TOPOGRAPHIC GUIDANCE SCAFFOLDS FOR PERIPHERAL NERVE INTERFACING

A Dissertation
Presented to
The Academic Faculty

By

Isaac P. Clements

In Partial Fulfillment
of the Requirements for the Degree
Doctor of Philosophy in the
School of Biomedical Engineering

Georgia Institute of Technology

December 2010

TOPOGRAPHIC GUIDANCE SCAFFOLDS FOR PERIPHERAL NERVE INTERFACING

Approved by:

Dr. Ravi V. Bellamkonda, Advisor
Department of Biomedical Engineering
Georgia Institute of Technology

Dr. Robert J. Butera, Co-Advisor
School of Electrical and Computer Engineering
Georgia Institute of Technology

Dr. Robert H. Lee
Department of Biomedical Engineering
Georgia Institute of Technology

Dr. Pamela T. Bhatti
School of Electrical and Computer Engineering
Georgia Institute of Technology

Dr. Arthur W. English
Department of Cell Biology
Emory University

Date Approved: November 18, 2010

ACKNOWLEDGEMENTS

This dissertation would not exist without the gracious support of colleagues, friends, and family. I'd first like to express gratefulness to my thesis committee and my advisor, Dr. Ravi Bellamkonda, who has always given me the guidance, resources, and freedom to conduct any and all research that interests me. Dr. Bellamkonda's enthusiasm for research and innovation are inspiring to those around him. My co-advisor Dr. Rob Butera gave me laboratory space to work in and was patient with my frequent drop-ins for on-demand advice. Dr. Arthur English discussed my research plans for hours on end and opened up his laboratory to me as one of his own students, (who were also very generous with their time and assistance). Dr. Bob Lee was always a great source of constructive feedback and was also generous in lending me lab equipment. Finally, Dr. Pamela Bhatti has been a source of helpful insight and a very gracious committee member.

I'd also like to express appreciation to my labmates and colleagues throughout the Neurolab. You've been a pleasure to work with and always generous with your time and advice. My former mentor, Dr. Young-tae Kim, trained me for hours at a time in basic techniques, and since then many others have offered countless hours of patient assistance. Vivek Mukhatyar, Akhil Srinivasan, Dr. George McConnell, Dinal Andreasen, Edgar Brown, Dr. Amanda Preyer, Dr. Rhadika Madhaven, Dr. Jeremy Lewi, Liang Guo, Brock Wester, Dr. Lohitash Karumbaiah, and Michael Tanenbaum are just a few of the people in the lab who have spent hours providing advice and technical aid. John Bentley, Gaurangkumar Patel, and many others in my "army of undergrads" have spent long days

and late nights working with me to obtain each figure and data point I present. I'd also like to thank, Dr. Laura O'Farrell and the staff in the Physiological Research Laboratory for making all of my animal research possible.

Outside of the lab, my friends and family have been a constant source of love and support. My sisters Chrissy and Andi have always been bright spot of joy and laughter in my life. My parents Mark and Melinda have given me unconditional love and always sacrificed to raise me with the best possible training, in both academics and also life values. I'm also thankful to my new family the Dysarts, who have welcomed me in love as one of their own. And I'd like to express special appreciation to my beautiful, soon-to-be wife, Rebecca: You see what my best can be and always challenge me to reach it. I love you, and I can't wait to begin the rest of my life with you. Above all, I'd like to acknowledge God for the many blessings and opportunities he has given me.

TABLE OF CONTENTS

LIST OF TABLES

Page

LIST OF FIGURES

Page

LIST OF ABBREVIATIONS

AC	Alternating current
ANOVA	Analysis of variance
CNAP	Compound nerve action potential
CNS	Central nervous system
DRG	Dorsal root ganglion
DAPI	4’,6-diamidino-2-phenylindole
ECM	Extracellular matrix
FINE	Flat interface nerve electrode
LIFE	Longitudinal intrafascicular electrode
LN	Laminin
NF-160	Neurofilament 160kDa.
NF-200	Neurofilament 200kDa.
PAN-MA	Poly(acrylonitrile-co-methylacrylate)
PBS	Physiologically buffered saline
PNI	Peripheral nerve interface
PNS	Peripheral nervous system
RSE	Regenerative scaffold electrode
Si	Silicon
SNR	Signal to noise ratio
SU-8	Photosensitive epoxy

SUMMARY

In response to high and rising amputation rates, significant advances have been made in the field of prosthetic limb design. Unfortunately, there exists a lag in the neural interfacing technology required to provide an adequate link between the nervous system and this emerging generation of advanced prosthetic devices. Novel approaches to peripheral nerve interfacing are required to establish the stable, high channel-count connections necessary to provide natural, thought driven control of an external prosthesis. Here, a tissue engineering-based approach has been used to create a device capable of interfacing with a regenerated portion of amputated nerve.

As part of this work, a nerve guidance channel in which small amounts of interior scaffolding material could be precisely positioned was developed and evaluated. Guidance channels containing a single thin-film sheet of aligned scaffolding were shown to support robust, functional nerve regeneration across extended injury gaps by minimally supplementing natural repair mechanisms. Significantly, these "thin-film enhanced nerve guidance channels" also provided the capability to control the path of axons regenerating from a cut nerve.

This capability to direct the course of axonal growth was next leveraged to create "regenerative scaffold electrodes (RSEs)" able to interface with axons regenerated from an amputated nerve. In the RSE design, low-profile arrays of interfacing electrodes were embedded within layers of aligned scaffolding material, such that regenerating axons were topographically guided by the scaffolding through the device and directly across the embedded electrodes. Chronically implanted RSEs were successfully used to record

evoked neural activity from amputated nerves in an animal model. These results demonstrate that the use of topographic cues within a nerve guidance channel might offer the potential to influence the course of nerve regeneration to the advantage of a peripheral nerve interface suitable for limb amputees.

CHAPTER 1

INTRODUCTION

1.1 Motivation

The Amputee Coalition of America cites that as of the year 2000, there are an estimated 1.6 million limb amputees live in the United States alone, with 185,000 new amputations performed annually. The escalating prevalence of major contributing factors threatens to increase amputation rates even further, and numbers are projected to double over the next several decades [1].

While significant development has occurred in the design of prosthetic limbs that cosmetically and functionally mimic natural limbs, advances in neural interfacing technology have not kept pace. As a result, existing prosthetic devices are typically controlled by simple, open-looped mechanisms. For example, artificial hand movements are often controlled by crude recordings of muscle signals in the residual limb, or more frequently by contralateral shoulder movements. These methods provide few independent control signals and do not provide a sense of feeling from the prosthetic limb. Even the most advanced interfacing approaches currently available in research clinics fail to provide sufficient numbers of control signals or adequate sensory feedback.

A fundamental goal in neuroprosthetic research has long been the development of a nerve/electrode interface that is able to seamlessly relay information between a surviving nerve stump and an external neuroprosthetic device. Ideally the interface should provide robust, high channel-count, bidirectional flow of information that remains

stable over the lifetime of the patient. The end goal for the functionality provided by this type of interface is as follows: The patient's natural attempts to move his or her amputated limb should result in the appropriate activation of the prosthetic device, and, likewise, input detected by sensors on the prosthetic device should be naturally perceived by the patient as coming from his or her original limb.

1.2 Project objectives

The objective of this project was to contribute towards these design goals through the application of tissue engineering principles to peripheral nerve interface design. Specifically, it was sought to embed interfacing electrodes within topographic guidance scaffolds capable of a) supporting regeneration from an amputated nerve, and b) directing the course of regenerating axons to within close proximity of the integrated electrodes. Significantly, the proposed "regenerative scaffold interface" (RSE) was designed to promote and control nerve regeneration, as opposed to existing regenerative electrodes that impede, or at best passively constrain regeneration.

As a first step, nerve guidance scaffolds containing anchored sheets of aligned nanofiber scaffolding were developed and demonstrated to exert controlled influence over the formative stages of the nerve repair sequence. Low-profile thin-film electrode arrays were next developed for integration within the nanofiber scaffolding sheets, with the intent that the scaffolding would support robust growth and direct the path of regenerating axons through the device and directly across the embedded array.

The details of this work are further described in the following chapters. Relevant background information is first provided in Chapter 2, and Chapter 3 details the development and characterization of topographic guidance scaffolds able to support and

direct nerve regeneration. Chapter 4 described the incorporation of interfacing electrodes into these scaffolds to create regenerative scaffold electrodes (RSEs). Finally, the broader implications and future goals regarding this work are discussed in Chapter 5.

CHAPTER 2

RELEVANT BACKGROUND

2.1 Peripheral nervous system structure and response to injury

2.1.1 Peripheral nervous system structure

The human nervous system gathers, transmits, processes, and stores information with remarkable speed and fidelity. These capabilities are made possible by networks of highly specialized neural cells, organized within an intricate 3D framework of interconnected neural tissue. The nervous system can be subdivided into the central nervous system (CNS) and peripheral nervous system (PNS). The chief components of the CNS are the brain and spinal cord, while the PNS includes the peripheral nerves that branch out from the CNS. Within both of these divisions, neural tissue is composed primarily of neurons and supporting glial cells. However, basic cell types and tissue organization vary greatly between the brain, spinal cord, and peripheral nerves. Here, we will focus on the peripheral nervous system.

Neurons of the PNS connect the CNS with sensory and motor targets. The cell body of each PNS neuron is located in or near the spinal cord or base of the brain. From this cell body, a long axon extends uninterrupted to the tissue it innervates (up to one meter or more). A single peripheral nerve can contain thousands of motor and sensory axons, enveloped along with other cell types within flexible tubes of collagen and other supporting extracellular matrix (ECM) components. The glial cells of the PNS are Schwann cells, which wrap around the axons in concentric layers to form insulating

sheaths rich in the protein myelin. These myelin sheaths enhance the speed of signal conduction down the length of the axon. Schwann cells also provide trophic support to the axons and play a major role in injury response.

2.1.2 Peripheral nerve regeneration after injury

When a peripheral nerve is damaged such that axons within it are severed, the portions of the affected axons lying distal to the injury site are cut off from the centrally located cell body. These distal axon segments subsequently degrade, and the resulting debris is cleared away by macrophages and Schwann cells as part of a process termed Wallerian degeneration. The Schwann cells proliferate and take on a pro-regenerative phenotype, rearranging themselves into aligned tracts called “bands of Bungner” and secreting factors conducive to the in-growth of regenerating axons.

Meanwhile, the portions of the injured neurons proximal to the damage site prepare for regeneration. The cell body of each injured axon undergoes major metabolic changes and initiates a program of protein synthesis to support axonal regeneration. At the tip of each injured axon, a growth cone develops and leads the regenerating axon through the intact structure of the distal nerve segment and back toward its original target at the approximate rate of 1-3 mm per day [2].

The process of peripheral nerve regeneration occurs spontaneously, as long as there is no extended nerve gap across the injury site. In cases where a small gap exists, the two nerve stumps can be surgically re-apposed. However when the nerve gap is longer, this procedure creates unacceptable tension on the nerve. In these cases, an autografted segment of nerve is the clinical gold standard for treatment. Healthy segments of nerve are harvested from elsewhere in the body, and used to bridge the gap

across the injury site. Unfortunately, this technique comes with several drawbacks, including the need for an additional surgery and a loss of function at the site from which the donor nerves are taken. Furthermore, patient recovery after autograft treatment is less than ideal.

Because of the drawbacks autograft repair, engineered guidance channels have been explored as an alternative treatment for nerve injury. For example, and empty silicone tube can be used to bridge and isolates a gap between injured nerve stumps, thereby facilitating a spontaneous repair sequence (Figure 2.1) [3]. A fibrin clot initially forms to bridge the gap, and non-neuronal cells migrate from both nerve stumps to restructure this acellular matrix, preparing the way for axons regenerating from the proximal nerve stump. The guidance channel walls block the in-growth of scar tissue forming cells, holding open a space through which regenerating cells and axons can grow. However, across gaps longer than a critical length (10-15mm through empty silicone tubes [4], initial steps in the regenerative sequence break down and regeneration fails.

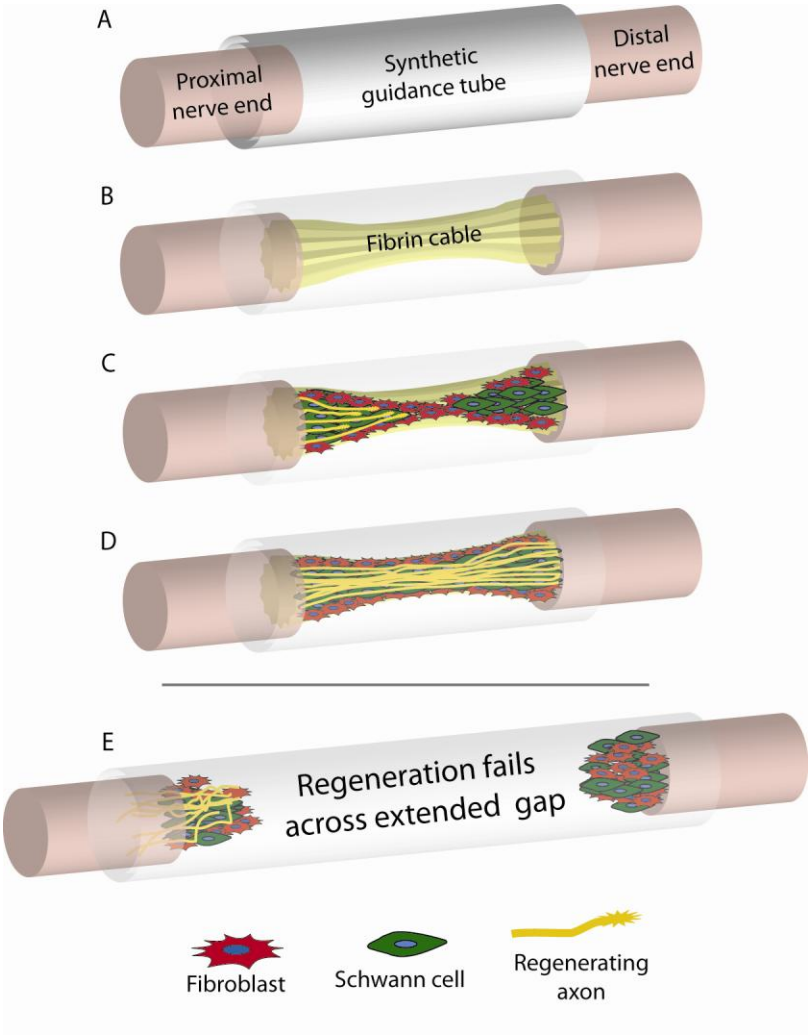

Figure 2.1: Peripheral nerve regeneration through an empty nerve guidance tube

Regeneration through the empty tube occurs in an ordered sequence. A: The ends of an severed nerve are attached into a nerve guidance tube. B: The tube fills with plasma derived from the nerve stumps. Fibrin precursors from within the plasma coalesce into an oriented fibrin bridge that physically bridges the nerve gap. C: Cells involved in regeneration, including fibroblasts and Schwann cells, migrate through this aligned fibrin cable and begin to proliferate and differentiate to prepare the way for regenerating axons. D: Axons regenerate from the proximal stump along with the migrating Schwann cells, bridging the gap and re-entering the distal nerve stump.

2.1.3 Response to topographic cues

Neural cells are highly responsive to natural cues present in their surrounding environment, especially during periods of growth and development. The course of a regenerating axon, for example, is guided by such factors as the physical topography and

chemistry of the surface along which it grows, as well as by signaling molecules in the local environment. These physical, biochemical, and even electrical cues exert great influence on cellular viability, growth, and activity. Thus, a fundamental strategy in tissue engineering-based approaches to injury repair is to artificially recreate environmental cues in such a way as to influence neural cell behavior.

2.1.3.1 Influence of topographic cues on cellular behavior

Topographic cues are physical features of the appropriate geometry and size to influence cellular behavior. Cellular attachment, alignment, migration, growth, and gene expression can all be regulated by controlling the nature and distribution of topographic cues provided by the component biomaterials of a tissue engineered construct.

The capacity of cells to respond to artificial topographic cues stems from the sensitivity of cells to natural topographic cues in their normal biological surroundings. Cells are particularly sensitive to topography during periods of growth, development, and regeneration. For example, during neural tissue development, aligned extracellular matrix (ECM) plays a major role in guiding neural cell migration and differentiation [5]. By mimicking the natural structures along which neural cells develop and reside, engineered substrates with particular topographies can greatly influence cellular behavior.

The mechanisms by which topographic cues influence cellular behavior are complex but involve interactions between the substrate topography and cellular structures that are sensitive to physical cues and able to effect cell-wide changes in behavior. For example, neural growth cones, located at the front of extending axons or neurites, are particularly sensitive to topographical features as they guide neuronal extension during periods of growth and development. Filipodial protrusions on the end of the growth cones

continually advance or retract in response to physical and chemical cues as they "explore" their surrounding environment. Ultimately, growth cones direct axon/neurite extension by mediating reorganization of the neuronal cytoskeleton.

This cytoskeletal reorganization is required for changes in cellular orientation as well as for growth and migration. The cytoskeleton is rearranged by depolymerization and polymerization of its component microtubules, intermediate filaments, and microfilaments [6]. It is hypothesized that these rod-like structures are limited in their capacity to bend, similar to a railroad track, and that their polymerization is thus dependent on the surrounding topography. This hypothesis might explain, for example, why cellular alignment and growth can be directionally constrained by certain types of topographic features such as aligned grooves (Figure 2.2).

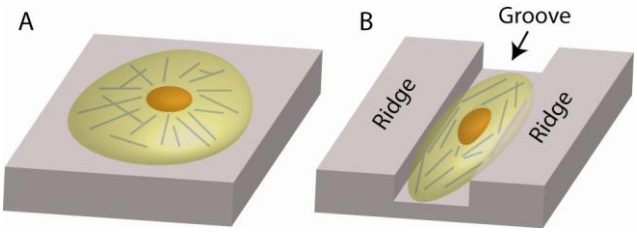

Figure 2.2: Example of topographic influence over cellular alignment and migration

The reorganization of cytoskeletal components can be constrained by the surface topography of the surrounding substrate, resulting in cellular alignment and directed migration. A: A cell cultured on a flat surface contains cytoskeletal components radiating predominantly from the centralized nucleus. B: When the same type of cell is cultured on a grooved surface, the orientation of the cytoskeletal components are constrained by the grooved surface topography.

2.1.3.2 Engineering topographic cues to control cell behavior

One of the most basic ways of altering the topography of a biomaterial is to vary its roughness by randomly modulating its surface texture [7]. Biomaterials roughened to include surface features at the appropriate size scales have been shown to promote

cellular adhesion and viability. For example, silicon substrates treated with chemical etchants or reactive ion etching techniques to include surface features down to the nanoscale have been shown to increase the adhesion and survival of both neurons and glia [8, 9]. It is proposed that nanoscale surface roughness promotes cellular adhesion by increasing cell membrane contact area as cells conform to fit the roughened surface [8].

More precisely defined topography can be used to influence cellular behavior in a more controlled manner. The ability to pattern arbitrary physical features allows for the fabrication of patterned surfaces that more closely mimic the surfaces of physiological structures and supporting cells. Cell culture experiments on topographically patterned substrates have explored the effects on cell behavior of a variety of patterned surface features, including grooves, pits, ridges, steps, and waves. These experiments have demonstrated the sensitivity of cells to geometric features down to nanoscale dimensions, and have shed light on the mechanisms by which cells are influenced by their surrounding topographies. Neurite extension, for example, can be directly guided along grooved or ridged surfaces, in a manner resembling fasciculation, the naturally occurring process in which axons grow along other preexisting axons [10, 11]. Other experiments have explored the effects of topographic cues presented in 3D. Matrices in the form of permissive gels or porous materials are useful for stimulating cell attachment and for providing a substrate for physical support and growth. Hydrogels, for example, are composed of a 3D structure of polymer cross-linkages that can be controlled to achieve desired properties such as stiffness and pore size. These parameters can be tailored to create biomaterial scaffolds with similar stiffness to soft-tissues and a low interfacial tension, favorable to cellular in-growth [12, 13].

Different types of oriented topographies can be created within 3D substrates using a variety of techniques. For example, gels can be given an aligned orientation by flowing them during gelling. Externally applied magnetic fields have been used to align collagen gels [14], and a variety of techniques have been used to create aligned subluminal or microchannels within 3D polymer substrates. Oriented 3D substrates have been use to create nerve guidance channels as well as guidance bridges for treating spinal cord injury gaps. Success has been met in both applications, though in the case of spinal cord repair, additional challenges must be addressed before clinically relevant results are achieved.

Although topographic cues can be used to directly influence neuronal growth, a potentially more effective strategy is to provide indirect guidance, by targeting the influence of patterned topography towards non-neuronal cells. For example, oriented topography can be used to align glial cells, which in turn can stimulate and support directed axonal growth not only through physical guidance cues, but also through aligned pathways of biochemical guidance cues, such as secreted ECM molecules [15, 16]. Fibroblasts, meningeal cells, astrocytes, and Schwann cells, aligned on topographically defined substrates, have all been demonstrated to promote and direct axonal growth [16-19].

2.1.3.3 Techniques for topographic patterning

Conventional photolithography techniques are most commonly used to pattern 2D surfaces with microscale features. Silicon is often used as a substrate, due to established patterning techniques developed for the microcomputing industry. Polymeric substrates can also be lithographically patterned, and are typically more suitable, due to their definable mechanical properties and/or biodegradability. Another advantage of polymeric

substrates is their capacity for direct pattern transfer via casting or embossing [20]. Polydimethylsiloxane (PDMS) and poly(methyl methacrylate) (PMMA) are two of the most commonly used materials for casting replicas of another patterned substrate.

While standard photolithography techniques can be used to pattern surfaces with microscale features, other techniques are required to pattern nanoscale features (100nm and below) [20]. For example, electron beam lithography (EBL) can be used to create arbitrary patterns with feature sizes as small as 3-5nm [21]. However, processing with EBL techniques is time consuming and requires expensive equipment [7]. To increase speed and reduce cost, patterns initially produced by EBL techniques can be replicated with polymer materials such as PDMS through techniques such as hot embossing and solvent casting [7, 11, 22]. While techniques such as EBL enable arbitrary control over nanoscale surface features, simpler and more inexpensive techniques are often preferable for patterning nanoscale topography when precise control over individual features is not required [7]. Electrospinning techniques, for example, can be used to create polymer fibers with diameters down to the nanoscale range (Figure 2.3). Aligned nanofibers are thought to mimic fibrous extracellular matrix proteins such as collagen and fibrinogen which have similar dimensions and alignment [7].

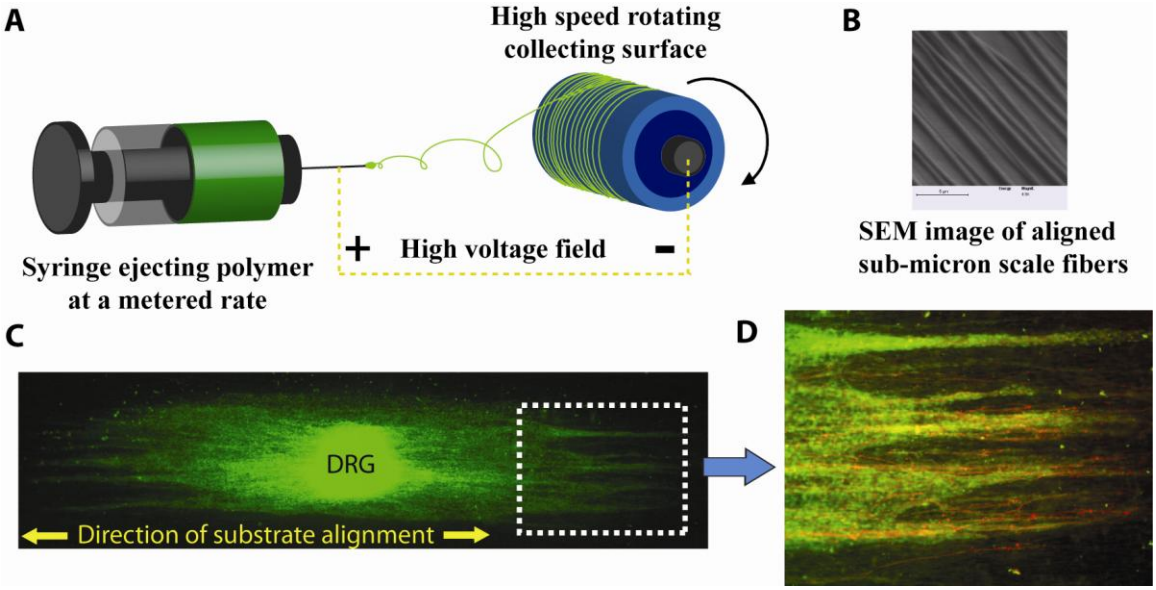

Figure 2.3: Electrospinning technique for creating aligned nanofibers and *in vitro* validation

A) To electrospin fibers, a liquid polymer melt is introduced to a high voltage field as it is slowly ejected from a syringe. Charge buildup on the drop of polymer at the syringe tip creates repulsive forces that cause tiny streams of polymer to be ejected towards a metal collecting surface. By collecting the ejected fibers on a high speed rotating cylinder, aligned films or sheets can be formed. B) SEM image of the surface of an aligned nanofiber sheet. C) Image of a rat dorsal root ganglion (DRG) cultured on an surface of an aligned nanofiber sheet. Schwann cells (green) migrate from the DRG, following the orientation of the fibers. D: In this magnified zoom-in, neurites are additionally labeled (red), and can be seen to grow along the aligned tracts of Schwann cells.

2.1.4 Nerve guidance scaffolds for peripheral nerve repair

Because of the influence of topography over cell behavior, particular during times of growth and regeneration, much research has been devoted to developing a biomaterials-based scaffold able to aid in the repair of extended nerve gap injuries. Such a scaffold should be implantable across an injury gap, and able to provide support and guidance to regenerating cells and axons in the place of an autograft. Such a construct would employ use topographic cues to recreate a pro-regenerative environment, similar to that which is found in the distal segment of injured nerve. For example, the Bands of

Bungner found in the distal nerve segment provide a physically aligned surface topography containing oriented tracks of adhesive molecules.

Due to the ability of aligned nanofibers to promote directed nerve regeneration [23, 24], a variety of nerve regeneration scaffolds employing electrospun nanofibers at their core has been shown to effectively facilitate nerve regeneration *in vivo* [25, 26]. As an example, scaffolds containing fifteen sheets of loosely stacked aligned nanofibers have been previously developed and tested in our lab [19]. The scaffold walls were produced from semipermeable polysulfone channels with a molecular weight cut-off of 50kDa, to allow the diffusion of natural biochemical factors, but black the influx of inflammatory cells. These topographic guidance scaffolds were shown to facilitate cell migration and functional nerve regeneration across critical length nerve gaps of 17mm. Notably, however, the loosely stacked films in this design tend to shift and settle, preventing precise spatial control over regeneration.

2.1.5 Axotomized peripheral nerves survive and regenerate even in the absence of the distal stump

Aebischer *et al.* have demonstrated robust peripheral nerve regeneration through empty semi-permeable guidance tubes in the absence of a distal nerve stump [27, 28]. By adding a fragment of nerve tissue to the distal end of a guidance tube, Williams *et al.*, among others, were able to increase this regeneration to match or exceed levels obtained in the presence of the distal stump. Their research demonstrated that an isolated nerve tissue fragment is able to support axonal regeneration at least as well as the intact distal nerve stump still connected to the end organ [29, 30]. Furthermore, it has been shown that even a very small segment of nerve tissue is more than sufficient for providing a source

of migrating Schwann cells, fibroblasts, etc., which support the regeneration of a nerve across a gap [31-34]. These studies demonstrate that mammalian peripheral nerves can be stimulated to regenerate normally after amputation by molecular signaling derived from sources other than the intact distal stump. (Also see our own results in the work to date section of Aim 2).

2.1.6 Axotomized peripheral nerves remain viable in the long term with help from Schwann cells

In their review on peripheral nerve regeneration, Fu and Gordon cite several prior experiments demonstrating that motoneurons branching from the spinal cord (spinal motoneurons) in adult mammals rarely die after peripheral nerve sectioning and that they remain viable indefinitely, even in the absence of a distal target [34-37]. The authors report that sensory neurons are less resistant to axotomy-induced death, yet are still able to sustain survival rates of at least 50% within a dorsal root ganglion after the same type of nerve sectioning. Thus, after limb amputation, the portion of the nerve proximal to the incision site remains largely viable. The mechanism by which axotomized spinal motoneurons are able to survive in the absence of a distal target lies in the neurotrophic support they receive from local sources, especially Schwann cells. As mentioned above, Schwann cells migrate after injury and differentiate to provide mechanical and neurotrophic support to injured axons [31, 32]. Schwann cells are capable of remaining in the proximal nerve stump indefinitely, providing a "substitute trophic target" for axons lacking their original targets [38].

This substitute distal support is not equivalent to that provided by the original distal target, however, and many of the surviving axons atrophy in size [34, 37].

Nevertheless, the state of the affected neurons grows stable, and they retain their ability to conduct action potentials, though their electrophysiological characteristics may be altered [37, 39]. Human amputee experiments with the aforementioned LIFE electrode have demonstrated the practical potential of the long-term viability of severed peripheral nerves [40]. Functional bidirectional interfacing with nerve stumps has shown that a high percentage of both afferent and efferent fibers survive a small distance back from the site of initial trauma, even in the absence of their original distal targets. Additionally the experimental results "indicate that both central and peripheral motor and somatosensory pathways retain significant residual connectivity and function for many years after limb amputation" [40].

2.2 Bioelectrical signaling and peripheral nerve interfacing

2.2.1 Electrical signaling of the nervous system

Neurons are electrically excitable cells, specialized to network with other neurons to store, process, and transmit information. Bioelectric signals propagate down the axon of a neuron in the form of shifting fluxes of ions termed an action potential. Neurons are specialized into many different forms within the central and peripheral nervous system. Two broad classes of neurons in the peripheral nervous system are motor and sensory neurons. Myelinated axons of the peripheral nervous system are enwrapped by Schwann cells such that extracellular currents appear only at gaps between the Schwann cells termed "nodes of Ranvier." Propagating action potentials are capable of propagating directly from node in a process called salutatory conduction. This process greatly increases the speed of signal conduction through myelinated axons.

Recording neural signals as they propagate down peripheral nerves is technically challenging because the extracellular voltage levels induced during action potentials are within the microvolt range. A whereas noise sources such motion artifact and electrical muscle activity can be several orders of magnitude higher. Furthermore extracellular voltage fluxes are not uniform across the membrane of myelinated axons, but rather localized to the nodes of Ranvier, which are spaced apart by approximately 0.5mm to 1mm apart down the length of the axon. Notably, smaller diameter axons produce smaller extracellular signals, which makes recording from regenerating axons even more difficult due to their reduced caliber.

2.2.2 Selecting the site of a neural interface

A neural interface provides a means of accessing the nervous system to record or stimulate neural signals. Despite the technical challenges involved with recording electrical signals from peripheral nerves, there are several reasons to choose peripheral nerve as the site to interface with the nervous system for the control of a prosthetic device. For example, a peripheral nerve interface is less invasive than an interface implanted in the central nervous system (CNS). The risks of surgery and consequences of possible infections are reduced in the periphery as compared to in the brain or spinal cord. Furthermore, if the interface is implanted at the time of amputation, there is no need for any additional surgical procedure.

Also, an interface at the level of peripheral nerve takes advantage of much of the natural processing in the nervous system. For example, in the formation of motor patterns, signals descending from the cortex are modified in subcortical regions such as the cerebellum and basal ganglia. Similarly, in sensory processing centers as low as the

spinal cord, ascending integration, filtering, and processing occur. A peripheral nerve interface will take advantage of this natural processing, which is left intact in the typical amputee.

Interfacing with peripheral nerve also allows for the most natural control for the patient. The electrodes can be mapped with patient feedback such that the original functions of the recorded neurons can be used to control corresponding functions on the prosthetic device. After this mapping, a peripheral nerve interface has the potential to offer a patient natural control of the prosthetic device, achieved by attempting to control the lost limb or organ. Similarly, stimulation patterns generated the prosthetic device can be mapped such that it is perceived as sensory and proprioceptive input coming from the lost limb or organ [40]. Achieving this arrangement of natural control and feedback by interfacing at the precise required locations of motor and sensory cortex would be a much more challenging task. Finally, peripheral nerve offers highly selective control over motor and sensory interfacing. Small groups of axons or even individual axons could be stimulated and recorded from, to provide the finest resolution of sensory modulation and motor control.

The peripheral nerve interfacing (PNI) problem is uniquely multidisciplinary. From an engineering perspective, an optimum interface will faithfully record from and stimulate small groups of axons in a stable and robust fashion. From a biological perspective, the nerve should be presented with an environment that encourages its stability and viability.

2.2.3 Peripheral nerve interfacing approaches

2.2.3.1 Extraneural Electrodes

Cuff electrodes have long been used as a means to stimulate and record from intact peripheral nerves. They offer a safe and stable interface, and their utility for certain applications (e.g. bladder control) has been clinically validated. There are several modified versions of the basic cuff design, including spiral nerve cuffs that self-regulate pressure on the nerve, and flat interface nerve electrodes (FINEs) developed by the Durand lab [41, 42]. FINEs can slowly flatten nerves, as well as take advantage of their natural eccentricity, to achieve an increased surface area for recording and stimulation. However, even the FINE electrode and other advanced versions of the basic cuff electrode design are extraneural in nature and may fail to contact enough small subsets of the nerve.

2.2.3.2 LIFE Electrodes:

Using longitudinal intrafascicular (LIFE) electrodes on human amputees, Kenneth Horch and colleagues have achieved a level of interfacing selectivity higher than that offered by extraneural electrodes [40]. The thin, needle-like electrodes have been demonstrated to achieve bidirectional interfacing with nerves stumps, even in long-term amputated nerves. However, while these experiments have been successful in terms of establishing functional sensory and motor interfacing with a few electrodes at a time, LIFE electrodes are not easily expanded to high channel counts. Additionally, LIFE electrodes are more invasive than other possible approaches, as they must be inserted into the proximal stump and pushed up into more proximal and viable regions of the amputated nerve.

2.2.3.3 Regenerative Electrodes

The sieve electrode is another interfacing approach that offers both higher channel counts and selectivity. First implemented decades ago [43], this device seeks to exploit the plasticity of a regenerating nerve. In the basic design, a disk containing electrode holes is inserted into a saline-filled silicone tube [44]. The tube is sutured to both cut ends of a transected nerve, and regenerating axons grow through vias surrounding by ring-shaped electrodes, able to contact regenerated axons for stimulation and recording. However, while the hollow silicone conduit used in this setup contributes to regeneration by confining the regenerating axons, it offers little support or influence over axonal growth. The situation is aggravated by the fact that the perforated electrode disk significantly impedes regeneration [45]. Additionally, the perforated disks are so thin (10 μm) that the nodes of Ranvier on each axons has a reduced chance of falling close enough to the disk for recording [45].

These shortcoming have driven the recent development of alternative designs [46-48]. Guidance channel structure and electrode types vary widely between these designs, but each seeks to minimize barriers to regeneration and produce stable, high channel count microelectrode / axon interfacing that is more sensitive to biological signals and more robust to noise. Such designs are early in development, but appear to offer little support or control over nerve regeneration. Furthermore, none of these designs have been adequately evaluated in an amputation case, when the intact distal nerve stump is not available as a target to the regenerating nerve.

CHAPTER 3

INFLUENCE OF TOPOGRAPHICALLY ALIGNED, NANOFIBER-BASED SCAFFOLDS ON NERVE REGENERATION

3.1 ABSTRACT

It has been demonstrated that nerve guidance channels containing stacked thin-films of aligned poly(acrylonitrile-methacrylate) fibers support peripheral nerve regeneration across critical sized nerve gaps, without the aid of exogenous cells or proteins. Here, we explore the ability of tubular channels mininally supplemented with aligned nanofiber-based thin-films to promote endogenous nerve repair. We describe a technique for fabricating guidance channels in which individual thin-films are fixed into place within the lumen of a polysulfone tube. Because each thin-film is <10μm thick, this technique allows fine control over the positioning of aligned scaffolding substrate. We evaluated nerve regeneration through a 1-film guidance channel - containing a single continuous thin-film of aligned fibers - in comparison to a 3-film channel that provided two additional thin-film tracks. Thirty rats were implanted with one of the two channel types, and regeneration across a 14 mm tibial nerve gap was evaluated after 6 weeks and 13 weeks, using a range of morphological and functional measures. Both the 1-film and the 3-film channels supported regeneration across the nerve gap resulting in functional muscular reinnervation. Each channel type characteristically influenced the morphology of the regeneration cable. Interestingly, the 1-film channels supported enhanced

regeneration compared to the 3-film channels in terms of regenerated axon profile counts and measures of nerve conduction velocity. These results suggest that minimal levels of appropriately positioned topographical cues significantly enhance guidance channel function by modulating endogenous repair mechanisms, resulting in effective bridging of critically sized peripheral nerve gaps.

3.2 INTRODUCTION

Peripheral nerves are capable of limited regeneration after injury, but regeneration across extended nerve gaps must be surgically facilitated. When the nerve stumps cannot be directly coapted without producing tension, the gap must instead be bridged - most commonly with autografted segments of nerve. Autograft bridging is limited, however, by the lack of availability of donor nerves, and drawbacks include the need for a secondary surgery and the loss of donor site function. Furthermore, the functional outcomes of autografting fall short of ideal, partly due to mismatch in dimension and modality between the injured and donor nerves [50, 51].

Due to these limitations, engineered guidance channels have been explored as an alternative to autografts for the repair of nerve injury. The most common example of a synthetic guidance channel is a saline filled polymer channel, used to bridge the two nerve stumps. The channel isolates the gap between the nerve stumps, thereby facilitating a well-documented wound-healing type process of endogenous nerve repair [3]. Briefly, plasma derived precursors first coalesce into an oriented fibrin matrix that physically bridges the nerve gap. Non-neuronal cell types including fibroblasts and Schwann cells migrate from the nerve stumps along this acellular matrix, where they multiply and differentiate, enriching and remodeling the matrix [52, 53]. Regenerating axons advance

in close association with the proximally derived Schwann cells through the regeneration matrix, crossing over the nerve gap and re-entering the distal stump. Continued nerve growth and migration follows along this developing matrix, and a regenerated nerve cable is gradually formed and matured through a continued series of complex neural-glial-matrix interactions [53].

While this sequence of endogenous repair can be modulated by altering the guidance channel's physical and chemical properties, such as its material composition, permeability, or texture [27], regeneration through empty channels is limited beyond a critical gap length of 10mm for rat sciatic nerve gaps [4].

The introduction of scaffolding within the lumen of a guidance channel can also increase the channel's ability to bridge nerve gaps. For instance, materials with oriented topography are able to stimulate cellular alignment and effect topographic guidance [20, 54-56], and have shown promise as scaffolding substrates. Classes of aligned scaffolding materials include patterned polymers, natural or synthetic microfilaments [57-59], and oriented gels and matrices composed of extracellular matrix (ECM) components [14, 60-62] or polysaccharides [63].

Significantly, electrospun meshes of aligned sub-micron scale polymer fibers have also been demonstrated as effective scaffolding substrates with unique properties, such as high surface area-to-volume ratio, mechanical strength, and a compactly aligned topography [24-26]. As an example, our lab has previously developed guidance channels containing stacked electrospun polyacrlonitrile-methacrylate (PAN-MA) thin-films and demonstrated their ability to promote Schwann cell migration and nerve regeneration

across critical sized nerve gaps without the aid of any exogenous ECM or trophic proteins [19].

Here, in a new design, we explore the concept of an enhanced nerve guidance channel, containing one or three aligned thin-films within the channel lumen. The organizing principle of this design is to modulate the regenerative wound-healing sequence to enable bridging of long gaps, while minimally obstructing the cross-sectional area available to the regenerating nerve. Briefly, the edges of electrospun thin-films are attached within the inner walls of the guidance channel, fixing the thin-films into place through the channel lumen. This arrangement enables fine control over the location of the thin-films within the lumen and furthermore prevents the thin-films from shifting over time. With a thickness of ~ 7μm, each thin-film sheet occupies only ~0.6% of the guidance channel's open cross-sectional area, yet provides a continuous track of densely aligned topographic cues, anchored through the length of the channel.

Using a 14mm tibial nerve gap model in rats, the regenerative potential of 1-film guidance channels, containing a single aligned thin-film, was compared to that of a 3-film design, in order to explore the design space of minimal enhancement to empty nerve guidance channels. Using a combination of morphological and functional measures, nerve regeneration was evaluated at 6 and 13 weeks.

3.3 MATERIALS AND METHODS

3.3.1 Design of aligned fiber-based thin-film channels

3.3.1.1 Fabrication of aligned fiber thin-films

Films consisting of aligned poly(acrylontrile-co-methylacrylate, random copolymer, 4 mole percent methylacrylate) (PAN-MA) fibers were created through an electrospinning process as in our previous studies [19]. Briefly, a 15% (w/v) PAN-MA solution was prepared by dissolving PAN-MA into the organic solvent N, N-Dimethyl Formamide (DMF, Acros Organics) at 60ºC. This solution was loaded into a metered syringe and dispensed for 15 minutes at a constant flow-rate of 1ml/hr through a 19 gauge needle across a voltage field of 15-18kV. The ejected polymer fibers were collected 10 cm away on a 3.8 cm diameter metal drum, rotating at approximately 2500 rpm to produce aligned fiber thin-films, which were baked for 4 hours at 60ºC to remove any residual DMF. Finally, 2.2 x 14mm sheets of aligned thin-films were manually cut with a razor blade and separated from the collected polymer mass with fine forceps for use in channel construction.

3.3.1.2 Construction of thin-film enhanced nerve guidance channels

Polysulfone nerve guidance channels (Koch Membrane Systems) were modified to create enhanced nerve guides with aligned thin-films incorporated in their lumens. The semipermeable polysulfone tubing (inner diameter: 1.6 mm, outer diameter: 2.2 mm, molecular weight cutoff: 50kDa) was first cut into tubes of 17 mm length. These tubes were next sectioned lengthwise into 4 longitudinal sections, using a custom machined aluminum template. Under a fabrication microscope, the thin-film enhanced channels

were then fabricated as part of a multistep process (Figure 3.1), with each layer secured into place with a medical grade UV light curing adhesive (1187-M-SV01, Dymax). In the 1-film case, a single thin-film was secured longitudinally through the length of the tube. In the 3-film case, two additional films were fixed through the tube, distributed from each other in a "Z" formation (Figure 3.1). This formation was chosen as opposed to a formation of three parallel thin-films because its construction was less complex, requiring that the polysulfone tube be split into four pieces rather than six. Notably, the 1-film guidance channels could have been constructed more simply by splitting the polysulfone tubes longitudinally into two pieces rather than four, but we fabricated the two channel types in an identical manner to minimize any structural variability. Significantly, due to the negligible thickness of each thin-film, there is minimal difference between the two designs in the percentage of luminal cross-sectional area occupied by scaffolding.

The channels were sterilized by overnight incubation under UV light followed by immersion in 70% ethanol for 30 minutes. This process was immediately followed by two 20 minute washes in sterilized deionized water and a final wash in sterilized phosphate buffered saline (PBS). The channels were then stored in sterile PBS until the implantation surgery.

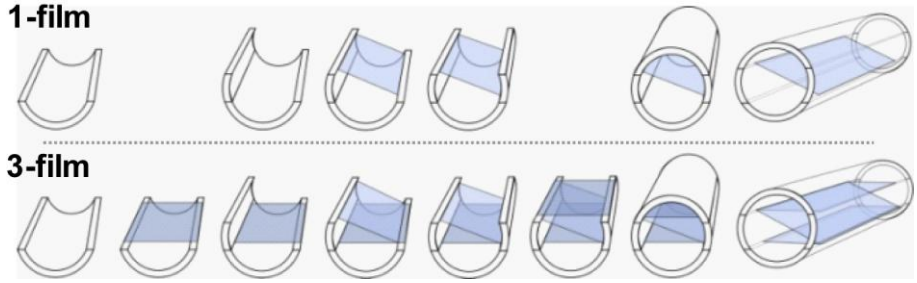

Figure 3.1: Illustration of the fabrication process for a 1-film and 3-film channel.

Under a microscope, longitudinal sections of polysulfone tubing and strips of electrospun PAN-MA thin-films were sequentially stacked and fixed into place with UV curing adhesive. The steps used to build the two channel types were identical, except for the addition of the two extra thin-films included in the 3-film channels (bottom row).

3.3.2 *In vivo* implantation of enhanced nerve guidance channels

Enhanced guidance channel implantations to bridge 14 mm gaps in the tibial branch of the sciatic nerve were performed on anesthetized Fischer 344 rats (250-300g), as described in [19]. Briefly, the rats were anesthetized with inhaled isoflurane gas, and the surgical site was shaved and sterilized. Marcaine (0.25% w/v, Hospira, Inc.) was next administered subcutaneously for post-surgical pain relief (0.3 ml/animal). A skin incision was then made along the femoral axis, and the underlying thigh muscles were delineated with a blunt probe to expose the sciatic nerve. After the nerves were freed from overlying connective tissue, microscissors were used to transect the tibial nerve branch, slightly distal to the common peroneal - tibial bifurcation, and the nerve stumps were pulled 1.5 mm into each end of a guidance channel and fixed into place with a single 10-0 nylon suture (Ethilon) to create a 14 mm gap. The muscles were then reapposed with 4-0 vicryl sutures (Ethicon Inc.) and the skin incision was clamped shut with wound clips (Braintree Scientific, Inc.). After the surgery, the rats were placed under a warm light, allowed to recover from anesthesia, and then housed separately with access to food and water *ad*

libitum in a colony room maintained at constant temperature (19-22^{o}C) and humidity (40-50%) on a 12:12 h light/dark cycle. To prevent toe chewing, a bitter solution (Grannick's Bitter Apple Co.) was applied twice a day to the affected foot. When further action was required, treatment with a mixture of New Skin (MedTech) and Metronidazole (ICN Biomedical Research Products) as described in [64] was administered and found to be effective. Animals were maintained in facilities approved by the Institutional Animal Care and Use Committee (IACUC) at the Georgia Institue of Technology and in accordance with the current United States Department of Agriculture, Department of Health and Human Services, and National Institutes of Health regulations and standards.

3.3.3 Evaluation of nerve regeneration

Nerve regeneration was assessed using histological and electrophysiological measures. Explanted channels were sectioned and evaluated (1) qualitatively, to examine the influence of the aligned thin-films in each channel type on the morphology of the regenerating nerve, and (2) quantitatively, to compare regeneration cable size and counts of numbers of regenerated axons. Functional recovery was assessed through electrophysiological measurements of nerve conduction velocity (NCV) and electromyographic (EMG) signals produced by the reinnervated muscles. Histological evaluation of motor endplates was also performed.

3.3.3.1 Experimental groups

Nerve regeneration through each channel type was evaluated at 6 weeks and 13 weeks post-implantation (Table 3.1). The 13 week time point (20 animals) was chosen to allow for an appreciable degree of functional recovery to take place, and electrophysiological assessments were conducted at this later time point only. Negative

control cases with empty guidance channels were not performed because it was anticipated that little to no regeneration would occur through empty channels at this 14 mm gap length. These assumptions were based on prior work in our lab in which regeneration through empty channels of the same material failed in most cases, even across less challenging 10 mm gaps [65].

We note here that for the 13 week group, the process of electrophysiological testing and tissue harvest required several hours per animal, and so this phase of evaluation spanned a period of approximately ten days. As a result, the exact regeneration times were actually 12.5-14 weeks, but for simplicity this time point is elsewhere referred to in this study as the 13 week time point. To prevent bias in regeneration times between the 1-film and 3-film groups, animals from each group were tested in alternating fashion.

The six week time point groups (10 animals) were used to study the role of the thin-films in affecting regenerative processes at an earlier stage. Based on prior experience in our lab, it was determined that six weeks would be long enough to allow for an appreciable degree of axonal regeneration through the full length of the guidance channels, but short enough that the regeneration cable across the gap would still be at an immature state. Regeneration in the six week groups was examined using histological techniques.

Table 3.1: Experimental groups

Groups	No. of rats
1-film, 13 weeks	10
3-film, 13 weeks	10
1-film, 6 weeks	5
3-film, 6 weeks	5

3.3.3.2 Electrophysiological assessment of nerve regeneration

In order to assess functional recovery in the 13 week groups, electrophysiological testing was performed. Each animal was deeply anesthetized with a mixture of ketamine (65mg/kg), xylazine (7.5mg/kg), and acepromazine (0.5mg/kg), and a catheter was sutured into the intraperitoneal (IP) space to allow continued dosage during the evaluation. The site of nerve injury was exposed as during the initial surgery, and the cavity was kept moistened with mineral oil warmed to 37ºC. Through the procedure, the animals were kept warm with an infrared light, and their breathing rates and reflex responses to toe pinch stimuli were closely monitored.

3.3.3.3 Nerve conduction velocity

A portion of the sciatic nerve, approximately 15 mm proximal to the proximal end of the channel, was freed from the surrounding tissue, as was a portion of the distal tibial nerve branch, approximately 15 mm past the distal end of the channel. Stainless steel bipolar hook electrodes were fixed to both exposed portions of nerve, and the separation distance between the pair of electrodes was precisely measured. The distally positioned pair of electrodes, which was attached to a stimulator (Model S88, Grass Technologies) and stimulus isolation unit (Model SIU5B, Grass), was used to stimulate the regenerated nerve with 100μs square pulses of variable amplitude, applied at a rate of 1Hz. The

evoked compound nerve action potentials (CNAPs) were recorded from the proximal pair of electrodes, amplified (G=1000), bandpass filtered (10-5000 Hz, Model 1700, A-M Systems), and digitally sampled. (25 kS/sec, Multichannel Systems DAQ card.) The recordings were averaged up to 200 times, using a trigger signal provided by the stimulator, and the latencies of the onset of the evoked CNAPs were determined off-line. The precise distances between stimulating and recording electrodes were measured and divided by the latencies to calculate the conduction velocity of the CNAPs through the regenerated nerves. Average conduction velocities through the 1-film and 3-film groups were compared using one-way ANOVA, with a *p*-value less than 0.05 considered statistically significant. Although the NCV does not provide a complete measure of functional recovery, this measurement is positively correlated with the size of myelinated axons and degree of myelination, and can thus be used to quantitatively assess the extent of reinnervation of the distal nerve segment.

3.3.3.4 EMG recordings

As an assessment of functional muscle reinnervation, bipolar patch electrodes were fixed to the surface of the denervated lateral gastrocnemius muscles (LG) and used to record evoked EMG activity. Briefly, the patch electrodes were constructed as previously described [66] by gluing two insulated, stranded, stainless steel wires through a Dacron mesh reinforced square of 0.01" thick silicone.

Hook electrodes were used to stimulate the regenerated tibial nerve with supramaximal square pulses of 300μs duration, delivered at 1Hz, and the evoked EMG signals were recorded with the patch electrodes. Recordings were amplified, filtered, and stored for off-line averaging and analysis. As a negative control, EMG activity from the

tibialis anterior (TA) muscle was recorded as well, since TA is not innervated by the tibial nerve. Additionally, near the end of the procedure, the regenerated nerve was crushed distal to the stimulating hook electrode to further demonstrate that the previously recorded EMG signals from LG were indeed the result of nerve activity traveling through the regenerated nerve. Because recorded EMG signal shape and amplitude can vary significantly based on electrode placement, EMG recordings were used primarily for qualitative analysis.

3.3.3.5 Immunohistochemical analysis of nerve regeneration

After electrophysiological evaluation, the rats were immediately perfused intracardially with saline followed by 4% paraformaldehyde in PBS (Sigma-Aldrich). The injury site was fully exposed, and the nerve guidance channels were explanted for histological analysis. The gastrocnemius muscles from the experimental and control legs were also explanted, and all harvested tissues were post-fixed overnight in 4% paraformaldehyde. The tissues were later washed and stored for several hours in PBS and then transferred to a 30% sucrose in PBS solution for cryoprotection and incubated at 4ºC for 1-2 days until saturation. Finally, the samples were embedded in O.C.T. gel (Tissue Tek) and frozen for cryosectioning (CM30505, Leica). Ten micron thick cross sections were collected at one millimeter intervals. In four channels, 18µm thick longitudinal sections were instead collected, to provide an alternative perspective of regeneration through the channels.

Sections were later reacted for immunofluorescent demonstration of markers on 1) axons (NF160, 1:500 dilution, Sigma-Aldrich); 2) Schwann cells, (S100, 1:250, Dako); 3) myelin (P0, 1:100, Chemicon Intl.); 4) macrophages (ED-1, CD-68, 1:1000,

Serotec); 5) fibroblasts (vimentin, 1:500, Sigma-Aldrich, as well as S100, to allow differentiation of weak reactivity of Schwann cells by anti-vimentin antibody). Nuclei were labeled with DAPI (Invitrogen) in PBS at a concentration of 10μM. The following secondary antibodies were used: Goat anti-rabbit IgG Alexa 488/594, goat anti-mouse IgG1 Alexa 488/594, and goat anti-chick IgG (Invitrogen).

Immunohistochemistry techniques were conducted as previously described [19]. Briefly, sections were first incubated for one hour at room temperature in a blocking solution of 4% goat serum (Gibco) in PBS containing 0.5% Triton X-100 (Sigma). Sections were then incubated overnight at 4ºC in a mixture of primary antibody and blocking solution, then washed and incubated once more for 1 hour at room temperature in a solution of secondary antibody, diluted 1:220 in 0.5% triton in PBS. This incubation was followed by a 10 minute incubation in DAPI solution. Finally, the sections were washed once more, dried, and cover-slipped for evaluation. Other slides were prepared for bright field microscopy using standard Masson's Trichrome staining techniques.

The cross sectional area of the regeneration cables was measured at the channel center (7 mm into the nerve gap) and at distances of 2.5 mm from each nerve stump in all 13 week channels. To perform these measurements, 4x magnified images of stained cross sections were analyzed with Image Pro software (Media Cybernetics). Within each imaged section, the cross-sectional area occupied by the regenerated tissue cable (comprised of the axonal/Schwann cell core as well the surrounding epineurial-like collagenous tissue) was selected and quantified, and means were calculated for each group.

Nerve regeneration was also quantified by counting the total number of NF-160^{+} axonal profiles at the center of the nerve gap. To perform this analysis, a confocal microscope (LSM 510, Zeiss) was first used to image a representative subset of the regeneration cable at 40x magnification. The number of NF160^{+} axons within this image was then quantified with Image Pro software and used to calculate a representative axonal density for each channel. Next, a composite 40x image of the entire regeneration cable cross section was obtained, using a microscope equipped with a computer controlled stage and Neurolucida software (MFB Bioscience). Image Pro software was then used to quantify the entire cross-sectional area of axonal regeneration, and this area was multiplied by the calculated axonal density to estimate the total number of axonal profiles. Accuracy of this technique was initially validated by comparing results with manual hand counts, and reproducibility/precision was demonstrated by repeating quantifications on sequential sections. One-way ANOVA was used for all statistical comparisons between the 1-film and 3-film groups, and a p-value < 0.05 was considered to be significant.

3.3.3.6 Evaluation of neuromuscular junctions re-innervation

Explanted gastrocnemius muscles were embedded in OCT gel in a process similar to the guidance channels and then cut with a cryostat into 25 µm thick longitudinal sections. Tissue sections were collected from the center of the muscle and reacted as previously described [19, 67] for fluorescent demonstration of axons, motor endplates, and synaptic vesicles. These structures were identified using markers for neurofilament 160 (anti-NF160, Sigma-Aldrich), (2) synaptic vesicles (anti-synaptic vesicle protein 2 (SV2), Developmental Studies Hybridoma Bank), and acetylcholine receptors

(tetramethlyrhodamine conjugated α-bungarotoxin, Sigma-Aldrich). Co-localization of markers for axons and motor endplates indicates morphological innervation of the neuromuscular synapses. The additional co-localization of synaptic vesicle markers is suggestive of functional regeneration. Healthy contralateral gastrocnemius muscles taken from the control limb were evaluated as positive controls.

3.4 RESULTS

3.4.1 Surgical outcomes

All 30 rats survived the guidance channel implantation surgery without complication, and most animals exhibited only minimal autotomy as a result of nerve transection. One animal from the 1-film channel, 13 week group excessively chewed the foot on the operated side and was euthanized at two weeks post-surgery. A second animal from the 3-film, 13 week group was electively euthanized as well to allow for a comparative example of early regeneration after two weeks through each channel type. The channels explanted from these two animals were cryosectioned longitudinally for histology. All other animals remained healthy and were sacrificed at their scheduled endpoints. At the time of explantation, all guidance channels were found to be structurally intact with the tibial nerve still firmly secured on each end. The guidance channels were encased in a characteristic thin envelope of fibrotic tissue, but the visible inflammatory response to the implanted channels was otherwise minimal.

3.4.2 Histological assessment of nerve regeneration

3.4.2.1 General observations

Explanted channels were sectioned and processed for histological analysis. Substantial regeneration of $NF160^+$ axons was observed through the full lengths of both types of guidance channels at both the 6 week and 13 week time points. The aligned PAN-MA thin-films were visible in the guidance channel cross-sections and were observed to have remained intact and fixed into place within the channel interiors. The thin-films were measured to have a relatively uniform thickness of approximately 7 µm.

The placement of the aligned thin-films influenced the positioning and morphology of the regenerated nerve structure, as observed in channel cross-sections. The regeneration cables in the 1-film channels were centered around the single thin-film, and consisted of a centralized core of axons and co-localized Schwann cells that was surrounded by epineurial-like tissue arranged into aligned bands (Figure 3.2 A,B). The regeneration cables in the 3-film channels were larger, but contained a fragmented core of axons/Schwann cells, with subsets of this core asymmetrically dispersed around and between the multiple thin-films (Figure 3.2 C,D).

A minimal inflammatory response to all implanted materials, including the polysulfone walls, UV curing adhesive, and PAN-MA thin-films was observed, which was consistent with the results of our previous studies [19, 68]. By the 13 week time point $ED\text{-}1^+$ macrophages were present in a thin layer on the interior and exterior surfaces of the guidance channel walls, within the walls, and were sparsely distributed within the channel interiors (data not shown). Several concentric layers of $vimentin^+$ fibroblasts surrounded the outer walls of the guidance channels, and in many of the channels

fibroblast in-growth occurred through cracks at the junctures where the channel walls were cut and glued during the fabrication process (Figure 3.6 A). Macrophage and fibroblast presence on the thin-films was minimal.

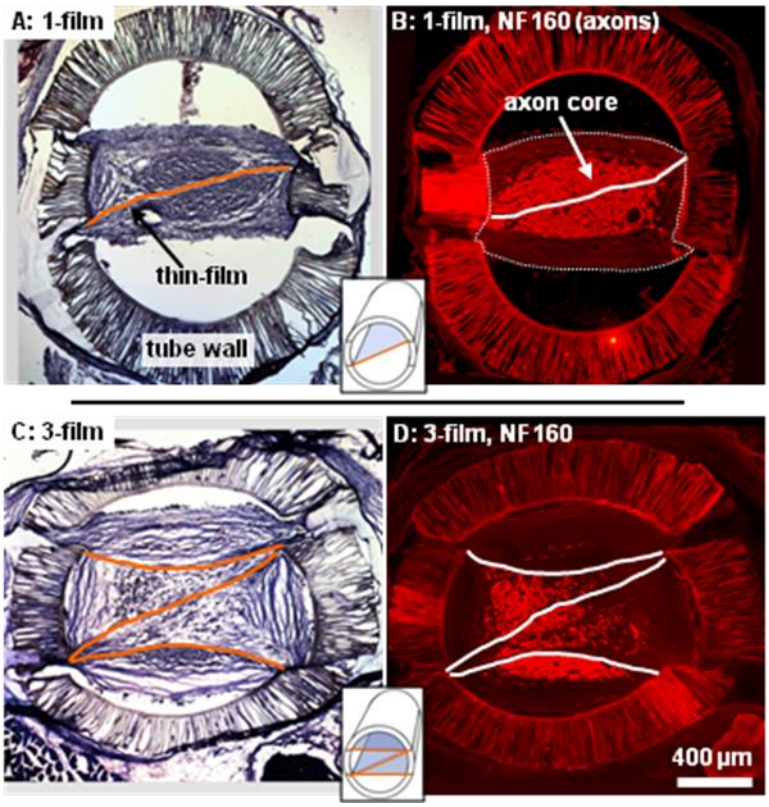

Figure 3.2: Representative cross-sections from a 1-film and 3-film channel at thirteen weeks.

False colored lines mark the locations of the aligned thin-films for a 1-film (A,B) and 3-film (C,D) channel. (A,C): Tissue stained cross-sections taken 3.5 mm into the nerve gap. The location and structure of the regenerated tissue cables were visibly influenced by the thin-films. (B,D): Cross-sections taken from 2.5 mm into the nerve gap, reacted with NF160 for immunofluorescent demonstration of axons. In the 1-film channels (B), regenerated axons were distributed within a consolidated core surrounding the single thin-film. This core was surrounded by aligned bands of epineurial-like tissue forming the periphery of the regeneration cable, (the outer border of which is marked with a thin dotted line). In the 3-film channels, the axonal core was fragmented around and between the aligned thin-films.

3.4.2.2 1-film channels, 13 week time point

To examine the influence of the aligned thin-films on regeneration cable morphology, cross-sections were taken at one millimeter intervals through the entire length of the channel. Characteristic patterns of regeneration observed in the 1-film channel, 13 week group are shown for a representative channel in Figure 3.3. Near the proximal edge of the channel, the intact nerve stump contained a core of axons arranged in a circular cross-section (Figure 3.3 A), but at further distances into the channel, regenerating axons were grouped together into a more centralized interior core with a cross-sectional shape that was elongated to match the orientation of the single aligned thin-film (Figure 3.3 B-D). This elongation of the axonal core's cross-sectional shape around the thin-film reached a maximum near the channel midpoint (Figure 3.3 C). At farther distances past the midpoint, the axonal core gradually regained a circular cross-section as it approached the intact distal nerve stump (Figure 3.3 D, E).

Patterns of cellular distribution within the core of regenerated axons also varied based on distance into the 1-film channel (Figure 3.3 F-H). Towards the proximal end of the regeneration cable, axons were grouped into a dense and uniformly organized pattern surrounding the single thin-film (Figure 3.3 F and inset). Towards the channel midpoint, the axons were aggregated into dense groups (Figure 3.3 G and inset). At distances past the channel midpoint, the axons were dispersed from this grouped arrangement and were distributed more uniformly, though more sparsely, across a wider cross-sectional area within the channels (Figure 3.3 H and inset). Co-localization of axons and Schwann cells, myelination of axons, and laminin deposition around axons were visualized at 40x magnification using confocal microscopy (Figure 3.3 J-L).

Surrounding the axonal core, aligned bands of epineurial-like collagenous tissue formed the periphery of the regeneration cable (Figure 3.2 A, 3I). These tissue bands were not attached to the smooth interior walls of the guidance channels, but in some channels attached to the junctures where the channel was cut and glued during the fabrication process, giving some of the regeneration cables a rectangular cross-sectional profile (Figure 3.2 A, Figure 3.3 B-D). The distribution of cells within the regeneration cable was correlated with the locations of the collagen bands. For example, the distribution of axons into elongated groups located within the collagen bands was apparent near the periphery of the axonal core, especially towards the distal end of the regeneration cable (Figure 3.3 H and inset).

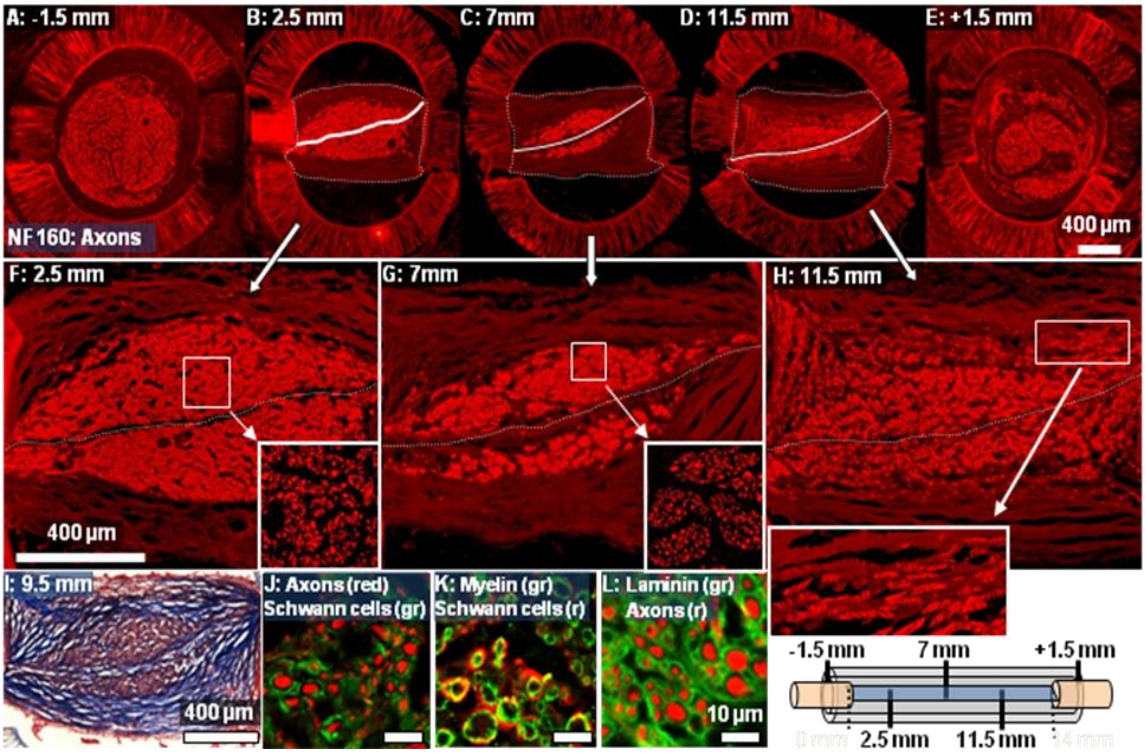

Figure 3.3: Cross-sections taken at increasing distances into a representative 1-film channel.

The scaffold was implanted at the 13 week time point and sectioned at the locations shown in the diagram at bottom right corner. (A-E): The brightly fluorescent core of $NF160^{+}$ axons is consolidated around the single aligned thin-film (marked by a solid white line.) This axonal core was surrounded by bands of collagenous tissue forming the regeneration cable periphery. (These bands are more dimly visible, and their outer border is marked with a dotted line.) (F-H): Magnified images of the regeneration cables shown in (B-D). Axons towards the proximal end of the channel were densely grouped into a consolidated core (F). Near the channel midpoint, axons were aggregated into isolated groups (G). Past the midpoint, axons were dispersed across a wider area and distributed in patterns correlated with the locations of the aligned collagen tissue bands (H and inset.) (I): These collagen bands were aligned in formations oriented in parallel to the surface of the aligned thin-film (Masson's Trichrome stain). Sections were reacted for immunofluorescent demonstration of (J): axons and Schwann cells (S100), (K): Schwann cells and Myelin (P0), and (L): axons and Laminin-1.

1-film guidance channel cross-sections were also reacted for immunofluorescent demonstration of fibroblasts (anti-vimentin antibody). Outside the regeneration cable, the densest regions of vimentin immunoreactivity were observed surrounding the outer wall of the channels and within the porous channel walls (Figure 3.4). Within the regeneration cable, $vimentin^{+}$ fibroblasts were concentrated within the collagenous periphery, and were aligned circumferentially within the collagen tissue bands, as described by others

[69] (Figure 3.4 C). Significantly, the axonal/Schwann cell core and the surrounding fibroblast-rich bands of collagenous tissue were well segregated into distinct regions with a defined border, (Figure 3.4 B,C) and only a sparse distribution of vimentin^{+} fibroblasts was observed within the axonal/Schwann cell core.

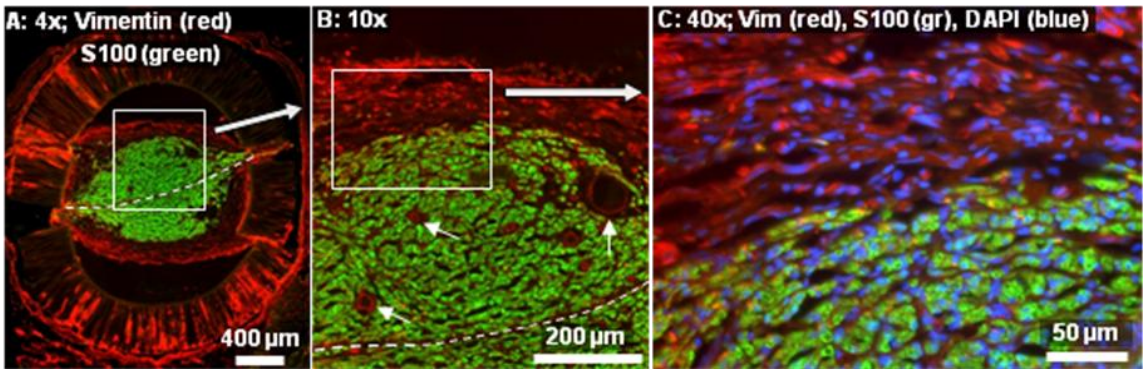

Figure 3.4: Cross-section from the same representative 1-film channel as in the previous figure.

This section was taken 1.5 mm into the nerve gap and processed for immunofluorescent demonstration of fibroblasts (vimentin: red) and Schwann cells (S100: green). (A): Vimentin^{+} fibroblasts were visible within the bands of collagenous tissue surrounding the axonal/Schwann cell core, particularly in the outer periphery. (B): Magnified view of the boxed region in (A). The axonal core is segregated from the surrounding fibroblast-rich collagenous tissue. Several example blood vessels are marked by small arrows. (C): Magnified view of the boxed region in (B). Fibroblasts were located mainly outside of the Schwann cell / axonal core and were aligned within the epineurial-like bands of collagenous tissue.

3.4.2.3 3-film channels, 13 week time point

Patterns of regeneration in the 3-film, 13 week channels differed characteristically from those observed in their 1-film counterparts. In 3-film channel cross-sections (Figure 3.5), the regeneration cables were compartmentalized by the thin-films into four distinct zones of differing cellular organization. For example, near the proximal end of this representative channel (Figure 3.5 B, F), an area of densely grouped axons was visible in the zone below the bottom thin-film (marked with a "4"), while few axons were located in the zone above the topmost thin-film (marked with a "1"). The inner zones of the 3-

film channels, (marked “2” and “3” in Figure 3.5 F), contained a more sparse and irregular distribution of axons. As in the 1-film channels, axons in all zones were aggregated into grouped formations towards the channel midpoint (Figure 3.5 C, G and inset), and at further distances in the channel were dispersed more sparsely in elongated distributions that correlated with the structure of the banded collagenous tissue (Figure 3.5 D, H and inset). Confocal microscopy was used to visualize axon / Schwann cell co-localization, myelination of axons, and laminin deposition around axons (Figure 3.5 J-L).

The collagen tissue bands in the 3-film channels were distinct not only on the periphery, but also within the interior regions of the regeneration cable (Figure 3.2 B, Figure 3.5 F-I). In the outer zones, the collagen bands had a predominantly linear / circumferential alignment as in the 1-film channels, but in the inner zones (between the outer two thin-films) alignment patterns were irregular. Rather than being arranged concentrically or in parallel, the collagen bands in these interior zones were formed into a branching structure with irregular alignment patterns that were visibly constrained by the thin-films.

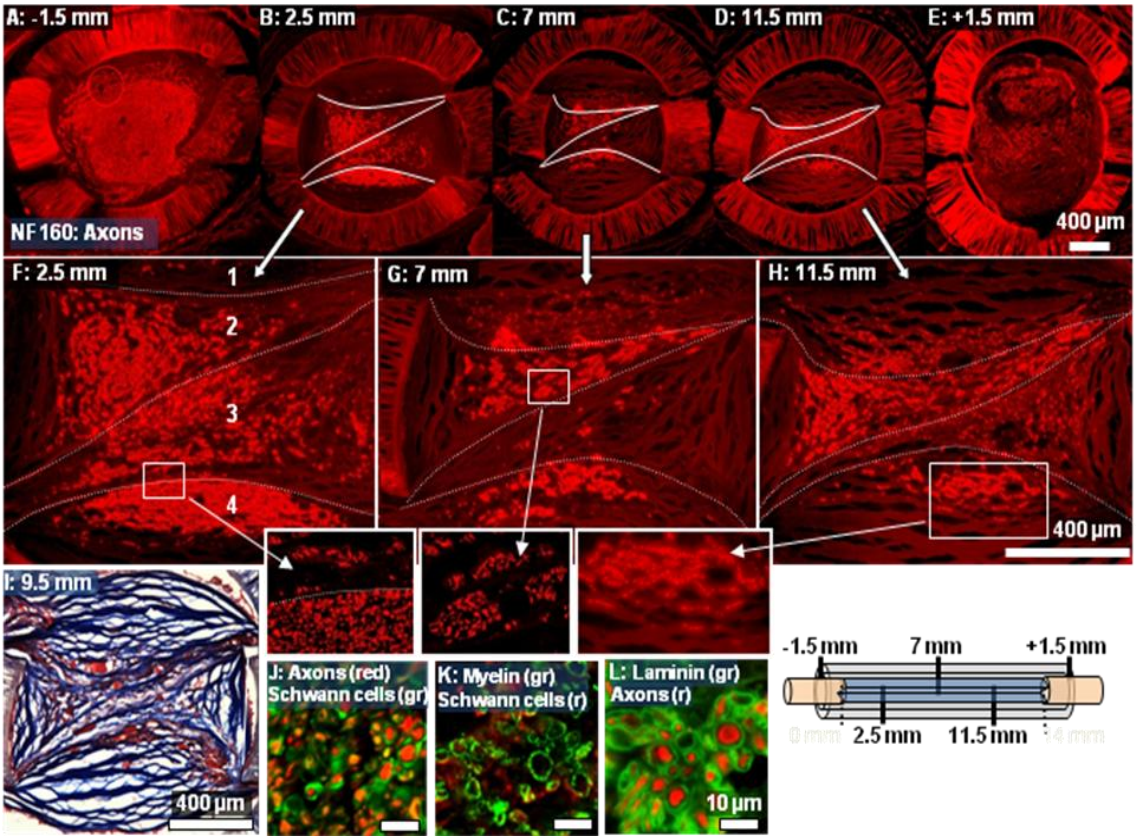

Figure 3.5: Cross-sections taken at increasing distances into a representative 3-film channel.

The scaffold was implanted at the 13 week time point and sectioned at the locations shown in the diagram at bottom right corner. (A-E): The axonal core (NF160) was fragmented asymmetrically around the thin-films, whose approximate location is marked with white lines. (F-H): Magnified images of (B-D). (F): The three thin-films compartmentalized the channel into four zones (labeled "1"-"4".) Axons in the lower outer zone (labeled "4") were densely grouped, but within the interior compartments ("2" and "3"), axons were more sparsely distributed. Little regeneration was observed in the top compartment, ("1"). (G): Axons showed a tendency to aggregate in tight groups near the channel mid-point. (H and inset): Axons were more dispersed past the channel midpoint and were distributed according to the structure of the collagenous bands. (I): In the interior zones of the channel, the alignment of the collagenous banded structure was disrupted (Masson's Trichrome stain). Sections were reacted for immunofluorescent demonstration of (J): axons and Schwann cells (S100), (K): Schwann cells and Myelin (P0), and (L): axons and Laminin-1.

Vimentin^{+} fibroblasts were again observed surrounding the outer wall of the guidance channel, within the channel walls, and within the collagenous outer periphery of the regeneration cable (Figure 3.6). However, the strict segregation of fibroblasts and Schwann cells noted in the 1-film channels was disrupted in the interior of the 3-film channels (Figure 3.6 B,C). In this representative channel, in the outer zone below the

lowest aligned thin-film, was a dense group of co-localized Schwann cells and axons, well segregated from the fibroblasts in the periphery of the regeneration cable (Figure 3.6 A, B). In contrast, within the inner zones, the distribution of Schwann cells / axons was sparse and irregular (Figure 3.6 B) and was intermingled with groups of unaligned fibroblasts (Figure 3.6 C).

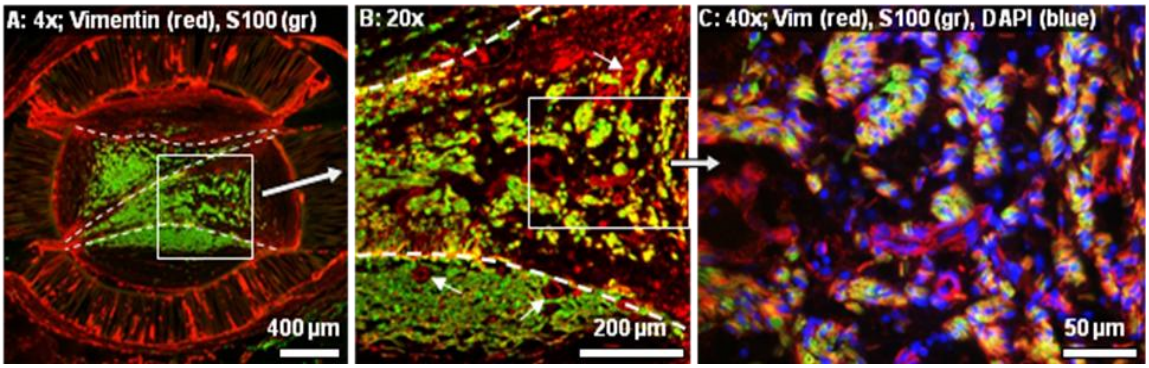

Figure 3.6: Cross-section from the same representative 1-film channel as in the previous figure.

This section was taken 1.5 mm into the nerve gap and processed for immunofluorescent demonstration of fibroblasts (vimentin: red) and Schwann cells (S100: green). (A): Vimentin$^+$ fibroblasts were visible in the outer bands of collagenous tissue. (B): Magnified view of the boxed region in (A). In the outer zone below the lower thin-film was a dense and consolidated portion of the axonal core. (Example blood vessels are indicated with small arrows). In the interior zone above this lower thin-film, the Schwann cells/axonal distribution was sparse, irregular, and intermixed with vimentin$^+$ fibroblasts. (C): Magnified view of the boxed region in (B). Schwann cells and randomly aligned fibroblasts intermingled within the interior compartments of the regeneration cable.

3.4.2.4 Quantitative comparisons of regeneration cable size and number of regenerated axons at 13 weeks.

The cross-sectional areas of all regeneration cables at the 13 week time point were quantified at three distances into the channels (Figure 3.7 A). The regeneration cables in the 3-film channels were found to be significantly larger at each of these distances. At the channel midpoint, for example, the regeneration cables of the 3-film channels were found

to be 1.35 times larger than the regeneration cables in the 1-film channels ($p<0.05$). In neither channel type did the size of the regeneration cable vary significantly based on distance into the channel.

Axons were regenerated through the full length all 1-film and 3-film channels in the 13 week groups. Despite the fact that the 3-film channels contained larger regeneration cables, the 1-film channels contained significantly higher numbers of $NF160^+$ regenerated axons (Figure 3.7 B, $p<0.01$). Compared to the 3-film channels, the 1-film channels contained on average 1.63 times the number of regenerated axon profiles, as measured from the channel midpoints (4383 ± 442 $NF160^+$ axons compared to 2691 ± 338 axons).

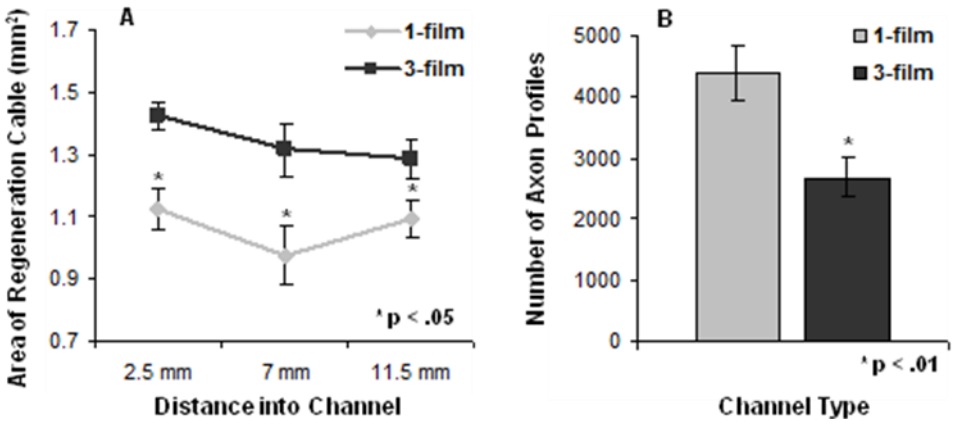

Figure 3.7: Quantitative comparison of regeneration cables in each channel type.

(A): Cross-sectional areas of the regeneration cables (including the collagenous tissue periphery) were quantified at three distances into each channel. The regeneration cables in the 3-film channels were significantly larger at each distance as compared to the 1-film channels. There were no significant differences in regeneration cable sizes between the different distances into the channels. (B): Axon profiles were quantified at the midpoint of each channel at the 13 week time point. Despite containing smaller regeneration cables, the 1-film channels supported significantly higher counts of regenerating axon profiles. (Error bars represent s.e.m.)

3.4.2.5 Six week time point

The six week time point was used to examine regeneration cable morphology at an earlier stage of development. By six weeks, substantial axonal regeneration had occurred through the full lengths of all 1-film channels, and through all but one of the 3-film channels. In both guidance channel types, general patterns of regeneration cable morphology were similar between the 6 and 13 week time points.

For example, characteristic differences in cellular organization between the inner and outer zones of the 3-film channels were apparent in the 6 week group (Figure 3.8). As at the 13 week time point, the outer zones contained a compact distribution of co-localized axons and Schwann cells, lying adjacent to aligned collagen bands containing aligned fibroblasts (Figure 3.8 B,C). The inner zones contained splintered groups of

axons and Schwann cells that intermingled with randomly aligned fibroblasts (Figure 3.8 B,D).

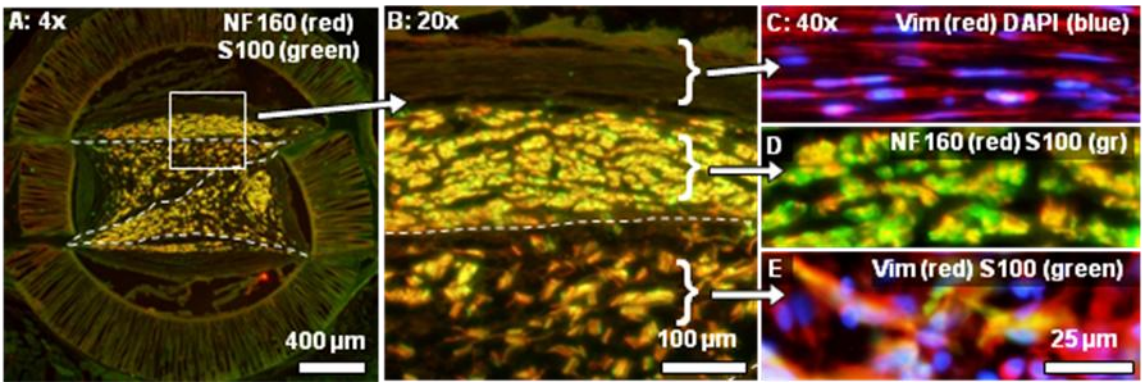

Figure 3.8: Cross-sections taken near the proximal end of a representative 3-film channel at 6 weeks.

These sections illustrate similarities in regeneration cable morphology between the 6 and 13 week time points. (A): Axons (NF160: red) and Schwann cells (S100: green) were co-localized and distributed within the compartments of the 3-film channels, as in the 13 week channels. (B): Magnified view of the boxed region in (A). Patterns of cellular organization in the inner and outer zones differed characteristically. (C): Fibroblasts (vimentin: red) in the epineurial-like collagenous bands were highly aligned and well segregated from underlying groups of axons/Schwann cells (D). (E): Within the interior compartments of the 3-film channel, randomly aligned fibroblasts intermingled with Schwann cells/axons.

Although the basic regeneration cable structure was in place by the 6 week time point, regeneration in both channel types was clearly less developed than at 13 weeks. For example, the areas occupied by axonal growth were comparatively smaller and less developed, especially towards the distal ends of the 6 week channels (Figure 3.9 A). Also, while $NF160^{+}$ axons were never observed apart from Schwann cells at either time point, there existed distal portions of the 6 week regeneration cables occupied by Schwann cells alone (Figure 3.9 B). The distribution of axons into elongated groups that followed the banded structure of the collagenous tissue was also more prominent at the six week time point (Figure 3.9 C). Aligned bands of collagenous tissue were visible not

only on the periphery, but also within the interior of the regeneration cables of the 1-film channels (data not shown).

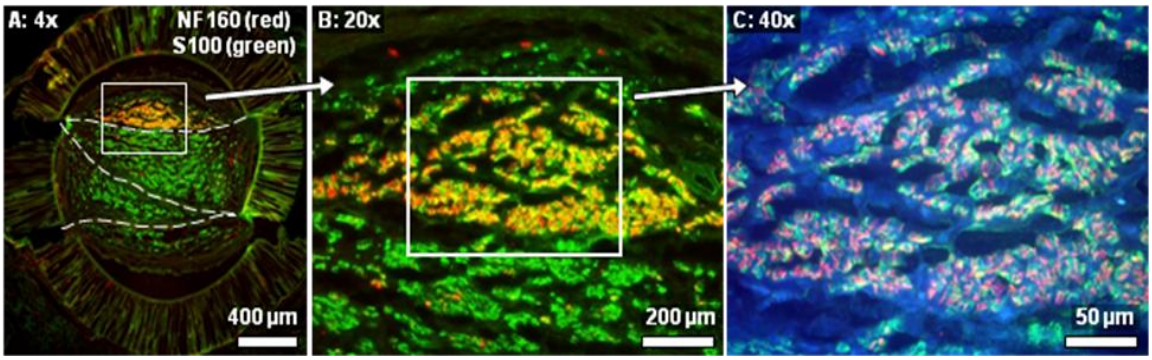

Figure 3.9: Cross-section taken near the distal end of a representative 3-film channel at six weeks.

(A): Migrated Schwann cells (S100: green) were distributed throughout the channel, but regenerated axons (NF160: red) were present mainly in the top outer zone of the channel. In the more mature regeneration cables at the 13 week time point, Schwann cells and axons were fully co-localized throughout the channel. (B): Magnified view of the boxed region in (A), showing the distribution of axons and Schwann cells. C): Further magnification of the boxed region in B). Schwann cell / axon localization within the collagenous bands was prominent. (The collagenous tissue is emphasized in blue).

3.4.2.6 Longitudinal sections of explanted channels

One channel of each type was sectioned longitudinally at the six week time point and also at two weeks post-surgery to give a perspective of nerve morphology along the axis of regeneration. In sections from the 3-film channel at the six week time point, patterns of longitudinal alignment differed between the zones (Figure 3.10). In the top outer zone, above the outermost thin-film (marked with a dashed line), axons, co-localized Schwann cells, and overlying collagenous tissue bands were all longitudinally aligned through the channel length (Figure 3.10 B, above the white dashed line). Within the inner zone on the opposite side of the same thin-film, axons/Schwann cells

intermingled with misaligned fibroblasts, and longitudinal alignment patterns were disrupted (Figure 3.10 C).

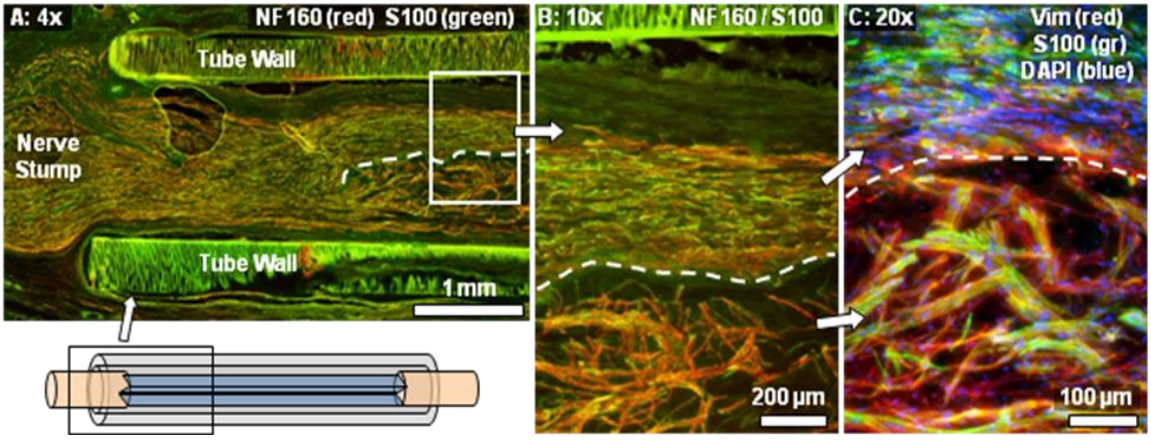

Figure 3.10: Longitudinal section from a 3-film channel at the six week time point.

(A): Axons (NF160: red) and co-localized Schwann cells (S100: green) were regenerated into the different zones of the channel. The top outer thin-film is marked with a dashed line, and a diagram in the lower left corner illustrates the approximate location within the channel of the image. (B): Magnified view of the boxed region in (A). Regenerated axons and Schwann cells in the top outer zone (above the labeled thin-film) were longitudinally aligned, growing in a core that made direct contact with the aligned thin-film. Overlying peripheral bands of collagenous tissue were longitudinally aligned as well. In the interior zones underneath the top outer thin-film, regenerating axons and co-localized Schwann cells displayed disrupted patterns of longitudinal alignment. (C): Vimentin+ fibroblasts were randomly aligned in the inner zones.

One guidance channel of each type was also sectioned longitudinally two weeks post-implantation (Figure 3.11). In both guidance channel types, axons (and co-localized Schwann cells) had migrated approximately 1/3 of the way through the length of the channels (Figure 3.11 A-C), and Schwann cells migrating from the distal end had covered a similar distance. Fibroblasts had migrated through the entire length of both channels by the 2 week time point.

The effects of compartmentalization within the 3-film channel were evident, as some of the zones were preferentially populated with axons and non-neuronal cells as compared to others. For example, axons had regenerated asymmetrically into the topmost

outer zone, perhaps influenced in this case by the off-center location of the proximal nerve stump. Migrated fibroblasts preferentially populated the lower two zones of the 3-film channel (Figure 3.11 D), and the cell density and degree of alignment differed within each of these adjacent zones. Highly aligned Schwann cells trailed the fibroblasts and had migrated directly on the thin-films, as well as some distance away from the films, both on top of each other and through the developing regeneration cable framework (Figure 3.11 E).

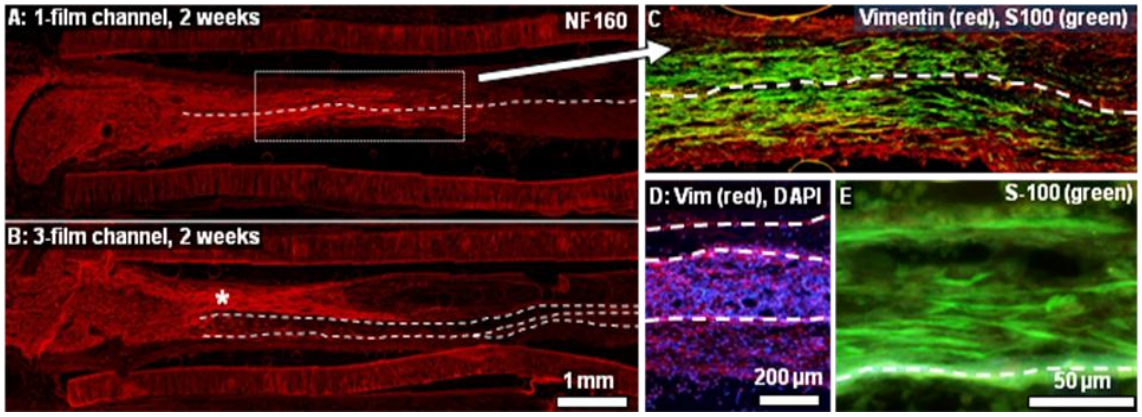

Figure 3.11: Longitudinal sections from a 1-film (A,C) and 3-film channel (B,D,E), at two weeks.

(A,B): NF160+ axons had regenerated approximately one third of the distance through each channel type. Asymmetric growth of the regenerating axons into the topmost zone of this 3-film channel ('*' symbol) might have been due in part to the off-center location of the proximal nerve stump. Regeneration in the 1-film channel (A,C) was symmetrically distributed around the single thin film, although this was not always the case. (C): Magnified view of the boxed region in (A). Fibroblasts had fully bridged the gap. (D): Image from near the midpoint of the 3-film channels. Fibroblasts had fully bridged the gap and were distributed asymmetrically between the different zones of the 3-film channel (image taken near channel midpoint.) (E): Cross-section taken towards the distal end of the 3-film channel. Schwann cells, seen here migrating from the distal end, were highly aligned along the aligned thin-films, growing in direct contact with the thin-films, on top of each other, and also through the tissue matrix of the developing regeneration cable.

3.4.3 Electrophysiological assessment of nerve regeneration

3.4.3.1 Nerve Conduction Velocity (NCV)

All 13 week time point animals from the 1-film and 3-film groups underwent electrophysiological testing at their end points. Nerve conduction velocities (NCV) across the regenerated nerves were determined by evoking compound nerve action potentials and dividing inter-electrode distance by conduction latency. A significantly higher average NCV was measured in nerves regenerated through 1-film channels as compared to nerves regenerated through the 3-film channels (20.55 ± 1.5 m/s vs. 15.86 ± 1.5 m/s, $p<0.05$) (Figure 3.12 A).

3.4.3.2 EMG signal measurements

In all animals from the 13 week time point, EMG activity was elicited by upstream stimulation of the regenerated nerve and recorded from the lateral gastrocnemius muscle (LG), which is normally innervated by the tibial nerve. In all regenerated animals, LG contracted visibly in response to tibial nerve stimulation produced a clearly distinguishable EMG signal (Figure 3.12 B). In contrast, the tibialis anterior (TA) muscle, normally innervated by the common peroneal nerve branch, exhibited no visible contractions in response to tibial nerve stimulation and produced no measurable EMG signal. At the end of the procedure, when the regenerated tibial nerve was crushed distal to the stimulating electrode, visible contractions and measurable EMG singles from LG disappeared in all cases. Thus, we conclude that the observed muscle contractions were indeed due to reinnervation by the regenerated tibial nerve.

3.4.3.3 Motor endplate reinnervation

As another assessment of muscle reinnervation by the regenerated tibial nerve, gastrocnemius muscles from the 13 week groups were longitudinally sectioned and reacted for immunofluorescent demonstration of axons, motor endplates, and synaptic vesicles (Figure 3.12 C-E). All muscle sections contained visible motor endplates, with a percentage of these endplates co-localized with synaptic vesicles and regenerated axons. These results indicate reinnervation in all animals from the 13 week group. The presence of synaptic vesicle proteins further suggests that the observed reinnervation was functional, agreeing with the results of EMG testing.

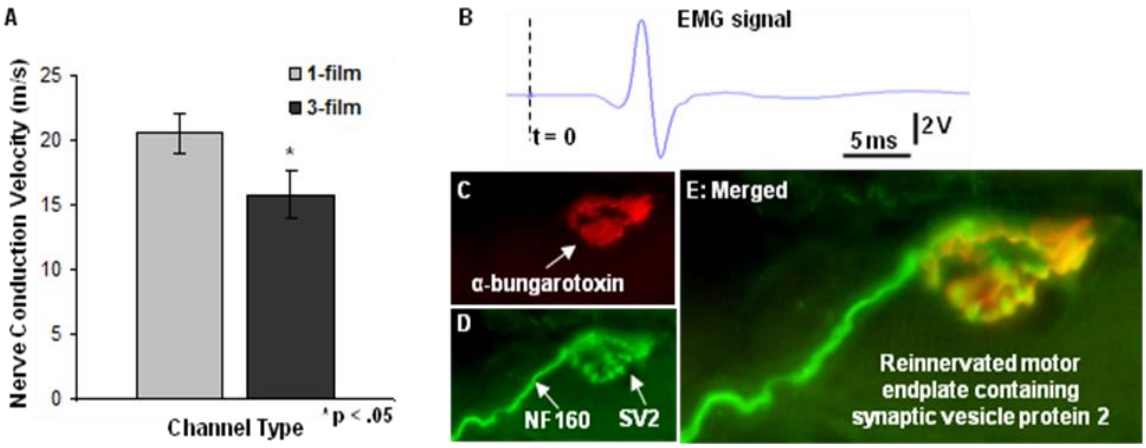

Figure 3.12: Evaluation of nerve conduction velocity and muscular reinnervation.

(A): Significantly higher compound action potential conduction velocities were measured from nerves regenerated through the 1-film channels. (B): All gastrocnemius muscles produced measurable EMG signals and visible contractions. (This representative trace was taken from a 3-film channel case.) (C-E): As a further evaluation of muscular reinnervation, sectioned gastrocnemius muscles were reacted for immunofluorescent demonstration of (C) motor endplates, (D) axons, and vesicles containing synaptic vesicles 2 (SV2) protein. (E) Co-localization of these three markers confirmed the presence of reinnervated motor endplates in all treated animals.

3.5 DISCUSSION

A critical first step in the sequence of endogenous nerve repair across a gap is the proper formation of an aligned, regenerative fibrin matrix/cable between the nerve stumps. The fibrin matrix provides physical support to the initial influx of migrating fibroblasts and Schwann cells, and the fine topographic structure of the matrix furthermore determines the distribution and alignment of these cells [52, 53]. The regenerating cells in turn form the framework of the regeneration cable, replacing the fibrin matrix with a more permanent network of ECM proteins, including collagens and laminins [30, 53, 70-73]. The initial formation of the fibrin cable thus predetermines at an early time the final morphology of the regenerating nerve [71, 74].

In similar fashion, scaffolding materials presented within a guidance channel can also impact early cellular migration and alignment to influence formative stages of endogenous nerve repair mechanisms. Internal scaffolding may act by a combination of (1) bolstering the fibrin matrix, by contributing to its proper formation and maintenance, and (2) replacing the function of the matrix, by serving as an alternative aligned substrate for glial and neuronal migration [58, 59]. In either case, the proper distribution of appropriately structured scaffolding material is critical in directing the ultimate migration and alignment of regenerating cells. Disorganized topographic guidance cues – provided directly by scaffolding substrate or indirectly by a malformed fibrin matrix – can disrupt regeneration [19, 70, 75].

With these issues in mind, we investigated how minimal amounts of precisely distributed PAN-MA thin-films, presenting topographic cues, might promote and influence regeneration cable formation and nerve regeneration, thus enhancing the

function of nerve guidance channels. We bridged critical sized nerve gaps with guidance channels containing one or three aligned thin-films, and in all 18 animals evaluated at the 13 week time point, we observed axonal regeneration and functional reinnervation of muscle. Functional reinnervation was evidenced by evoked muscle twitches and EMG recordings, and was further suggested by immunohistochemical analysis of reinnervated motor end plates. While EMG signals from reinnervated LG were measurable in all animals from each group, we observed variability in EMG signal shape and amplitude based on the precise orientation of the recording electrode on the muscle. Due to this uncontrollable variability, we used EMG measurements to qualitatively detect successful regeneration but not to quantitatively assess and compare functional recovery between the two groups. In future studies, analysis of muscle force generation in response to nerve stimulation might represent a more ideal measure of functional recovery.

The ability of the thin-film enhanced guidance channels to promote nerve regeneration across critical sized gaps was significant, given the small amounts of scaffolding material used within the guidance channels. Each thin-film occupied only 0.6% of the guidance channel's open space. (Elsewhere this measurement is termed the "packing density [59]," or, conversely, the "void fraction [76]."") The packing density of our 3-film, and especially our 1-film channels, was substantially lower than in other guidance channels containing internal scaffolding described in the literature [59, 75-78].

While both the 1-film and 3-film guidance channels supported regeneration across the nerve gap, regeneration through the 1-film channels was superior in terms of morphological and functional measures. Although NCV values of neither experimental group was large enough in comparison to intact rat nerve to indicate complete

regeneration at this 13 week time point, these measurements demonstrate a more complete stage of regeneration in the animals treated with the 1-film channels.

The sequence of regeneration through the 1-film channels was characteristically shaped by the presence of the single aligned thin-film. Two weeks after channel implantation, a cellular matrix including aligned Schwann cells and regenerating axons had bridged the nerve gap and was centralized around the thin-film. By the six week time point, the bulk of the developing regeneration cable's framework consisted of an orderly collagenous tissue structure, arranged into aligned bands that were shaped around the thin-film.

This aligned banded configuration of collagen tissue potentially shaped the sequence of development observed in the 1-film channels. By the 13 week time point, elongated groupings of axons/Schwann cells within prominent bands of aligned collagen tissue were visible only within cross-sections taken towards the less mature distal ends of the channels (Figure 3.3 H and inset). These observations suggest a possible sequence of nerve maturation in which bands of axons and Schwann cells growing within the aligned bands of tissue matrix gradually merge and compact to form a more uniform and consolidated core. In this scenario, the orderly compaction of the collagen bands would be made possible by their parallel aligned structure, which formed around the single aligned thin-film early in the regeneration process. The eventual structure of the nerves regenerated through the 1-film channels consisted of a consolidated axonal core, segregated from a surrounding periphery of fibroblast-rich bands of epineurial-like tissue.

These outcomes differ from earlier reports describing regeneration across shorter gaps through guidance channels that were similarly bisected, but with thicker substrate

dividers of smooth or rough (but not aligned) topographies [75, 79]. These reports describe the formation of two discrete regenerated nerve cables on either side of the non-aligned divider, with each cable surrounded with an epineurial-like periphery. The aligned topography of our thin-films likely played a role in causing the differences we observed, by contributing to the proper formation of the initial regeneration cable and the directed migration and alignment of regenerative cells. Another possible contributing factor was the comparatively higher permeability and molecular weight cutoff of our PAN-MA thin-films (at least as high as 70 KDa in unpublished experiments). Biochemical factors able to pass through the permeable thin-film might have influenced cells on the opposite side, helping to consolidate the nerve cables.

In contrast to the 1-film case, regeneration cables in the 3-film channels were characterized by disrupted patterns of cellular distribution and alignment, and contained a fragmented core of fewer overall axons. Because all other design features of the two guidance channel types were identical, we conclude that the differences in regeneration stemmed from the inclusion of the two additional thin-films, which likely affected endogenous regenerative processes by a combination of mechanisms.

One effect of the additional thin-films was to compartmentalize the guidance channel into four zones. Regenerating axons and cells migrating from the nerve stumps often traveled preferentially into one or more of these zones, possibly due in part to the relative location of the sutured nerve stumps (Figure 3.11 B). The resulting asymmetric distribution of regeneration between the zones potentially affected regeneration adversely in at least two ways. First, constraining regeneration to a subset of the guidance channel decreases the open space available for continued growth and maturation. Secondly, as we

observed at the earlier six week time point, the zones that receiving the most regeneration from the proximal end were not necessarily the same zones receiving the most regeneration from the distal end. This mismatch in symmetry is undesirable because if non-neuronal cells and axons traveling from the proximal and distal ends do not unite at the midpoint of a given zone, initial cellular bridging fails, potentially disrupting subsequent regeneration in that zone. Indeed in the 3-film 13 week case, we observed that axon populations within a given zone sometimes began high on the proximal end and then often tapered off sharply before reaching the channel midpoint - potentially due to failed initial cellular bridge formation within that zone. Although the 1-film channels were similarly divided into two zones, the observed degree of asymmetry in regeneration between these two zones was far less than in the 3-film channels. This is possibly due to the fact that, with each compartment comprising half of the channel's cross-sectional area, the possibility of regeneration from either nerve stump significantly missing either zone was reduced.

Another potential cause for disrupted regeneration through the 3-film channels was the rearranged distribution of topographical cues caused by the additional two thin-films. Of the four zones delineated by the thin-films, the two semi-circular outer zones, (labeled "1" and "4" in Figure 3.5 F), were bordered by the smooth wall of the guidance channel on the outer side, and by an aligned thin-film on their interior side. This arrangement of border topography is similar to each of the two zones of the 1-film channel. Indeed, the patterns of regeneration in the outer two zones of the 3-film channels were typically comparable to those in the 1-film case in terms of cellular distribution, alignment, and segregation. In contrast, the two triangular "inner" zones of the 3-film

channels, (labeled “2” and “3” in Figure 3.5 F), were bordered on their two long sides by the aligned thin-films, with only the third, shorter border formed by the smooth channel wall. Within the inner compartments, misaligned fibroblasts intermingled with sparse distributions of poorly aligned axons and Schwann cells, and the organization of the aligned collagen bands was also disrupted. The rearranged border topography within these inner zones potentially affected regeneration by altering the initial polymerization of aligned fibrin strands [75]. An altered initial fibrin matrix would then interfere with Schwann cell and fibroblast distribution and alignment, possibly disrupting the natural sequence leading to their segregation. Additionally, the resulting irregularly branched structure of the regeneration cable’s collagenous framework in the inner zones potentially interfered with normal maturation processes leading to a consolidated axonal core.

While the arrangement of three thin-films into a ‘Z’ formation represents one of many possible configurations for a multiple thin-film channel, results from the 3-film channels can be extended to guidance scaffold design in general. Increased amounts of scaffolding material, even with negligible change in packing density, do not necessarily translate into enhanced regeneration. Compartmentalization of the guidance channel interior and altered distributions of topographic cues are examples of factors that can impact endogenous repair processes from an early time point and significantly impact regenerative outcomes.

3.6 CONCLUSIONS

In this study, nerve guidance channels enhanced with aligned thin-films presented within their lumen were designed to modulate endogenous repair processes and enhance regeneration across critically sized peripheral nerve gaps. These thin-film enhanced

guidance channels contained minimal internal scaffolding, and yet promoted robust levels of axonal regeneration, without the aid of any exogenous ECM or trophic factors. When comparing regeneration through guidance channels containing one or three thin-films, significantly greater regeneration was observed in the 1-film channels. Furthermore, regenerated nerve cables through the 1-film channels were structurally more akin to normal nerve in terms of patterns of cellular distribution and alignment. These results highlight the potential influence of internal scaffolding on the endogenous repair sequence. By providing minimal, yet appropriate topographic cues, a guidance channel's ability to bridge critically sized nerve defects may be significantly enhanced.

3.7 ACKNOWLEDGMENTS

The authors would like to acknowledge support from the following grants: NIH R01 44409, NSF GTEC EEC-9731643, NSF CBET 0651716, and NSF IGERT-0221600. We would also like to thank He Zheng and Alex Stroh for their assistance with microscopy and quantification techniques, Dr. Brani Vidakovic for his assistance with statistical methods, and Dr. Laura O'Farrell, for her assistance with animal care.

CHAPTER 4

REGENERATIVE SCAFFOLD ELECTRODES FOR PERIPHERAL NERVE INTERFACING

(This chapter is has been submitted for publication to the Journal of Neural Engineering)

4.1 ABSTRACT

Advances in neural interfacing technology are required to enable natural, thought-driven control of prosthetic limbs. In traditional "regenerative electrode" approaches to peripheral nerve interfacing, an array of microelectrodes is positioned in the path of axons regenerating from a transected nerve. Here, we describe an augmented regenerative electrode design in which aligned scaffolding materials are incorporated to influence regeneration and guide axonal growth to within close proximity of an integrated microelectrode array.

Thin-film electrode arrays on SU-8 substrates were custom fabricated and embedded within thin-film sheets of aligned polyacrylonitrile-methacrylate (PAN-MA) nanofibers, such that regenerating axons might be topographically guided along the direction of nanofiber alignment and directly across the embedded electrodes. *In vitro* cell culture experiments were used to explore design parameters and to characterize cellular migration and neurite extension across the nanofiber / electrode array boundary. "Regenerative scaffold electrodes" (RSEs) were subsequently fabricated and implanted across rat tibial nerve gaps to evaluate device recording capabilities and influence on nerve regeneration. In twenty of these animals, regeneration was compared between a nerve gap repair model and a simulated amputation model in which the distal nerve was

replaced with an isolated fragment of nerve. In both groups, characteristic influence over regenerated nerve morphology was observed and counts of regenerated axon profiles were similar at an eight week time point (7077 ± 546 vs. 7945 ± 1144). Chronically implanted RSEs were successfully used to record evoked neural activity after as long as twenty-two weeks. These results demonstrate that the incorporation of scaffolding-based topographic cues within a regenerative electrode can provide influence over the course of nerve regeneration, to the potential benefit of a peripheral nerve interface suitable for limb amputees.

4.2 INTRODUCTION

An estimated one out of every two hundred people living in the United States has suffered the loss of a limb, and this rate is projected to double over the next few decades [1]. Sophisticated prosthetic limbs with advanced features such as computerized controllers and lifelike joints have been developed in response, but neuroprosthetic devices are limited by current neural interfacing technology. Providing an amputee with natural, thought-driven control of a prosthetic limb will depend on improved capabilities to interface with the nervous system for extracting motor commands and providing sensory feedback.

Peripheral nerve tissue provides an ideal neural interfacing site for prosthetic limb control. An amputated peripheral nerve contains all of the motor and sensory pathways associated with the lost limb, and these pathways retain significant function after injury[40]. As opposed to other candidate sites, such as the motor and sensory cortex of the brain, accessing amputated peripheral nerves is relatively non-invasive as they are not encased in the cranium or vertebral columns. Furthermore, a peripheral nerve interface

takes advantage of the remaining information processing neural circuitry left intact after amputation. “Raw” motor signals originating in the cortex are refined by descending pathways of the brain and spinal cord as they travel to the peripheral nerve. Likewise, afferent feedback applied at the level of the peripheral nerve are correctly routed and processed by intact ascending pathways [80-82].

Another useful property of an amputated peripheral nerve is its ability to regenerate, affording the opportunity to engineer nerve growth into an interfacing device. The term “regenerative electrode” refers to a peripheral nerve interface design in which an array of electrodes is incorporated within a nerve guidance channel, such that a regenerating nerve grows through the channel and within recording/stimulation range of the electrodes. Traditional sieve type regenerative electrodes consist of a nerve guidance channel containing a thin disk, perforated with small diameter electrode “vias” for axons to grow through [43, 83-87]. The ability of sieve electrodes to stimulate and record neural activity from regenerated axons has been established, but drawbacks, such as the barrier posed by the electrode array to regeneration, have driven the recent development of alternative designs [46-48]. Guidance channel structure and electrode geometries vary widely between these designs, but each seeks to minimize barriers to regeneration and produce stable, high channel count microelectrode / axon interfacing that is more sensitive to biological signals and more robust to noise.

A common feature of all regenerative electrodes is that they take advantage of the inherent plasticity of regenerating nerve morphology, allowing the developing nerve to conform to the intraluminal device structure. However, existing designs typically influence regeneration in a passive manner. An augmented design such as we describe

here might use tissue engineering-based principles to exert more control over the regenerating nerve structure. For example, topographic cues are physical features of the appropriate geometry and size to influence cellular alignment, growth, migration, and behavior [20, 54-56]. Significantly, the incorporation of topographically patterned scaffolding within a guidance channel has been shown to influence formative stages of nerve regeneration, thereby directing nerve growth [14, 19, 57-59].

In this study, we explore the use of scaffold-based topographic cues to shape regenerating nerve structure and guide axonal growth to within close proximity of interfacing electrodes. The design of our device is based on a nerve guidance scaffold previously demonstrated by our lab to support and guide nerve regeneration across extended injury gaps [49]. These guidance scaffolds contain a single aligned sheet of electrospun polymer nanofibers and have been shown to influence regenerating nerve morphology and guide regeneration across long nerve gaps. Here, we adapt this design and embed thin-film electrode arrays within the nanofiber sheets, for the intended purpose of shaping nerve regeneration around the electrode arrays and guiding axons across individual electrodes. Significantly, this low-profile design minimally obstructs the cross-sectional area available to the regenerating nerve. As opposed to a conventional regenerative electrode, we term this type of design a regenerative scaffold electrode (RSE).

SU-8 based thin-film electrode arrays were custom designed and fabricated at Georgia Tech's Nanotechnology Research Center (NRC). Dorsal root ganglia (DRG) cultures were used to explore design parameters associated with embedding a thin-film array within a sheet of aligned nanofibers. Based upon *in vitro* outcomes, regenerative

scaffold electrodes (RSEs) were constructed and evaluated using a rodent tibial nerve gap model for up to twenty two weeks of regeneration time. Histological testing was used to evaluate the morphology of the regenerated nerves and to observe the proximity of axons/fascicles to the electrode array. Electrophysiological testing was used to evaluate the extent of nerve regeneration as well as the ability of the scaffold to stimulate and record neural signals. Additionally, outcomes in a conventional nerve gap case were compared to outcomes in a simulated amputation model, where the distal nerve stump was replaced with an isolated fragment of nerve [29, 30]. In both test groups, electrophysiological and histological testing were performed after eight weeks of regeneration time.

4.3 MATERIALS AND METHODS

4.3.1 Electrode array design, fabrication, and characterization

Thin-film electrode arrays were designed for integration within sheets of nanofiber scaffolding using L-EDIT CAD design software (Tanner EDA). Variations of the same basic design were laid out on the same wafer, with up to sixteen electrode channels per array. Traces and interconnection pads were designed such that lead wire connections could be established at the outer wall of the device and encapsulated with an insulative and protective coat of epoxy. Minimum traces widths were 10µm, and all electrode arrays included an additional ground pad measuring 50x1000 µm. Both the choice of SU-8 photoresist as the substrate material and the dimensions of the recording electrode sites were modeled after previous work [47]. As in these prior experiments, electrodes were 12 µm by 500 µm, and set within a trench of 10µm depth, included such that limited numbers of axons might grow within the recording zone of any one electrode.

Electrode array fabrication took place at Georgia Tech's Nanotechnology Research Center (NRC) (Figure 4.1). A 4 μm base layer of SU-8 photoresist (SU-8 2005, Microchem) was first spin coated and patterned on an oxidized silicon wafer (Figure 4.1A). A layer of SPR220 photoresist was next spin coated and patterned before the deposition of metal layers (Ti(300 Å)/Au(3000 Å)/Ti(300Å))) using electron beam evaporation (Figure 4.1B-D). Micro-electrodes were then obtained by lifting off the extra deposited metal. After that, a top layer of 10 μm SU-8 was spin coated and patterned (Figure 4.1E-F). Finally, the gold electrodes and bonding pads were opened using a plastherm reactive ion etching process (Figure 4.1G-H). Completed electrodes arrays were later delaminated from the Si wafer surface by soaking in a 45% KOH solution. Electrode impedance magnitudes were evaluated at 1kHz using an impedance testing device (ICM, Neurocraft.)

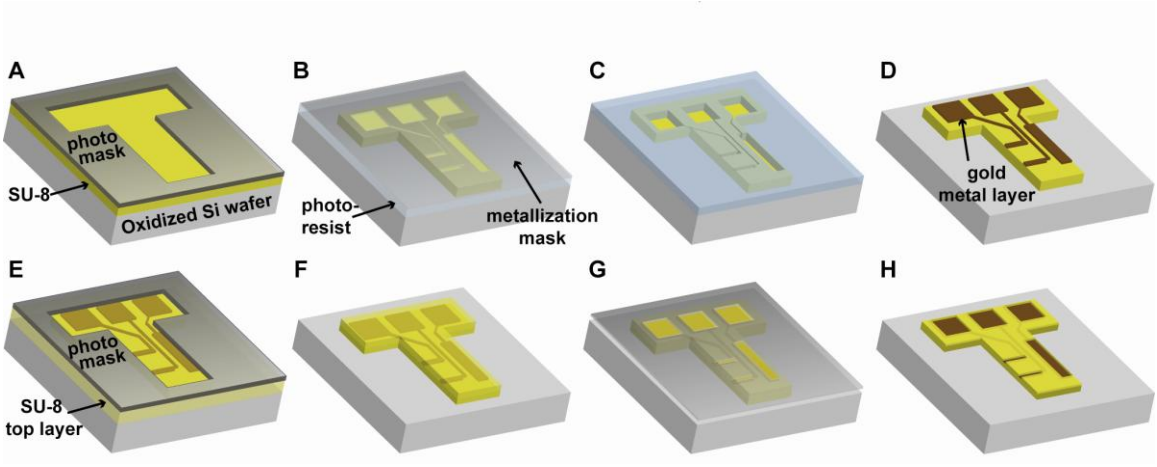

Figure 4.1: Electrode array fabrication steps (simplified schematic).

(A): A base layer of SU-8 is spin coated and patterned with a photomask. (B-D): SPR-220 positive photoresist is spin-coated and patterned with a metallization mask. (C-D): Gold is deposited, and the photoresist layer is dissolved in a lift-off process. (E): The top layer of SU-8 is spin-coated and patterned. (G-H): An RIE process is used to expose the active electrode sites and bond pads.

To evaluate SU-8 biocompatibility, cortical neurons were plated on fabricated electrode arrays. Neurons were derived from embryonic day 18 rats fetuses by isolating the cerebral cortices, which were dissociated using trypsin (0.25%) + 1mM EDTA (10 minutes at 37°C) followed by DNase (0.15 mg/mL). Neurons were plated at a density of 1M cells/2 mL media on SU-8 electrode arrays fixed to the bottom of 35mm culture wells using UV curing adhesive (1187-M-SV01, Dymax). The array surfaces were treated with poly-D-Lysine overnight and thoroughly washed before the time of culturing. The cultures were maintained in a tissue culture incubator for up to two weeks, within Neurobasal medium + B-27 + GlutaMAX (Invitrogen).

4.3.2 Electrospinning of aligned nanofiber scaffolding

An electrospinning process was used to create thin-films of aligned poly(acrylontrile-co-methylacrylate, random copolymer, 4 mole percent methylacrylate)

(PAN-MA) fibers, as in previous studies [19, 49]. Briefly, PAN-MA (Sigma) was dissolved into N, N-Dimethyl Formamide (DMF, Acros Organics) at 60ºC to create a 7% (w/v) PAN-MA solution. This solution was dispensed through a 19 gauge needle for 15 minutes at a flow-rate of 1ml/hr across a voltage field of 6-10kV. The ejected polymer fibers were collected 10 cm away on a 3.8 cm diameter metal drum, rotating at approximately 2500 rpm to produce aligned fiber thin-films of thickness under 10 µm. These thin-films which were baked for 4 hours at 60ºC to remove any residual DMF. Sheets of aligned thin-films were manually cut to size with a razor blade and peeled away with fine forceps for use in *in vitro* and *in vivo* experiments.

4.3.3 *In vitro* validation of electrode / nanofiber integration

Dorsal root ganglia (DRGs) were used to iteratively evaluate and refine techniques used to embed the SU-8 based thin-film electrode arrays within nanofiber sheets. In each round of *in vitro* experimentation, 5-7 culture dishes were prepared, with each dish containing a sheet of aligned nanofibers and several embedded SU-8 electrode arrays. In different dishes, electrode arrays were embedded into the fibers using different distributions of UV curing adhesive. DRGs were seeded on the nanofiber sheet near the nanofiber / electrode array boundary and allowed to grow for a period of fourteen days. Dishes were then prepared and analyzed to characterize cellular migration and neurite extension through the aligned nanofibers, across the nanofiber / electrode array boundary, and across the electrode array (Figure 4.2A).

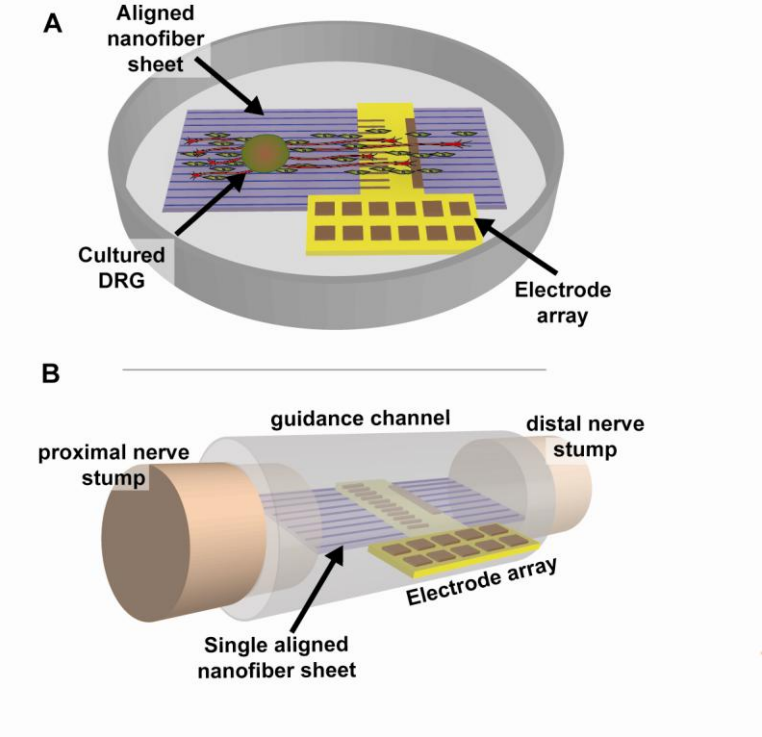

Figure 4.2: Experimental schematics

(A): In order to to test neural growth across a scaffolding material / electrode array boundary, dorsal root ganglia (DRGs) were cultured on aligned nanofiber sheets adjacent to embedded electrode arrays. (B): To create implantable RSE devices, sheets of nanofiber scaffolding along containing embedded electrode arrays were incorporated within nerve guidance channels.

4.3.3.1 Culturing harvested DRGs on nanofibers adjacent to embedded electrodes

Nanofiber sheets were first cut into rectangular strips and affixed at the corners to the bottom of a 35 mm Petri dish (BD Falcon) with UV curing adhesive. The same adhesive was next used to embed an electrode array within the nanofibers. Different proportions of the adhesive were placed in different locations on the electrode. The completed dishes were sterilized by a twenty minute soak in 70% ethanol, followed by three five minute washes in sterile deionized water. After the last wash, the dishes were filled with culture media (DMEM/F12 + 10% FBS) and placed in an incubator until the time of DRG seeding.

DRGs were harvested from P3 rat pups under a microscope. Each DRG was stripped of its nerve roots and stored in L15 hibernate media at 4ºC until the time of seeding. To seed the DRGs, the Petri dishes were removed from the incubator and the media was removed from each dish, leaving a moistened nanofiber surface. Several DRGs were seeded between 1-3 mm from each electrode array. To encourage attachment to the nanofibers, the ganglia were incubated for several hours with only a few drops of culturing medium (DMEM/F12 + 10% fetal bovine serum). Afterwards, the dishes were slowly filled with the culture media, also containing 50 ng/ml nerve growth factor (NGF, Roche Applied Science). Culture media including NGF was replaced every two to three days.

4.3.3.2 Immunohistochemical analysis of cell migration and neurite outgrowth

DRGs were maintained in culture for fourteen days and then fixed for 20 minutes with 4% paraformaldehyde in PBS. To visualize cell migration and neurite outgrowth, the dishes were reacted for immunofluorescent demonstration of markers on axons (anti-NF160/NF200, 1:500 dilution, Sigma-Aldrich) and Schwann cells, (anti-S100, 1:250, Dako). Nuclei were labeled with DAPI (10µM, Invitrogen). The following secondary antibodies were used: Goat anti-rabbit IgG Alexa 488/594 and goat anti-mouse IgG1 Alexa 488/594.

Immunohistochemistry techniques were conducted as in prior studies [19, 49]. Briefly, the fixed DRGs were first incubated for one hour at room temperature in a blocking solution of 4% goat serum (Gibco) in PBS containing 0.5% Triton X-100 (Sigma), followed by an overnight incubation at 4ºC in a mixture of primary antibody and blocking solution. After three washes, the dishes were incubated once more for 1 hour at

room temperature in a solution containing the secondary antibodies, diluted 1:220 in PBS. This incubation was followed by a ten minute incubation in DAPI solution. After three final washes, the dishes were maintained in PBS at 4ºC for evaluation.

4.3.4 Construction of nerve guidance scaffolds embedded with thin-film electrode arrays

A multistep process was used to fabricate the electrode embedded regeneration tubes (Figure 4.2B). Semipermeable polysulfone tubing (Koch Membrane Systems: 1.6mm inner diameter, 2.2mm outer diameter, molecular weight cutoff: 50kDa) was first cut into 7mm long segments. These segments of tubing were cut lengthwise into 2 longitudinal sections, using a custom machined aluminum template. Under a fabrication microscope, a single sheet of aligned PAN-MA fibers was laid down across the length of one of the longitudinal sections, and was secured into place with a medical grade UV light curing adhesive (1187-M-SV01, Dymax). The same adhesive was lightly coated on the bottom surface of an electrode array, and the array was pressed down into the mid-point of the channel, with bonding pads extending from the side of the tube. The top section of polysulfone was fitted and secured into place using the same adhesive. Fine stainless steel wire coated with Teflon (AS-631, Cooner Wire, Inc.) was attached to the bonding pads of the electrodes with conductive silver epoxy (EpoTek H20-S, Epoxy Technology, Inc.). UV curing adhesive was used to insulate the bonding pads and to provide mechanical support and strain relief. The teflon coated wires were attached to gold pins and fixed into a head cap (Plastics One) using gel epoxy (Ace).

The constructs were sterilized by UV light exposure followed by immersion in 70% ethanol for 20 minutes and three ten minute washes in sterilized deionized water. The channels were then stored in sterile PBS until the implantation surgery.

4.3.5 *In vivo* implantation of regenerative scaffold electrodes

4.3.5.1 Experimental groups

After a series of exploratory surgeries used to optimize parameters such as gap length and scaffold construction techniques, regenerative scaffold electrodes were used to bridge tibial nerve gaps in twenty male Lewis strain rats. Regeneration was allowed to proceed for eight weeks, until terminal electrophysiological experimentation and scaffold explantation. The animals were split between two test groups. In ten animals, the distal nerve stump was left intact, allow regenerating axons to travel back to their original innervations sites. Nerve regeneration through scaffolds in this "distal-nerve-intact" case was compared to regeneration in a "distal-nerve-absent" case, designed to model an amputation scenario. In this separate group of ten animals, the distal nerve was resected as far distally as possible, and only an isolated 2-3mm fragment of nerve was attached to the distal end of the scaffold [29, 30]. Regeneration in these "distal-nerve-intact" and "distal-nerve-absent" groups was allowed to proceed for eight weeks until terminal electrophysiological experimentation and scaffold explantation. This time point was chosen based on prior experience to allow for a large degree of nerve regeneration to progress through the scaffolds and to any attached innervation sites. Due to problems in initial implantation groups with headcaps not staying firmly mounted, some of the animals implanted in later groups were mostly implanted with subcutaneous lead wires,

but no headcap. At the time of terminal electrophysiological evaluation, direct connections were made to these wires for device evaluation.

4.3.5.2 Surgical procedures

To implant the regenerative scaffold electrodes, the rats were first anesthetized with inhaled isoflurane gas, and the surgical site was shaved and sterilized. Marcaine (0.25% w/v, Hospira, Inc.) was administered subcutaneously for post-surgical pain relief (0.3 ml/animal), and a skin incision was then made along the femoral axis of the right leg. The underlying musculature was delineated with a blunt probe to expose the sciatic nerve and its tibial branch, which was isolated and freed from surrounding connective tissue. The tibial nerve was transected approximately five millimeters distal to the common peroneal - tibial bifurcation, and its nerve stumps were pulled one millimeter into each end of a guidance channel and fixed into place with a single 10-0 nylon suture (Ethilon) to create a five millimeter gap. In the simulated amputation case, the sutured distal nerve stump was then cut and resected as far distal as possible, leaving only a 2-3 mm fragment of isolated nerve attached to the distal end of the scaffold. In all cases, the muscles were next reapposed with 4-0 vicryl sutures (Ethicon Inc.) The percutaneous headcap and attached electrode leads were tunneled subcutaneously to a one centimeter skin incision at the top of the skull. To provide the headcap with a firm attachment site, four stainless steel screws (Fine Science Tools, Inc.) were screwed into into the skull, through one mm diameter drill holes. The headcap was affixed to the screws using dental acrylic (Lang Dental Mfg. Co.). The skin incision in the leg was clamped shut with wound clips (Braintree Scientific, Inc.).

4.3.5.3 Post-operative care

After the surgery, the rats were placed under a warm light to recover from anesthesia then given a subcutaneous injection of buprenorphine (.03mg/kg) for pain relief. Rats were housed separately with access to food and water *ad libitum* in a colony room maintained at constant temperature (19-22^{o}C) and humidity (40-50%) on a 12:12 h light/dark cycle. Cages were filled with soft bedding (Diamond Soft, Harlan) to prevent the onset of pododermatitis. Animals were maintained in facilities approved by the Institutional Animal Care and Use Committee (IACUC) at the Georgia Institue of Technology and in accordance with the current United States Department of Agriculture, Department of Health and Human Services, and National Institutes of Health regulations and standards.

4.3.6 Recordings of neural activity using implanted regenerative scaffold electrodes.

4.3.6.1 Chronic recordings through headcap connector

After surgical implantation, weekly recording sessions were performed to measure neural activity. Rats were briefly anesthetized with isofluorane gas and placed within their cages inside a faraday chamber. Short wires were attached between their headcap pin connectors and a Multichannel Systems (MCS) headstage, providing buffering and an initial gain of ten. The connections were then sent to a wideband MCS filter and amplifier (0.1-5000 Hz, gain=1000), before being sampled at 50 kHz through a MCS DAQ card. MCS software was used to visualize recordings and to provide additional bandpass filtering (300-3000Hz). Recordings were taken from the

anesthetized animals in response to stimuli such as light toe pinch. Recordings were also taken from animals freely moving within their cages.

4.3.6.2 Terminal electrophysiological testing

At its scheduled end point, each animal was anesthetized with isofluorane gas for terminal electrophysiological experimentation. The implantation site was exposed as during the initial surgery, and the sciatic nerve was dissected and freed from surrounding tissue up as far proximally as possible. Gastrocnemius muscles, normally innervated by the tibial nerve, were also exposed. The surgical cavity was kept moistened with mineral oil warmed to 37ºC. Throughout the procedure, the animals were kept on an insulated pad and their breathing rates and reflex responses to toe pinch stimuli were closely monitored.

As a brief test of functional innervation by the tibial nerve, all other nerves branching from the sciatic nerve were cut, and a pair of stainless steel bipolar hook electrodes, spaced 1.5 mm apart, was fixed to the sciatic nerve as far proximally as possible. A stimulator (Model S88, Grass Technologies) and stimulus isolation unit (Model SIU5B, Grass), were used to stimulate the nerve with 50-100μs square pulses of variable amplitude, applied at a rate of 1Hz. Muscles were closely observed for twitch-type contractions of the same frequency. In some cases, EMG recordings were taken as previously described [49], but visual assessment was typically sufficient as a test of reinnervation.

RSEs were used to take recordings of evoked neural activity to characterize their recording capabilities. Compound nerve action potentials (CNAPs) evoked from the proximal nerve were recorded by the chronically implanted electrode arrays and amplified and filtered as described above. The recordings were averaged up to 128 times,

using a trigger signal provided by the stimulator, and recorded data was saved for each electrode channel. In some animals stimulation was applied through the implanted electrode arrays, using the same stimulus patterns as described above. Any resulting muscular contractions were noted, and evoked CNAPs were recorded from upstream electrodes.

4.3.7 Histological evaluation of nerve regeneration

After terminal electrophysiological evaluation, the regenerative electrode scaffolds were explanted, rinsed in PBS and post-fixed for one hour in 4% paraformaldehyde in PBS (Sigma-Aldrich). The samples were next rinsed again in PBS and transferred to a 30% sucrose in PBS solution for cryoprotection and incubated at 4ºC overnight. The samples were then embedded in O.C.T. gel (Tissue Tek) and stored at -80ºC until the time of cryosectioning. A cryostat (CM30505, Leica) was used to collect ten micron thick cross sections at nine intervals through the length of the scaffolds. Some scaffolds were instead reserved for obtaining18µm thick longitudinal sections, to provide an alternative perspective of regeneration through the channels. Sectioned slides were reacted for immunofluorescent demonstration of relevant markers as described above for the cultured DRGs. Markers were also selected for macrophages (anti-ED-1, CD-68, 1:1000, Serotec) and fibroblasts (anti-vimentin, 1:500, Sigma-Aldrich, as well as S100, to allow differentiation of weak reactivity of Schwann cells by anti-vimentin antibody). At the conclusion of the immunostaining process, the slides were dried and coverslipped using Fluoromount G solution. (Southern Biotech).

Nerve regeneration was quantified by counting the total number of NF-160^{+} axonal profiles at the center of the nerve gap, as described previously [49]. Briefly,

representative portions of the regenerated nerve cable were imaged at 40x with a confocal microscope (LSM 510, Zeiss). Using Image Pro software (Media Cybernetics), the number of $NF160^{+}$ axons within this image was quantified and used to calculate a representative axonal density values. To accurately calculate total nerve cross-sectional area, a composite 40x image of the entire nerve cross-section was obtained using a computer controlled microscope stage and Neurolucida software (MFB Bioscience). Axonal density measurements were used in conjunction with total area measurements to estimate the total number of axonal profiles. One-way ANOVA was used for all statistical comparisons between experimental groups, and a p-value < 0.05 was considered to be significant.

4.4 RESULTS

4.4.1 Electrode array characterization

The structural integrity of the fabricated thin-film electrode arrays was verified under a light microscope (Figure 4.3A). Several electrode array design variations were included on the same wafer, with up to sixteen channels per array. For these experiments, a four channel design was selected, and to further reduce packaging complexity, lead wire connections were made to just two of these electrodes as well as the ground electrode (Figure 4.3C-G). Dissociated neurons survived and grew well on the SU-8 substrates, forming extensive branched connections after two days in culture (Figure 4.3B). The measured impedance magnitudes at 1kHz of the recording electrodes ranged from 30-300 kΩ, but the majority of these values fell within the range of 30-90 kΩ. For the ground electrodes, the majority of the measured impedance magnitudes were between 10-20kΩ.

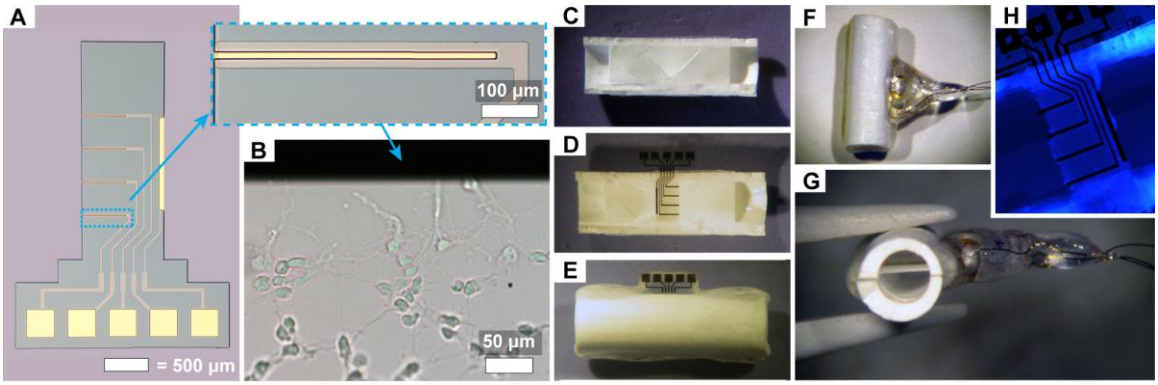

Figure 4.3: Electrode array characterization

(A): Micrograph of a 4-channel electrode on the Si wafer. Inset: magnified view of a single recording electrode. (B): Dissociated neurons grew well on SU-8 electrode arrays in culture, suggesting substrate biocompatibility (image here taken two days after culturing). (C-H): Step-by-step images of the RSE fabrication process. (C): A single nanofiber sheet was fixed to the walls of a longitudinally bisected polysulfone channel. (D): An electrode array was embedded within the fiber sheet using a UV curing adhesive. (E, F): The same adhesive was also used to close the channels and to encapsulate the connector end of the electrode array after making lead wire connections with conductive epoxy. (G): Negligible cross-sectional area of the channel was blocked by the fibers and electrode. (H): Fluouresence of the adhesive under UV light allowed precision application and validation.

4.4.2 Dorsal root ganglia culturing experiments

Cultured DRGs were fixed after fourteen days and reacted for immunofluorescent demonstration of cellular markers. The DRGs were observed to have adhered well to the PAN-MA nanofiber sheets and extended neurites and migrating non-neuronal cells in an oriented fashion, along the direction of nanofiber alignment (Figure 4.4A). Robust growth of neurites and migrating cells was observed on all surfaces, further suggesting biocompatibility of the implant materials.

As expected [68], patterns of DRG growth were influenced by the distribution of adhesive used to embed the SU-8 based electrode arrays within the nanofiber sheets. For example, in zones where the nanofibers were saturated with adhesive, the organization and alignment of cell growth were disrupted. The presence of adhesive was critical at the boundary between the nanofiber sheets and the electrode array. In zones where adhesive

was lacking this boundary, cell migration and neurite outgrowth continued uninterrupted along the nanofiber sheet and underneath the overlying electrode array. In dishes where adhesive was present at this boundary line, sealing the gap between the nanofiber sheet and the electrode array, robust growth across the boundary was observed.

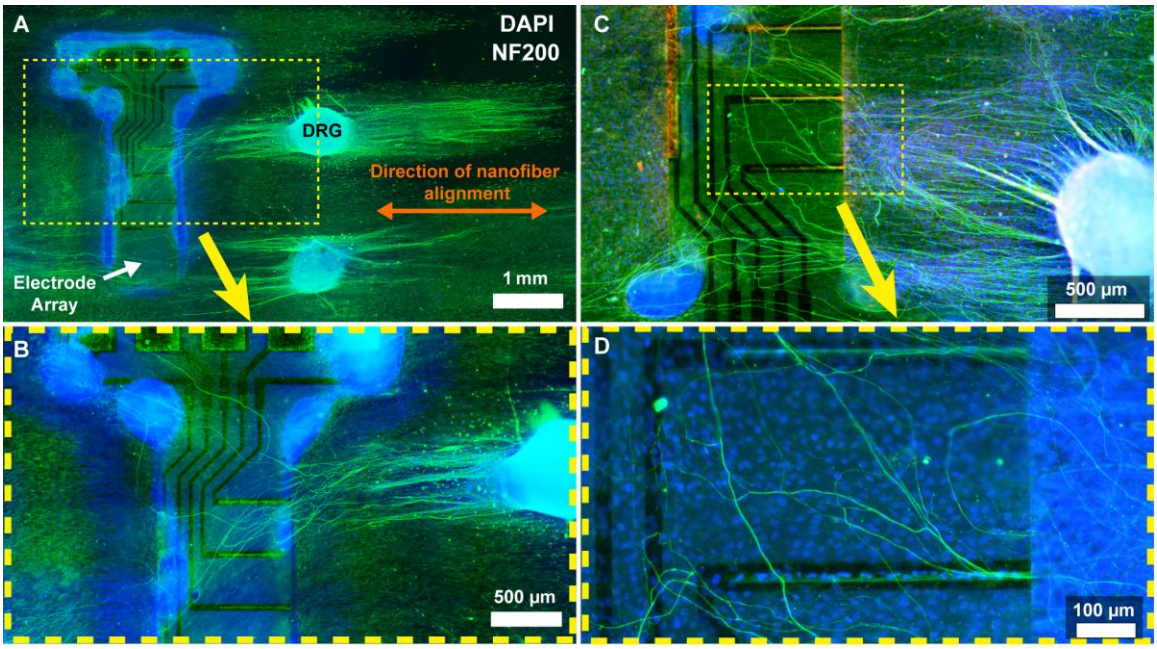

Figure 4.4: Dorsal root ganglia (DRG) cultures.

(A): DRGs cultured on aligned nanofiber substrates extended neurites and migrating Schwann cells in an oriented fashion, matching the direction of nanofiber alignment. The UV curing adhesive fluorescences blue, along with cell nuclei stained with DAPI. (B): Neurites crossed the nanofiber / electrode array boundary and grew along the surface of the SU-8 based electrode array. (C,D): The direction of alignment of neurite growth across the surface of the electrode arrays was more randomly oriented. (D): Grooved recesses filled with migrated non-neural cells, and neurite growth was for the most part not constrained by the grooves.

As compared to the aligned growth observed through the nanofiber sheets, directionality of neurite extension across the smooth surface of the electrode array was reduced (Figure 4.4B,D). Growth of neurites crossing the nanofiber / electrode array boundary often spanned the full width of the array surface and back onto the nanofibers on the opposite side, but the path of growth was typically not direct. In some cases

neurites on the array surface reversed course, crossing back onto the nanofibers on the same side of the array (Figure 4.4D). Notably, neurites did not appear constrained to grow within the electrode array's grooved recesses, which were typically instead filled with non-neuronal cells. Neurites typically grew directly across the grooves, although in some cases neurites grew along the pattern of the grooves for a limited distance (Figure 4.4D).

4.4.3 Surgical outcomes

Implanted animals recovered from surgery without complication remained healthy until their scheduled endpoints. As expected from past experience with Lewis strain rats, animals exhibited no signs of autotomy as a result of nerve transaction. At the time of explantation, all guidance channels were found to be structurally intact with the tibial nerve still firmly secured on each end. Implanted devices were characteristically encased in fibrotic tissue, but the visible inflammatory response was otherwise minimal. One complication observed in many of the animals was the eventual loss of the percutaneous headcap connectors, along with attached lead wires. To ensure intact connections for terminal electrophysiological recordings, many of the animals in later groups were implanted with devices containing subcutaneous leads but no headcaps.

4.4.4 Histological assessment of nerve regeneration

4.4.4.1 Axonal profile counts

All explanted RSEs were sectioned at regular intervals and processed for histological analysis. Robust regeneration of $NF160^{+}$ axons was observed through the full lengths of all implanted devices. For both the distal-nerve-intact group and the distal-

nerve-absent group, regenerated axon profiles were counted at the RSE midpoint (Figure 4.5). Axon counts were not significantly different between these groups at the eight week end point. In the distal-nerve-intact group, an average of 7077 ± 546 axons was counted, while in the distal-nerve-absent group an average of 7945 ± 1144 axons was counted.

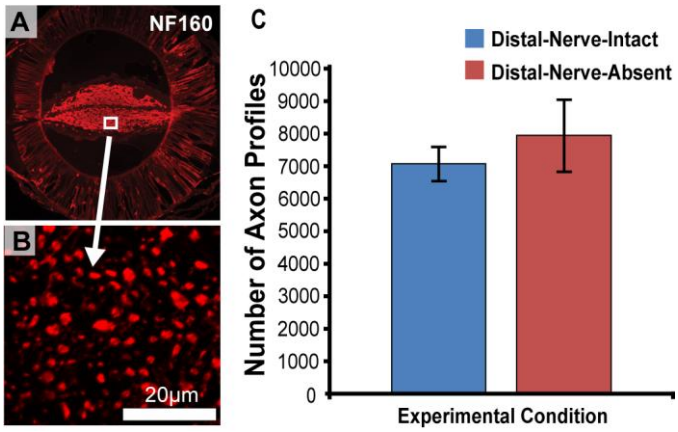

Figure 4.5: Axon profile count comparison between the two experimental groups

(A), (B): Representative images taken during the quantification process. (C): Axons counts for the distal-nerve-intact group and the distal-nerve-absent group at the 8 week end point (7077 ± 546 vs. 7945 ± 1144 axons). Axon counts were not significantly different between the two groups, suggesting the applicability of the RSE design in the case of amputation.

4.4.4.2 Regenerated nerve morphology

Characteristic patterns of regeneration were observed through the implanted RSEs. Near the proximal end of each scaffold, the intact nerve stump contained an axonal core that was circular in cross-section (Figure 4.6A). At further distances along the length of the device, the core gradually flattened out to take an increasingly elongated spindle shape (Figure 4.6B,C) that conformed to the nanofiber sheet and embedded electrode array. Past the scaffold mid-point, the regenerated nerve gradually regained a circular cross-section as it approached the distal end of the device (Figure 4.6D,E).

Axons and co-localized Schwann cells regenerated in consolidated cores that were centered around the electrode array (Figure 4.6F). Axons grew to within close proximity of the array surface, often making direct contact (Figure 4.6G). (Note that the cracked appearance of the electrode array in some of these images is due to effects of the cryosectioning process.) In cases where axons did not make direct contact with the electrode array, one or more layers of elongated fibroblasts were typically observed coating the array surface. Fibroblasts were also observed to fill up the electrode grooves, similarly to what was observed in the DRG culturing experiments (data not shown).

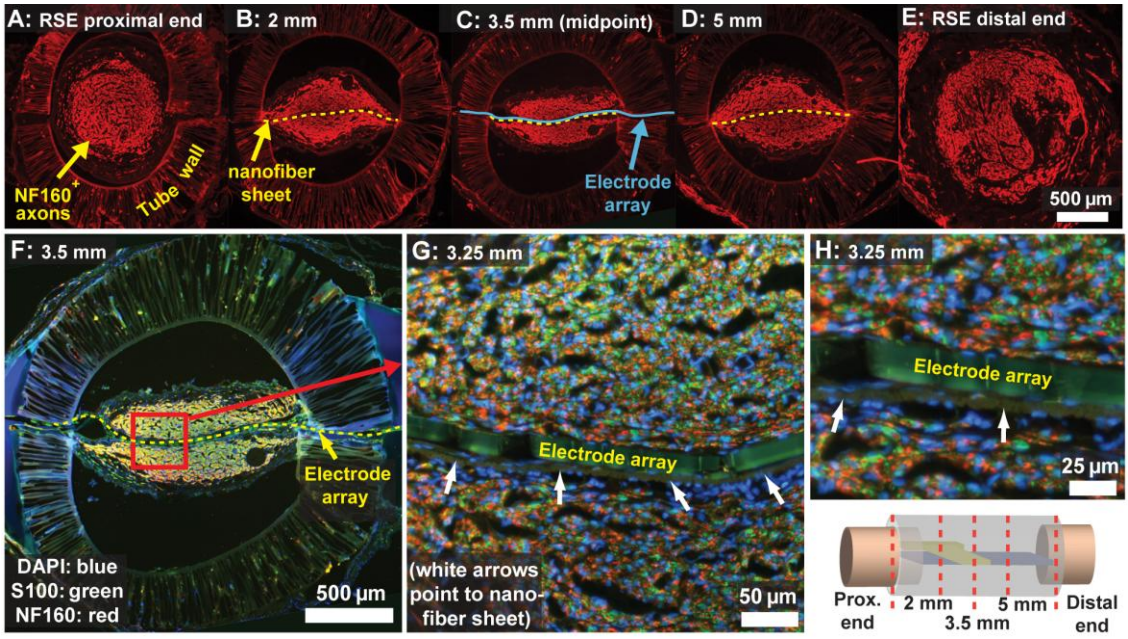

Figure 4.6: Cross-sections from within a representative distal-nerve-absent scaffold

The diagram on the lower right illustrates the location of the cross-sections. (A): Near the proximal end of each scaffold, the intact nerve stump contained an axonal core that was circular in cross-section. (B,C): At farther distances through the device, the axonal core gradually flattened out to take an increasingly elongated spindle shape, conforming to the nanofiber sheet (location marked with a yellow dashed line) and embedded electrode array (location marked with a solid blue line). (D, E): Past the scaffold mid-point, the regenerated nerve gradually regained a circular cross-section as it approached the distal end of the device. (F): Larger view of the same image as in (C), with additional Schwann cell and DAPI labeling. Axons were co-localized with Schwann cells, in a consolidated core that was centered around the electrode array (marked with red arrows.) (G): Magnified view of a different sample, taken 3.25 mm into the RSE. Axons and Schwann cells are growing in close proximity to the electrode array. (H): Magnified view of (G) showing individual axons / Schwann cells in direct contact with the surface of the electrode array.

Several RSEs were sectioned longitudinally to provide a representative view of regeneration from an alternate perspective (Figure 4.7A). Again, regenerated axons and migrating non-neuronal cells were observed to grow in a regeneration cable centered around the nanofiber sheet, and this centralized growth continued uninterrupted across the surface of the embedded electrode array. Significantly the low-profile electrode arrays did not appear to impede or redirect general growth patterns of regenerating axons (Figure 4.7B).

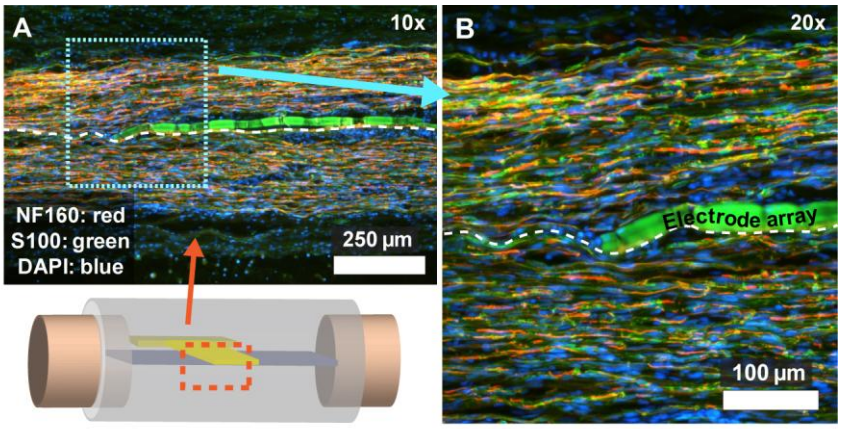

Figure 4.7: Longitudinal view of regeneration through a RSE.

The diagram in the bottom left corner illustrates the location within the channel where the image was taken.(A): Axons (NF160: red) and co-localized Schwann cells (S100: green) grew through the center of the polysulfone tube in a cable centered around the nanofiber sheet, whose location is indicated with a dashed white line. The electrode array fluoresces yellow-green in the image. (B): Higher magnification view of the boxed region in (A). Axons grew uninterrupted, directly across the low-profile embedded electrode array.

4.4.5 Electrophysiological assessment of nerve regeneration

Regular recording sessions were performed with animals implanted with percutaneous headcap connectors, but issues with headcap integrity were encounted. In many of the animals, the headcap connectors pulled off before scheduled end points,

typically pulling out attached lead wires as well. In other animals where headcaps stayed mounted, the continuity of the signal leads in the area of the headcaps was likely interrupted. This lead damage was sometimes indicated by the presence of heartbeat noise that went away when the headcap region was bypassed. Due to these issues, animals in later surgical groups were implanted with devices containing subcutaneous lead wires, but no percutaneous connections.

All animals underwent electrophysiological testing at their scheduled end points. In all distal-nerve-attached animals, electrical stimulation of the proximal sciatic nerve via hook electrodes elicited visible contractions of the gastrocnemius muscles as well as ankle extension, thereby demonstrating functional reinnervation by the regenerated nerve. Notably, in many of the distal-nerve-absent animals, proximal stimulation elicited faint twitch-type muscle contractions that were highly localized to the muscle bed underlying the distal end of the RSE. These twitches stopped when the distal end of the scaffold was separated from the underlying musculature, suggesting that axons regenerated through many of the RSEs formed functional neuromuscular junctions with local muscle tissue.

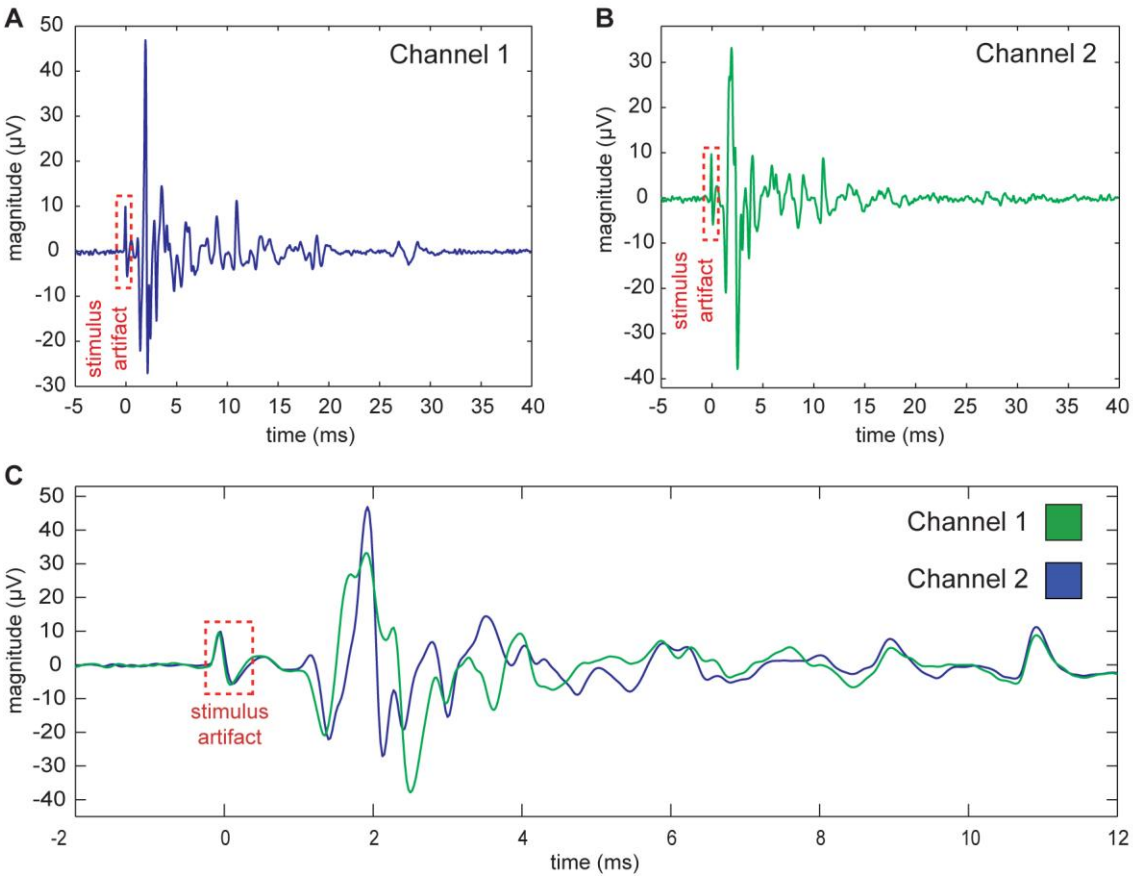

Figure 4.8: Nerve compound action potentials recorded with implanted RSEs.

These representative signals were recorded from a distal-nerve-absent case at the 8 week end point. (A,B): Recordings from two different channels of the electrode array with the ground electrode used as a common reference. (C): Overlaid and expanded view of the signals recorded from each channel.

Subcutaneous lead wires were exposed for attachment several centimeters away from the scaffolds so that neural recordings could be taken through the chronically implanted electrodes. In all cases, implanted RSEs with attached lead wires were able to record evoked compound nerve action potentials (CNAPs) (Figure 4.8). In distal-nerve-intact animals, stimulation through the RSE devices resulted in gastrocnemious muscle contractions, and in both groups, RSE stimulation resulted in the initiation of CNAPs, measurable upstream by hook electrodes, although the necessary voltages required to elicit measurable responses in these cases was high (data not shown). Some animals in

the initial, exploratory groups were kept until later time points. Successful stimulation and recording results were obtained in even the longest surviving of these animals – up to twenty-two weeks post-surgery.

4.5 DISCUSSION

Neural cells are highly responsive to physical and biochemical cues present in their surrounding environment, especially during periods of tissue growth or repair [20]. The course of a regenerating axon, for example, is guided by such factors as the physical topography and chemistry of the surface along which it grows, as well as by signaling molecules in the local environment. These types of topographic, biochemical, and electrical cues exert great influence on cellular viability, growth, and activity. A fundamental strategy in tissue engineering-based treatment of neural deficit or injury is to artificially recreate environmental cues in such a way as to influence neural cell behavior.

The objective of this study was to develop topographic scaffold-based regenerative electrodes and evaluate their ability to support and direct nerve regeneration for the purpose of interfacing with regenerated axons. *In vitro* experimentation demonstrated device biocompatibility and helped refine methods of integrating thin-film electrode arrays within sheets of nanofiber scaffolding. Cellular growth was strongly influenced by substrate topography, as evidenced by the highly directed neurite extension and Schwann cell migration observed on the aligned nanofiber sheets. Significantly, this growth was directed onto and across the surface of the embedded electrode arrays, a result that provided initial validation of the electrode integration techniques.

Within the implanted RSE devices, the aligned nanofiber scaffolding exerted strong influence on regenerated nerve morphology. Most visibly, the cross-sectional

shape of the regenerated nerves within the scaffold interior were elongated to conform to the nanofiber sheet and embedded electrode array. This type of flattened nerve structure might be valuable for certain interfacing applications. For example, an elongated nerve structure might offer the ability to interface more selectively with subsets of a regenerated nerve, in a manner analogous to the flat interface nerve electrodes (FINE) of the Durand lab [42].

Not only was the regenerated axon core centered around and flattened to conform to the embedded electrode arrays, but individual axons grew within close proximity to the arrays, in many cases making direct contact with the array surface. Minimal separation distance between axons and electrodes is critical, since extracellular signals strength decreases sharply with distance from the axon membrane. The low-profile electrode arrays also appeared to pose minimal disturbance to the course of axonal growth. Notably, the 7μm thick nanofiber sheet and embedded 14μm thick electrode array occupy a small fraction of guidance channel's open cross-sectional area available to the regenerating nerve (~1.7%). Thus, in future designs, not only might electrode density on individual arrays be increased, but additional layers might conceivably be integrated within a single guidance channel to achieve channel counts in the hundreds or higher. Also in future designs, the use of grooved recesses above the microelectrodes might be questioned, based on the lack of axons observed within these recesses during histological characterization.

In comparing axonal regeneration through the nerve gap case and the simulated amputation case, we observed substantial equivalence at the eight week time point. These results agreed with previous nerve regeneration studies over similar time lengths in which

isolated nerve fragments were used in place of isolated distal stumps [29, 30]. It is known, however, that extended axotomy affects the long-term viability of peripheral neurons [40, 88-92], and long-term studies are required to characterize the steady-state condition of axons within RSEs in the case of amputation. Nevertheless, the results we observed at the eight week time point are significant, because it is within this time frame that the formative steps of nerve repair occur and the overall structure of the regenerated nerve is determined [3, 53, 71, 74]. In future designs, natural or engineered sources of trophic feedback might be arranged to ensure the long-term viability of regenerated axons.

The ability of chronically implanted RSEs to record neural activity was demonstrated through recordings of evoked compound nerve action potentials. In all attempted trials, RSEs were able to successfully record and also stimulate CNAPs from regenerated nerves. It is important to note, however, that the embedded electrode arrays were designed for interfacing with small groups or individual axons, and the electrode layouts were not optimized for recording or stimulating evoked group activity. Possibly due in part to packaging issues we encountered, difficulties were encountered obtaining recordings of spontaneous neural activity from freely moving animals. To better obtain and characterize single unit activity, future work will be required to optimize electrode geometry and device packaging.

4.6 CONCLUSIONS

In this study, embedded interfacing electrodes were integrated within topographic guidance scaffolds, such that nerve regeneration could be supported and controlled. Regenerated nerve structure within our regenerative scaffold electrodes (RSEs) was

shaped around the embedded electrode array, and separation distances between regenerated axons and interfacing electrodes were minimal. Implantations with and without an intact distal nerve stump were also performed, and regeneration in these cases was not significantly different at the eight week time point. In both cases, devices were capable of stimulating and recording evoked neural signals. Future work is required to optimize electrode design and packaging in order to achieve robust recordings of single unit spiking. For the simulated amputation case, further research is required to characterize the long term viability of regenerated axons and the resulting effects on interfacing capabilities. Overall, our results suggest the potential benefit of using a scaffold-based design to influence nerve regeneration to the advantage of a peripheral nerve interface.

4.7 ACKNOWLEDGMENTS

The authors would like to acknowledge support from the following grants: NIH R01 44409, NSF GTEC EEC-9731643, NSF CBET 0651716, and NSF IGERT-0221600. We would also like to thank Dr. Arthur English and his laboratory for their assistance, Eric Gaupp, Patrick Malone, James Hyun, Safkat Al-Kibria, and Gaurangkumar Patel for assisting with histological techniques, and Dr. Laura O'Farrell, for her assistance with animal care.

CHAPTER 5

CONCLUSIONS AND FUTURE DIRECTIONS

5.1 Summary of work and novel contributions

5.1.1 Promoting and controlling nerve regeneration with nanofiber-based topographic cues

The objective of this project was to apply tissue engineering principles to peripheral nerve interface design in order to contribute towards the development of an interface able to provide seamless link between the nervous system and an advanced neuroprosthetic device.

A major first component of this work was to develop topographic guidance scaffolds able to promote nerve regeneration while exerting fine control over the course of axonal growth. Nanofiber-based regeneration scaffolds that had been pioneered in the Bellamkonda laboratory by Dr. Young-tae Kim were used as a starting point for the design [19]. Dr. Kim's existing devices contained stacked sheets of aligned electrospun nanofibers, and were shown to promote directed neural outgrowth *in vitro* and regeneration over long nerve gaps *in vivo*. This design did not, however, provide control over the path of regenerating axons or the morphology of the regenerated nerve segment. The loosely stacked nanofiber sheets in these devices tended to shift and settle unpredictably, resulting in a generally robust but uncontrolled course of regeneration.

In this work, the previously existing nanofiber-based scaffold design was modified such that nanofiber sheets could be fixed into place through the length of the

guidance channels. Towards this end, custom fabricated molds were used to slice guidance channel tubing into longitudinal sections, so that a layer by layer fabrication approach could be used to anchor individual nanofiber sheets into the channel walls through the length of the scaffold. The end result of this design was that scaffold-based topographic cues could be precisely positioned through the length of the guidance channels in a controlled and stable fashion.

It was expected that there would be an approximately linear correlation between the level of nerve regeneration observed and the amount of scaffolding used (i.e. the number of sheets fixed through the length of each regeneration channel. Preliminary experiments, however, demonstrated surprising results: Guidance channels containing only a single sheet of nanofiber scaffolding material fixed through the center length of the scaffold supported robust levels of regeneration. A full study was performed to further explore the mechanisms of influence of the nanofiber sheets on nerve regeneration. This study demonstrated that a single sheet of aligned nanofiber scaffolding, taking up only fraction of the channel's interior cross-sectional area, was able to support robust levels of nerve regeneration across critical length nerve gaps by providing a continuous bridge of topographic cues to migrating cells. Additional nanofiber sheets in this scaffold design only fragmented the endogenous nerve repair sequence and negatively impacted regeneration. Significantly, the fixed nanofiber sheets were shown to provide fine control over the course of regenerating axons and the morphology of the regenerated nerve segment, which consistently regenerated in a consolidated core conforming to the single thin-film of scaffolding.

5.1.2 Integrating electrode arrays within nanofiber-based regeneration scaffolds to create a neural interface

Nanofiber-based scaffolds containing a single sheet of fixed scaffolding material were able to shape nerve regeneration around the nanofiber sheet. In order to take advantage of this capability in a peripheral nerve interface, electrodes would need to be embedded in the nanofiber sheet in a low-profile, non-invasive manner. A thin-film electrode array design was selected and iterative rounds *in vitro* DRG culturing experiments were performed with various array substrates and designs to determine a method for integrating the electrode array within the nanofiber thin-film. A design in which the array was directly embedded into a continuous thin-film layer, using controlled proportions of biocompatible adhesive, was selected, and embedding techniques were further refined and validated through continued experimentation.

Several thin-film electrode designs were explored with the collaboration of Dinal Andreasen of the Georgia Tech Research Institute. A total of three custom electrodes were designed and fabricated and compared alongside commercially available probes in initial experiments. In the end, a custom electrode design that was fabricated in Georgia Tech's Nanotechnology research center was selected. Using techniques that had been explored using the other electrode types, these electrodes were embedded within nanofiber scaffolds and packaged for implantation across rat tibial nerve gaps.

Implantation studies with the resulting regenerative scaffold electrodes (RSEs) were performed to characterize their effect on regeneration and ability to interface with regenerated nerves in a chronic setting. RSEs were demonstrated to guide neural regeneration to conform to the embedded array, and to guide the course of regenerating

axons to within close proximity to the embedded electrode. Significantly the course of regenerating axons did not appear to be disturbed by the presence of the electrode array embedded within the nanofiber thin-film. RSEs were demonstrated to record neural activity for as long as the devices were implanted - up to twenty-two weeks. Significantly, robust regeneration was observed and recordings of neural activity were recorded from nerves regenerated in a simulated amputation case, in which no intact distal nerve target was attached to the RSE.

5.2 Remaining challenges and future directions

Attempts to interface with peripheral nerves using current microelectrode-based designs have been met with some success. For example, studies describing the successful use of regenerative electrodes to record neural activity have been steadily published for over three decades [43, 46, 47, 83, 84, 86]. Yet, a clinically viable peripheral nerve interfacing device for the purpose of prosthetic limb control has yet to emerge, suggesting that major technical challenges remain. Further evidence that the peripheral nerve interfacing problem is far from solved is given by the fact that some of the largest research funding agencies in the United States (for example, the National Institutes of Health, Nation Science Foundation, Defense Advanced Research Project Agency) are currently devoting considerable resources towards the development of a peripheral nerve interface suitable for prosthetic limb control.

The enormous amount of effort and resources that have contributed towards the yet unsolved the peripheral nerve interfacing problem speaks to the problem's challenging nature and to the need for innovative solution strategies. In this thesis project, a tissue engineering-based paradigm involving the use of topographic guidance cues in

regenerative electrode design has been introduced and validated. It is vital to note that it is not the intention of this work to present itself as yet another solution to the problem of peripheral nerve interfacing. Rather, it should be explicitly stated that the work described here is meant to be an incremental step in a new direction that potentially represents one aspect of the solution. As such, this work demonstrates techniques for achieving greater control over the course of nerve regeneration and regenerated nerve morphology, for purposes beneficial to an electrical interface, such as reducing separation distances between axons and interfacing electrodes.

Some of the challenges yet to be faced in the improvement of the described RSE design, and in the improvement of other similar nerve interfaces, are described in the following sections.

5.2.1 Electrode design

The capability of the chronically implanted RSE devices described in this study to interface with neural tissue was demonstrated through the recording and stimulation of evoked neural activity in the form of compound action potentials. There exists a range of clinical applications in which the stimulating and recording of bulk neural activity within a nerve is valuable, but for the fine control of prosthetic limbs, it will likely be necessary to reliably interface with smaller groups of axons. In future RSE devices, modifications such as improvements to electrode design will contribute towards this capability. The SU-8 patterned trench structures, which did not result in the isolation of small groups of axons, should be abandoned in favor of an alternative electrode geometry. Electrode materials or coatings should be selected to achieve high surface areas for the same geometric footprint, for the purpose of reducing electrode impedance.

Significantly, however, iterations of microelectrode devices for interfacing with peripheral nerves have been developed and refined for many decades, and yet even the most recent devices fail to provide adequate SNR (signal to noise ratio) under conditions approximating those of everyday life. The use of more sophisticated electrode materials, better electrical shielding, more advanced signal conditioning techniques, and other incremental improvements always have the potential to extend device capabilities, and this fact is often noted in the discussion sections of PNI studies. Yet, it is perhaps more likely that novel approaches will be required to obtain signals robust to EMG and electrical noise, motion artifact, and other electrical transients. Some examples of different types of future approaches are described in the final section.

5.2.2 System miniaturization and signal processing

The addition of integrated circuitry onto or adjacent to RSE devices would improve interfacing capabilities by (1) using multiplexing to reduce the number of unwieldy and fragile signals leads required, (2) increasing signal quality by applying initial amplification and filtering closer to the recording site, (3) eliminating the need for percutaneous connections through the addition of wireless technology. Advanced signal processing algorithms have been previously implemented on implanted chips for the purpose of identifying spikes or other relevant markers or patterns of information and relaying only the occurrence of these events, for the purpose of reducing bandwidth. Sophisticated signal processing techniques will also be vital for decoding patterns representing muscle activity and for encoding appropriate stimulation patterns to convey sensory information.

5.2.3 Long term system viability

Longer term studies are required to characterize the steady-state condition of axons regenerated through RSE devices in an amputation case. Based on prior studies, it is known that some degree of cell death and atrophy will occur, but it is not known to what degree or how these long term changes will affect device function. Further tissue engineering based strategies might be required to maintain axonal viability. For example, alternate natural or engineered sources of trophic feedback might be necessary to provide. This type of trophic support might be arranged through a wide variety of approaches, including drug delivery constructs, cell transplantion, or surrogate target tissues for the regenerating axons. Nevertheless research such as the studies performed on long term amputees using LIFE electrodes [40] give hope that peripheral nerves can remain viable indefinitely if given the proper environment.

Advances in device packaging will be required to ensure that implanted engineered devices are just as long-lived. Advancements in battery technology will be required for supplying power efficiently over extended periods of time over repeated cycling. Reduction of form factors will be important for implanted batteries as well as computerized electronics. Other issues are critical as well, such as the development of modular architecture for easier component replacement in case of failure.

5.2.4 Other future directions

In closing, several examples of newly emerging peripheral nerve interfacing strategies will be mentioned, representing only a few of the possible future directions PNI design. For instance, it has been proposed and demonstrated in recent years that a microchannel-type architecture might offer the potential to boost amplitudes of recorded

neural signals [93, 94]. If individual or small groups of axons from an amputated nerve can be induced to regenerate through microdiameter tubes of sufficient length, the tube walls can potentially constrain extracellular charge densities that would otherwise fall off quickly with distance from the nodes of Ranvier. Other researchers have recently proposed the use of muscle cells or slips of ectopic muscle to serve as surrogate targets for regenerating axons within a bioengineered construct [93, 95]. Because muscle-based targets would produce much larger extracellular signals, they have the potential to serve as biological amplifiers, in a manner similar to the targeted muscle reinnervation strategy developed by Dr. Todd Kuiken [96]. As a final example, other researchers are exploring the possibility of interfacing with peripheral nerves using other modalities such as light (neurophotonics), that might be more cell specific and resistant to electrical noise.

The above examples illustrate the type of directions neural interfacing might go beyond the simple co-localization of a peripheral nerve and an array of microelectrodes. Significantly, the success of each of these strategies will depend on the implementation of tissue engineering-based principles, and each approach could possibly benefit from the application of topographic cues to promote support and guidance of the regenerating nerve. Any road taken will face major technical challenges, but technology will be ultimately driven to the ultimate goal of providing amputees with natural control of a lifelike prosthetic device.

APPENDIX A

A REGENERATIVE ELECTRODE SCAFFOLD FOR PERIPHERAL NERVE INTERFACING

A.1 Abstract

Novel approaches to peripheral nerve interfacing are required to establish the stable, high-resolution connections demanded by the emerging generation of advanced neuroprosthetic devices. Here we propose a nanofiber scaffold-based design for a regenerative electrode capable of establishing significant numbers of stable and selective electrical connections with subsets of peripheral nerve. The design features one or more polyimide thin-film electrode arrays integrated within a layered nanofiber scaffold such that regenerating axons from a transected nerve are directed across the embedded electrodes. *In-vitro* and *in-vivo* experiments with a rat peripheral nerve model were performed to validate and optimize the ability of our regenerative electrode scaffold (RES) to direct axonal regeneration across an implanted electrode array. Immunostaining of cultured dorsal root ganglia revealed that migrating Schwann cells and extending neurites can be directed along oriented nanofibers and across an overlaid polyimide electrode *in-vitro*. RES's were then fabricated and implanted between the stumps of transected rat tibial nerves (n=10). After 3-6 weeks the scaffolds were explanted and stained to characterize regeneration through the RES's. Staining revealed robust axonal regeneration through the scaffolds. This regeneration was directed as close as several microns to the surfaces of the integrated electrode arrays. Staining also

revealed minimal inflammatory response at the electrode array site. Additionally, the same results were obtained in the absence of an intact distal stump. In conclusion, our results suggest the feasibility of this design for use in interfacing an amputated nerve stump. Electrophysiological capabilities of the interface and facilitation of long term trophic support for the nerve will be examined in future experiments.

A.2 Introduction

The Amputee Coalition of America cites that as of the year 2000 there are an estimated 1.6 million limb amputees living in the United States, with 185,000 new amputations performed annually. The escalating prevalence of major contributing factors threatens to increase amputation rates even further. In response, significant advances are occurring in the design of prosthetics that cosmetically and functionally mimic natural limbs.

Unfortunately, a critical gap exists in present technology: current neural interfaces do not enable prosthetic limbs to be controlled in a natural, biomimetic manner. Existing prosthetics are typically controlled by simple, open-looped mechanisms. For example, artificial hand movements are often controlled by electromyograms or contralateral shoulder movements. These methods provide few independent control signals and do not enable afferent sensory feedback from the prosthetic. The holy grail of neuroprosthetics research has long been the design and implementation of a seamless, bi-directional nerve-electrode interface between a surviving nerve stump and an external, biomimetic prosthesis. Ideally the interface should offer high-resolution communication that remains stable over the lifetime of the patient. Also, a patient's natural attempts to move the amputated limb should result in the appropriate activation of the prosthetic device, and,

likewise, sensory input from the prosthetic should be naturally perceived by the patient as coming from the original limb.

As a step towards this goal, we propose a regenerative scaffold-based design for the next generation peripheral nerve interface. The scaffolds in our design are based on layered nanofiber scaffolds recently developed by our lab that enable robust regeneration of a severed nerve as well as control over the physical location of regenerating axons [19]. In our proposed regenerative electrode scaffolds (RES), one or more thin-film electrode arrays are integrated into the layers of the scaffold, such that axons regenerating from a nerve stump are guided along the along each nanofiber layer and then across the plane of an embedded electrode array (Figure A.1). The ultimate goal is that such a device will be implantable at the time of amputation, capping the severed nerve and helping to establish an interface capable of supporting high-resolution, closed-loop control of a prosthetic device.

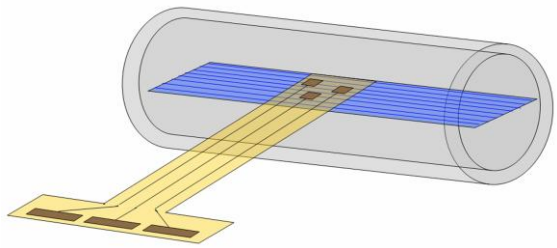

Figure A.1: Simplified illustration of the design of a prototype regenerative electrode scaffold (RES).

A thin-film polyimide electrode array (32 channels in our experiments) is integrated into a scaffold containing a single sheet of oriented nanofibers. The nanofiber layer directs regenerating axons through the tube and across the electrode surface. The electrode's connector end extends through the outside of the tube where it is enclosed in a silicone envelope and sutured beneath the skin.

A.3 Methods

In-vitro experimentation

The regenerative nanoscaffolds previously developed by our lab [19] consist at their core of layers of oriented nanofibers (PAN-MA, poly acrylonitrile-co-methylacrylate, 200-800nm diameter). These oriented nanofiber films, 10-20μm thick, are produced using an electrospinning process. Briefly, a high voltage (20kV) is applied between a syringe as it slowly ejects a liquid polymer melt and a high speed rotating metal drum. Fibers ejected from the syringe are collected on the rotating drum, from which they can later be extracted in oriented sheets.

To validate and refine the technique for integrating a polyimide thin-film electrode array into one of these oriented sheets, several iterations of culturing experiments were performed. Whole dorsal root ganglia (DRGs) from P3 rat pups were extracted and seeded on top of a sheet of oriented nanofiber film that was secured at the corners to the bottom of a Petri dish with biocompatible glue. This aspect of the setup is identical to previous experiments in our lab, in which robust Schwann cell migration and neurite extension from the seeded DRGs were shown to follow the orientation of the nanofibers in the sheets. However, in these new experiments, a modification was made to assess growth not only along a nanofiber layer but also growth across a nanofiber/polyimide boundary onto a 12μm thick polyimide sheet, chosen to simulate the surface of a polyimide electrode array.

The nanofiber/polyimide interface was created in several different configurations. These design conditions included whether the nanofiber layer was overlapped, underlapped, or laid flush to the polyimide boundary. Other conditions included the

presence or absence of surface modification to the polyimide surface, such as directional scratches or addition of extracellular matrix (poly$_l$lysine or laminin).

DRGs were seeded on the nanofiber sheet 1-5 mm from the polyimide boundary and after 10-14 days the dishes were fixed and immunostained for axons (NF-160), Schwann cells (S-100), and cell nuclei (DAPI). Migration of Schwann cells and extension of neurites through the nanofibers and across the polyimide boundary was assessed using a fluorescent microscope.

Regenerative electrode scaffold (RES) fabrication

Nanofiber scaffolds, or nanoscaffolds, have previously been shown by our lab to bridge long peripheral nerve gaps (>17mm in rats) as effectively as autografts [19]. The scaffolds are fabricated by stacking layers of PAN-MA nanofibers within a polymeric (polysulfone) tube. Here, we suggest the integration of thin-film electrode(s) into individual layers of nanofiber scaffold to create a RES, a novel device capable of establishing a stable, high resolution, peripheral nerve interface.

For our initial *in-vivo* experiments, we chose a prototype design consisting of a nanofiber scaffold containing a single nanofiber layer affixed down the mid-horizontal plane of the tube, with a polyimide electrode array embedded within the layer at the center of the tube (see Figure A.1). Results of the *in-vitro* DRG culturing experiments were used to optimize the techniques for integrating the polyimide electrode (2mm x 2mm active area) into the center of the scaffold. In most cases, a non-functional electrode, consisting of the polyimide substrate alone, was used to make the RES's. After fabrication, tubes were UV sterilized overnight and stored in sterile saline until implantation.

Preliminary in-vivo experimentation

RES's were fabricated to accommodate nerve gaps of 6, 10, and 13mm. Different gaps were tested since a gap too short would result in nerve regeneration that is not dependent on or guided by scaffold topography. In this case regeneration might occur throughout the cross-sectional area of the tube and would not be directed across the electrode site. Too long of a gap would result in sub-maximal regeneration. Thus, an optimal nerve gap length was sought in which robust regeneration was enabled, but directed entirely along the oriented nanofiber layer fixed in the tube.

Initial surgeries were performed on 6 anesthetized Fischer 344 rats (250-300g), 2 rats per gap length. Briefly, the sciatic nerve was exposed, and the tibial nerve was transected several millimeters distal to the tibial/common peroneal bifurcation. The proximal and distal stumps of the cut nerve were then secured into either end of the RES with 10-0 sutures.

The nerve was allowed to regenerate through the scaffolds for periods of 3-6 weeks, (more time was allowed for regeneration to occur through the longer scaffolds), and the rats were perfused transcardially with a 4% paraformaldehyde mixture. The scaffolds were then explanted and prepared for cryosectioning in a 30% sucrose solution. 18μm thick longitudinal sections were obtained with a cryostat, collected on glass slides, and double immunostained with markers for axonal regeneration and Schwann cell migration (NF-160 and S-100 staining). On some samples, double staining was performed using S-100 and either ED-1 or Vimentin, for macrophages and fibroblasts/macrophages, respectively.

Further in-vivo experimentation

Two additional "blind-ended" implantations, in which no intact distal nerve stump was present, were performed to better simulate the amputation case. In these blind-ended cases, all procedures were the same, except that after nerve suturing, the distal portion of the tibial nerve was cut and resected up to the muscles. Only an isolated fragment of nerve (2-3mm) was left at the end of the tube to supply a source of migrating Schwann cells [29, 30]. The nerve gap in these cases was chosen to be 6mm, based on the results of the first experiments.

Also, two rats were implanted with RES's containing functional 32-channel microfabricated polyimide electrode arrays containing gold traces and 30μm^2 electrodes coated with titanium nitride (purchased from Multichannel Systems.) The gap length in these implants was again 6mm.

A.4 Results and Discussion

In-vitro DRG cultures

DRGs cultured on a nanofiber layer adjacent to a polyimide surface demonstrated the ability to extend neurites and migrating Schwann cells through the nanofibers and across the nanofiber-to-polyimide boundary. Figure A.2 shows an example of robust Schwann cell migration from a DRG through the oriented nanofiber layer and across an overlaid polyimide surface. Oriented neurite extension through the nanofibers was strong as well, but extension of neurites onto the polyimide surface was relatively weak as compared to the observed Schwann cell migration across the same boundary. However, many examples of boundary crossings by extending neurites were observed,

demonstrating the potential of an *in-vivo* design to foster axonal regeneration along oriented nanofibers and onto an integrated polyimide electrode array site.

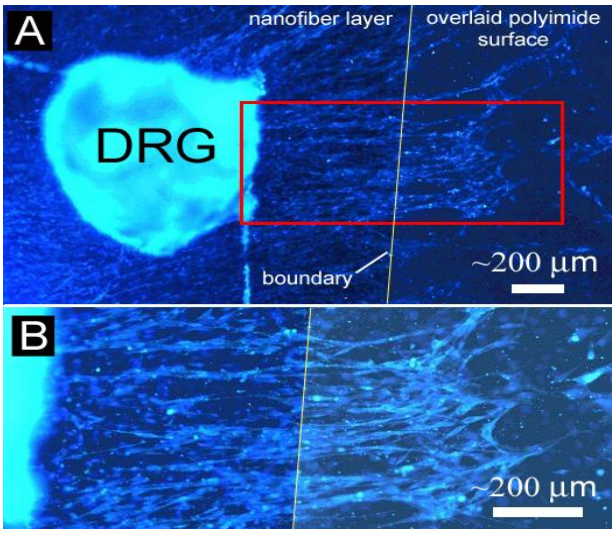

Figure A.2: *In vitro* results

(A): S-100 and DAPI double staining of a DRG seeded on a nanofiber film near an overlaid polyimide surface. A line marking the boundary has been added for clarity. (B): Zoomed in view of the boxed region in (A), better showing Schwann cell migration across the polyimide boundary.

In-vitro culturing experiments also helped in evaluating techniques for embedding a polyimide electrode array into a regenerative scaffold designed for *in-vivo* implantation. For example, it was shown that surface modification of the polyimide surface was unnecessary, but that the right proportion of biocompatible adhesive was important to enable growth from the nanofiber layer up and onto an overlaid polyimide surface.

In-vivo implants

In all 10 rats implanted with a RES, localized Schwann cell migration and axonal regeneration through the length of the scaffold and across the embedded polyimide layer was observed. In the 6 initial implants, in which the nerve gap lengths were varied, this regeneration was robust, even for the longest nerve gap length of 13mm. Additionally, in

all cases, regeneration was localized almost exclusively in regeneration cables on either side of the nanofiber layer. This localization occurred even for the shortest nerve gap lengths of 6mm, despite the fact that at these short gap lengths, regeneration could have occurred even through an empty tube [4]. This finding demonstrates the strong preference of regenerating nerves for the nanofiber layer surface. A gap length of 6mm was used in subsequent experiments for simplicity, but it is probable that localized, directed growth through even a shorter gap would be feasible.

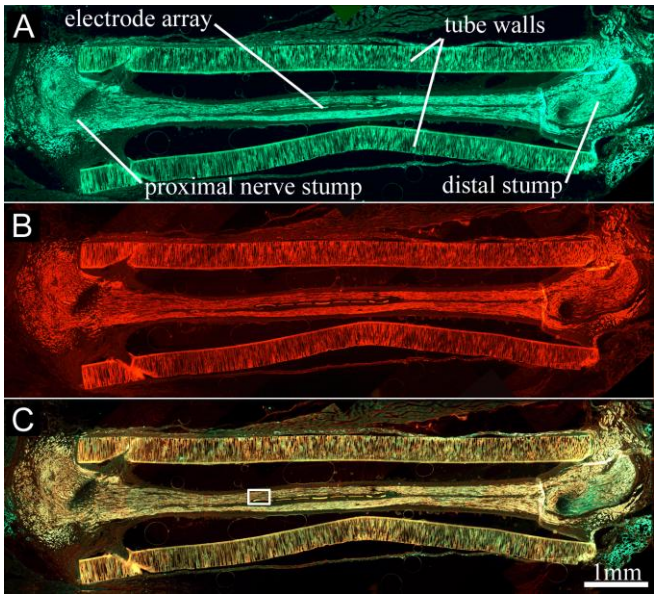

Figure A.3: Longitudinal cross section of an RES implanted for 4 weeks

Localized nerve regeneration occurred through the scaffold and across the electrode array surface in the scaffold's center. The "gaps" visible on the electrode array surface are individual electrode sites from one row of the array. (The arrays contain a total of 5 rows of 6 electrodes, plus 2 larger ground electrodes.) (A): S-100 staining for Schwann cells. (B): The same section stained with NF-160 for axons (C): Merged image of S-100 and NF-160 staining showing the co-localization of axonal regeneration and Schwann cell migration.

Figure A.3 shows different fluorescent stainings of a longitudinal section obtained from a typical RES. This particular RES was explanted after 4 weeks and contained a functional polyimide electrode array. Figure A.3A shows Schwann cell migration through

the scaffold, and Figure A.3B shows axonal regeneration. These images demonstrate that the configuration of the RES enabled directed axonal regeneration in a localized fashion through the mid-horizontal plane of the scaffold and across the embedded electrode. Figure A.3C, which shows a merged image of Figure A.3A and Figure A.3B, demonstrates the co-localization of axons and migrated Schwann cells through the length of the RES.

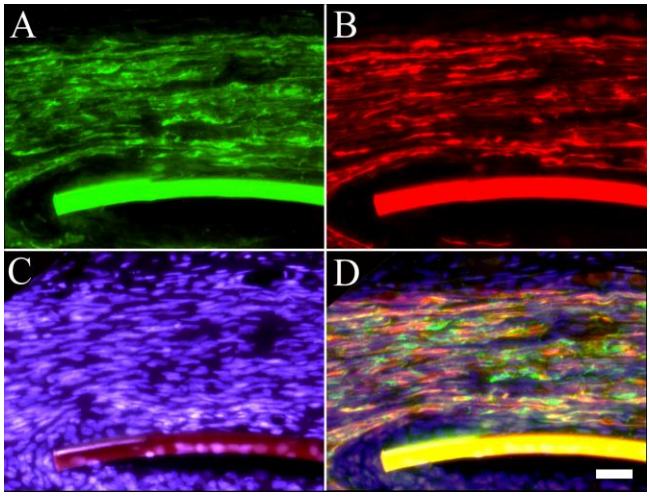

Figure A.4: Higher magnification of the proximal end of the polyimide electrode surface and overlying regeneration (zoomed in view of the boxed region in Figure A.3C.

(A): S-100 stain of migrated Schwann cells (B): NF-160 stain of regenerated axons. Note the proximity of axons to the electrode surface. (C): DAPI nuclear stain)D): Merged image showing all three stains. (scale bar ~ 25µm)

Figure A.4 provides higher magnification of the proximal end of the of the electrode array (the small white boxed region in the center of Figure A.3C) and demonstrates the close proximity of directed axonal regeneration to the array surface. DAPI staining, shown in Figure A.4C, indicates that the space that exists between regenerated axons and the electrode surface is cellular in nature. Figure A.5 confirms this finding and characterizes this tissue as consisting of macrophages and fibroblasts. This

typical observed inflammatory response was minimal and is characteristic of any implanted foreign object within the body. The semipermeable nature of the polysulfone tubes used in our RES's (molecular weight cutoff of 50kD) is thought to help limit the inflammatory response during nerve regeneration [27, 28]. Within all implanted RES's, separation distances between regenerated axons and the electrode surface were small, varying from as low as several microns to a few tens of microns at most.

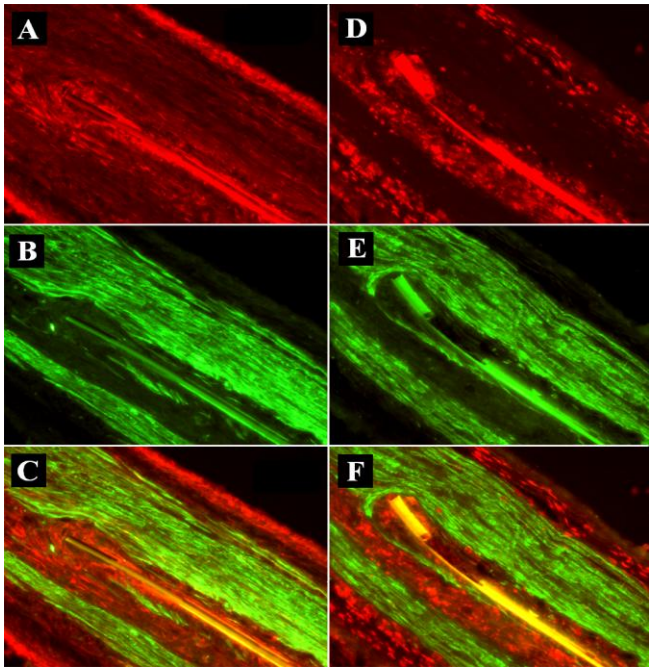

Figure A.5: ED-1, Vimentin, and S-100 staining to characterize the inflammatory response around the polyimide electrode. (Separate sections of the same RES as in Figure A.3 and Figure A.4.)

(A-C): Vimentin (red) and S-100 (green) double staining reveals a layer of fibroblasts on the electrode surface. (D-F): ED-1 (red) and S-100 (green) double staining reveals the presence of macrophages, primarily underneath the electrode surface (bottom side), not on the active side. (Missing notch on the polyimide is where a ground electrode was located)

In the two rats implanted with scaffolds attached to only a nerve fragment at the distal end (as opposed to the intact distal stump), healthy regeneration was again observed. In one of these animals, axonal regeneration through the RES occurred, but to a

lesser degree than in previous implants. This result was later found to be due to a partial blockage of the tube with the glue used in scaffold fabrication. In the other animal, regeneration was found to be as robust as in the best intact distal stump cases (see Figure A.6). This finding agrees with previous experiments showing that regeneration with a distal nerve fragment can be at least as robust as with an intact distal stump [29, 30]. Further considerations will likely be necessary to ensure a permanent source of distal trophic support for the regenerated nerve in the blind-ended case.

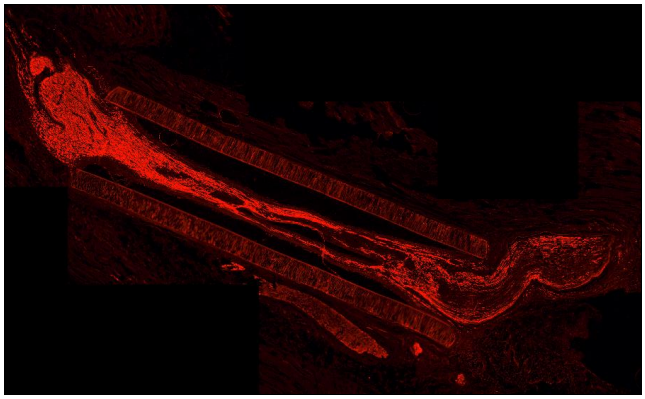

Figure A.6: Longitudinal cross section of regeneration scaffold with an isolated nerve segment sutured to the distal end.

NF-160 staining shows robust regeneration of axons through the length of the scaffold.

Overall, our results are encouraging for the design of an electrode able to interface with the nerve stump of an amputee. The recording and stimulating capabilities of RES's will be characterized in future experiments.

REFERENCES

[1] Ziegler-Graham K, MacKenzie EJ, Ephraim PL, Travison TG, Brookmeyer R. Estimating the prevalence of limb loss in the United States: 2005 to 2050. Arch Phys Med Rehabil. 2008;89:422-9.

[2] Gutmann E, Guttmann L, Medawar PB, Young JZ. The rate of regeneration of nerve. Journal of Experimental Biology. 1942;19:14-44.

[3] Williams LR, Longo FM, Powell HC, Lundborg G, Varon S. Spatial-temporal progress of peripheral-nerve regeneration within a silicone chamber - parameters for a bioassay. Journal of Comparative Neurology. 1983;218:460-70.

[4] Lundborg G, Dahlin LB, Danielsen N, Gelberman RH, Longo FM, Powell HC, et al. Nerve regeneration in silicone chambers - influence of gap length and of distal stump components. Experimental Neurology. 1982;76:361-75.

[5] Rakic P. Neuron-glia relationship during granule cell migration in developing cerebellar cortex-golgi and and electron microscopic study in macacus rhesus. Journal of Comparative Neurology. 1971;141:283-312.

[6] Wilkinson CDW, Riehle M, Wood M, Gallagher J, Curtis ASG. The use of materials patterned on a nano- and micro-metric scale in cellular engineering. Materials Science & Engineering C-Biomimetic and Supramolecular Systems. 2002;19:263-9.

[7] Norman J, Desai T. Methods for fabrication of nanoscale topography for tissue engineering scaffolds. Annals of Biomedical Engineering. 2006;34:89-101.

[8] Fan YW, Cui FZ, Chen LN, Zhai Y, Xu QY, Lee IS. Adhesion of neural cells on silicon wafer with nano-topographic surface. Applied Surface Science. 2002;187:313-8.

[9] Turner S, Kam L, Isaacson M, Craighead HG, Shain W, Turner J. Cell attachment on silicon nanostructures. 1997;2848-54.

[10] Rajnicek AM, Britland S, McCaig CD. Contact guidance of CNS neurites on grooved quartz: influence of groove dimensions, neuronal age and cell type. Journal of Cell Science. 1997;110:2905-13.

[11] Johansson F, Carlberg P, Danielsen N, Montelius L, Kanje M. Axonal outgrowth on nano-imprinted patterns. Biomaterials. 2006;27:1251-8.

[12] Bellamkonda R, Ranieri JP, Bouche N, Aebischer P. Hydrogel-based 3-dimensional matrix for neural cells. Journal of Biomedical Materials Research. 1995;29:663-71.

[13] Woerly S, Marchand R, Lavallee C. Interactions of copolmyeric poly(glyceryl methacrylate)-collagen hydogels with neural tissue - effects of structure and polar groups. Biomaterials. 1991;12:197-203.

[14] Ceballos D, Navarro X, Dubey N, Wendelschafer-Crabb G, Kennedy WR, Tranquillo RT. Magnetically aligned collagen gel filling a collagen nerve guide improves peripheral nerve regeneration. Experimental Neurology. 1999;158:290-300.

[15] Thompson DM, Buettner HM. Oriented Schwann cell monolayers for directed neurite outgrowth. Annals of Biomedical Engineering. 2004;32:1120-30.

[16] Biran R, Noble MD, Tresco PA. Directed nerve outgrowth is enhanced by engineered glial substrates. Experimental Neurology. 2003;184:141-52.

[17] Walsh JF, Manwaring ME, Tresco PA. Directional neurite outgrowth is enhanced by engineered meningeal cell-coated substrates. 2005;1085-94.

[18] Miller C, Jeftinija S, Mallapragada S. Micropatterned Schwann cell-seeded biodegradable polymer substrates significantly enhance neurite alignment and outgrowth. Tissue Engineering. 2001;7:705-15.

[19] Kim YT, Haftel VK, Kumar S, Bellamkonda RV. The role of aligned polymer fiber-based constructs in the bridging of long peripheral nerve gaps. Biomaterials. 2008;29:3117-27.

[20] Curtis A, Wilkinson C. Topographical control of cells. Biomaterials. 1997;18:1573-83.

[21] Vieu C, Carcenac F, Pepin A, Chen Y, Mejias M, Lebib A, et al. Electron beam lithography: resolution limits and applications. Applied Surface Science. 2000;164:111-7.

[22] Dalby MJ, Gadegaard N, Riehle MO, Wilkinson CDW, Curtis ASG. Investigating filopodia sensing using arrays of defined nano-pits down to 35 nm diameter in size. International Journal of Biochemistry & Cell Biology. 2004;36:2005-15.

[23] Bini TB, Gao SJ, Wang S, Ramakrishna S. Poly(l-lactide-co-glycolide) biodegradable microfibers and electrospun nanofibers for nerve tissue engineering: an in vitro study. Journal of Materials Science. 2006;41:6453-9.

[24] Huang ZM, Zhang YZ, Kotaki M, Ramakrishna S. A review on polymer nanofibers by electrospinning and their applications in nanocomposites. Composites Science and Technology. 2003;63:2223-53.

[25] Yang F, Murugan R, Wang S, Ramakrishna S. Electrospinning of nano/micro scale poly(L-lactic acid) aligned fibers and their potential in neural tissue engineering. Biomaterials. 2005;26:2603-10.

[26] Schnell E, Klinkhammer K, Balzer S, Brook G, Klee D, Dalton P, et al. Guidance of glial cell. migration and axonal growth on electrospun nanofibers of poly-epsilon-caprolactone and a collagen/poly-epsilon-caprolactone blend. Biomaterials. 2007;28:3012-25.

[27] Aebischer P, Guenard V, Winn SR, Valentini RF, Galletti PM. Blind-ended semipermeable guidance channels support peripheral-nerve regeneration in the absence of a distal nerve stump. Brain Research. 1988;454:179-87.

[28] Aebischer P, Guenard V, Brace S. Peripheral-nerve regeneration through blind-ended semipermeable guidance channels - effect of the molecular-weight cutoff Journal of Neuroscience. 1989;9:3590-5.

[29] Jenq CB, Coggeshall RE. Regeneration of transected rat sciatic-nerves after using isolated nerve fragments as distal inserts in silicone tubes. Experimental Neurology. 1986;91:154-62.

[30] Williams LR, Powell HC, Lundborg G, Varon S. Competence of nerve-tissue as distal insert promoting nerve regeneration in a silicone chamber. Brain Research. 1984;293:201-11.

[31] Frostick SP, Yin Q, Kemp GJ. Schwann cells, neurotrophic factors, and peripheral nerve regeneration. Microsurgery. 1998;18:397-405.

[32] Taniuchi M, Clark HB, Johnson EM. Induction of nerve growth-factor receptor in schwann-cells after axotomy. Proceedings of the National Academy of Sciences of the United States of America. 1986;83:4094-8.

[33] Zhang WG, Ochi M, Takata H, Ikuta Y. Influence of distal nerve segment volume on nerve regeneration in silicone tubes. Experimental Neurology. 1997;146:600-3.

[34] Vandennoven S, Wallace N, Muccio D, Turtz A, Pinter MJ. Adult spinal motoneurons remain viable despite prolonged absence of functional synaptic contact with muscle. Experimental Neurology. 1993;123:147-56.

[35] Fu SY, Gordon T. Contributing factors to poor functional recovery after delayed nerve repair - prolonged axotomy. Journal of Neuroscience. 1995;15:3876-85.

[36] Fu SY, Gordon T. The cellular and molecular basis of peripheral nerve regeneration. Molecular Neurobiology. 1997;14:67-116.

[37] Gordon T, Gillespie J, Orozco R, Davis L. Axotomy-induced changes in rabbit hindlimb nerves and the effects of chronic electrical-stimulation. Journal of Neuroscience. 1991;11:2157-69.

[38] Snider WD, Thanedar S. Target dependence of hypoglossal motor neurons during development and in maturity. Journal of Comparative Neurology. 1989;279:489-98.

[39] Titmus MJ, Faber DS. Axotomy-induced alterations in the electrophysiological characteristics of neurons. Progress in Neurobiology. 1990;35:1-51.

[40] Dhillon GS, Lawrence SM, Hutchinson DT, Horch KW. Residual function in peripheral nerve stumps of amputees: Implications for neural control of artificial limbs. Journal of Hand Surgery-American Volume. 2004;29A:605-15.

[41] Naples GG, Mortimer JT, Scheiner A, Sweeney JD. A spiral nerve cuff electrode for peripheral-nerve stimulation. Ieee Transactions on Biomedical Engineering. 1988;35:905-16.

[42] Tyler DJ, Durand DDM. Functionally selective peripheral nerve stimulation with a flat interface nerve electrode. Ieee Transactions on Neural Systems and Rehabilitation Engineering. 2002;10:294-303.

[43] Mannard A, Stein RB, Charles D. Regeneration electrode units - implants for recording from single peripheral-nerve fibers in freely moving animals. Science. 1974;183:547-9.

[44] Lago N, Ceballos D, Rodriguez FJ, Stieglitz T, Navarro X. Long term assessment of axonal regeneration through polyimide regenerative electrodes to interface the peripheral nerve. Biomaterials. 2005;26:2021-31.

[45] Rutten WLC. Selective electrical interfaces with the nervous system. Annual Review of Biomedical Engineering. 2002;4:407-52.

[46] Garde K, Keefer E, Botterman B, Galvan P, Romero MI. Early interfaced neural activity from chronic amputated nerves. Front Neuroengineering. 2009;2:5.

[47] Cho SH, Lu HM, Cauller L, Romero-Ortega MI, Lee JB, Hughes GA. Biocompatible SU-8-Based Microprobes for Recording Neural Spike Signals From Regenerated Peripheral Nerve Fibers. IEEE Sens J. 2008;8:1830-6.

[48] Lacour SP, Atta R, FitzGerald JJ, Blamire M, Tarte E, Fawcett J. Polyimide micro-channel arrays for peripheral nerve regenerative implants. Sensors and Actuators a-Physical. 2008;147:456-63.

[49] Clements IP, Kim YT, English AW, Lu X, Chung A, Bellamkonda RV. Thin-film enhanced nerve guidance channels for peripheral nerve repair. Biomaterials. 2009;30:3834-46.

[50] Nichols CM, Brenner MJ, Fox IK, Tung TH, Hunter DA, Rickman SR, et al. Effect of motor versus sensory nerve grafts on peripheral nerve regeneration. Experimental Neurology. 2004;190:347-55.

[51] Matsuyama T, Mackay M, Midha R. Peripheral nerve repair and grafting techniques: A review. Neurologia Medico-Chirurgica. 2000;40:187-99.

[52] Williams LR. Exogenous fibrin matrix precursors stimulate the temporal progress of nerve regeneration within a silicone chamber. Neurochemical Research. 1987;12:851-60.

[53] Liu HM. The role of extracellular-matrix in peripheral-nerve regeneration - a wound chamber study. Acta Neuropathologica. 1992;83:469-74.

[54] Miller C, Shanks H, Witt A, Rutkowski G, Mallapragada S. Oriented Schwann cell growth on micropatterned biodegradable polymer substrates. Biomaterials. 2001;22:1263-9.

[55] Thompson DM, Buettner HM. Neurite outgrowth is directed by Schwann cell alignment in the absence of other guidance cues. Annals of Biomedical Engineering. 2006;34:669-76.

[56] Manwaring ME, Walsh JF, Tresco PA. Contact guidance induced organization of extracellular matrix. Biomaterials. 2004;25:3631-8.

[57] Matsumoto K, Ohnishi K, Kiyotani T, Sekine T, Ueda H, Nakamura T, et al. Peripheral nerve regeneration across an 80-mm gap bridged by a polyglycolic acid (PGA)-collagen tube filled with laminin-coated collagen fibers: a histological and electrophysiological evaluation of regenerated nerves. Brain Research. 2000;868:315-28.

[58] Lundborg G, Kanje M. Bioartificial nerve grafts - A prototype. Scandinavian Journal of Plastic and Reconstructive Surgery and Hand Surgery. 1996;30:105-10.

[59] Ngo TT, Waggoner PJ, Romero AA, Nelson KD, Eberhart RC, Smith GM. Poly(L-lactide) microfilaments enhance peripheral nerve regeneration across extended nerve lesions. Journal of Neuroscience Research. 2003;72:227-38.

[60] Whitworth IH, Brown RA, Dore C, Green CJ, Terenghi G. Orientated mats of fibronectin as a conduit material for use in peripheral-nerve repair. Journal of Hand Surgery-British and European Volume. 1995;20B:429-36.

[61] Dodla MC, Bellamkonda RV. Differences between the effect of anisotropic and isotropic laminin and nerve growth factor presenting scaffolds on nerve regeneration across long peripheral nerve gaps. Biomaterials. 2008;29:33-46.

[62] Stokols S, Tuszynski MH. Freeze-dried agarose scaffolds with uniaxial channels stimulate and guide linear axonal growth following spinal cord injury. Biomaterials. 2006;27:443-51.

[63] Chamberlain LJ, Yannas IV, Hsu HP, Strichartz G, Spector M. Collagen-GAG substrate enhances the quality of nerve regeneration through collagen tubes up to level of autograft. Experimental Neurology. 1998;154:315-29.

[64] Zhang YP, Onifer SM, Burke DA, Shields CB. A topical mixture for preventing, abolishing, and treating autophagia and self-mutilation in laboratory rats. Contemporary Topics in Laboratory Animal Science. 2001;40:35-6.

[65] Yu XJ, Bellamkonda RV. Tissue-engineered scaffolds are effective alternatives to autografts for bridging peripheral nerve gaps. Tissue Engineering. 2003;9:421-30.

[66] Loeb GE, Gans C. Electromyography for Experimentalists. Chicago: The University of Chicago Press; 1986.

[67] Dodla MC, Bellamkonda RV. Differences between the effect of anisotropic and isotropic laminin and nerve growth factor presenting scaffolds on nerve regeneration across long peripheral nerve gaps. Biomaterials. 2008;29:33-46.

[68] Clements IP, Kim YT, Andreasen D, Bellamkonda RV. A regenerative electrode scaffold for peripheral nerve interfacing. Proceedings of the 3rd International Conference IEEE Engineering in Medicine and Biology Society Conference on Neural Engineering Kohala Coast, HI. 2007;390-3.

[69] Scaravilli F. Regeneration of the perineurium across a surgically induced gap in a nerve encased in a plastic tube. Journal of Anatomy. 1984;139:411-24.

[70] Aebischer P, Guenard V, Valentini RF. The morphology of regenerating peripheral-nerves is modulated by the surface microgeometry of polymeric guidance channels. Brain Research. 1990;531:211-8.

[71] Williams LR, Varon S. Modification of fibrin matrix formation insitu enhances nerve regeneration in silicone chambers. Journal of Comparative Neurology. 1985;231:209-20.

[72] Williams LR, Danielsen N, Muller H, Varon S. Exogenous matrix precursors promote functional nerve regeneration across a 15-mm gap within a silicone chamber in the rat. Journal of Comparative Neurology. 1987;264:284-90.

[73] Scaravilli F. The influence of distal environment on peripheral-nerve regeneration across a gap. Journal of Neurocytology. 1984;13:1027-41.

[74] Zhao Q, Dahlin LB, Kanje M, Lundborg G. Repair of the transected rat sciatic-nerve - matrix formation within implanted silicone tubes. Restorative Neurology and Neuroscience. 1993;5:197-204.

[75] Guenard V, Valentini RF, Aebischer P. Influence of surface texture of polymeric sheets on peripheral-nerve regeneration in a 2-compartment guidance-system. Biomaterials. 1991;12:259-63.

[76] Li JM, Shi RY. Fabrication of patterned multi-walled poly-L-lactic acid conduits for nerve regeneration. Journal of Neuroscience Methods. 2007;165:257-64.

[77] Itoh S, Takakuda K, Ichinose S, Kikuchi M, Schinomiya K. A study of induction of nerve regeneration using bioabsorbable tubes. Journal of Reconstructive Microsurgery. 2001;17:115-23.

[78] Lundborg G, Dahlin L, Dohl D, Kanje M, Terada N. A new type of "bioartificial" nerve graft for bridging extended defects in nerves. Journal of Hand Surgery-British and European Volume. 1997;22B:299-303.

[79] Danielsen N, Vahlsing HL, Manthorpe M, Varon S. A 2-compartment modification of the silicone chamber model for nerve regeneration. Experimental Neurology. 1988;99:622-35.

[80] Baldissera F, Hultborn H, Illert M. Integration in spinal neuronal systems. In: VB B, editor. Handbook of Physiology. Washington, D.C. : American Physiological Society; 1981;509-95.

[81] Poppele R, Bosco G. Sophisticated spinal contributions to motor control. Trends in Neurosciences. 2003;26:269-76.

[82] Rudomin P, Schmidt RF. Presynaptic inhibition in the vertebrate spinal cord revisited. Exp Brain Res. 1999;129:1-37.

[83] Edell DJ. A peripheral-nerve information transducer for amputees - Long-term multichannel recordings from rabbit peripheral-nerves. IEEE Transactions on Biomedical Engineering. 1986;33:203-14.

[84] Kovacs GTA, Storment CW, Rosen JM. Regeneration microelectrode array for peripheral-nerve recording and stimulation. IEEE Transactions on Biomedical Engineering. 1992;39:893-902.

[85] Akin T, Najafi K, Smoke RH, Bradley RM. A micromachined silicon sieve electrode for nerve regeneration applications. IEEE Transactions on Biomedical Engineering. 1994;41:305-13.

[86] Navarro X, Calvet S, Rodriguez FJ, Stieglitz T, Blau C, Buti M, et al. Stimulation and recording from regenerated peripheral nerves through polyimide sieve electrodes. Journal of the Peripheral Nervous System. 1998;3:91-101.

[87] Stieglitz T, Beutel H, Meyer JU. A flexible, light-weight multichannel sieve electrode with integrated cables for interfacing regenerating peripheral nerves. Sensors and Actuators a-Physical. 1997;60:240-3.

[88] Horch KW, Lisney SJW. On the number and nature of regenerating myelinated axons after lesions of cutaneous nerves in the cat. Journal of Physiology-London. 1981;313:275-86.

[89] Hoffer JA, Stein RB, Gordon T. Differential atrophy of sensory and motor fibers following section of cat peripheral nerves. Brain Research. 1979;178:347-61.

[90] Milner TE, Stein RB. the effects of axotomy on the conduction of action-potentials in periphearl sensory and moter-nerve fibers. Journal of Neurology Neurosurgery and Psychiatry. 1981;44:485-96.

[91] Lago N, Navarro X. Evaluation of the long-term regenerative potential in an experimental nerve amputee model. Journal of the Peripheral Nervous System. 2007;12:108-20.

[92] Carlson J, Lais AC, Dyck PJ. Axonal atrophy from permanent peripheral axotomy in adult cat J Neuropathol Exp Neurol. 1979;38:579-85.

[93] Edell DJ. Long Term Bi-Directional Axon-Electronic Communication System. (PCT patent application: 06009722, PCT/US-5/021081) World Intellectual Property Organization 2006.

[94] FitzGerald JJ, Lacour SP, McMahon SB, Fawcett JW. Microchannels as axonal amplifiers. Ieee Transactions on Biomedical Engineering. 2008;55:1136-46.

[95] Egeland BM, Urbanchek M, Martin DC, Kipke DR, Kuzon W, Cederna PS. Engineering and development of a stable, low-impedance, bioelectrical peripheral nerve interface. J Am Coll Surg. 2009;209:S76-S.

[96] Kuiken TA, Dumanian GA, Lipschutz RD, Miller LA, Stubblefield KA. The use of targeted muscle reinnervation for improved myoelectric prosthesis control in a bilateral shoulder disarticulation amputee. Prosthetics and Orthotics International. 2004;28:245-53.